DISSERTATION

INVESTIGATION OF ENVIRONMENTAL FACTORS ON THE INTRANUCLEAR LANDSCAPE OF MESENCHYMAL STROMAL CELLS

Submitted by

Samantha Kaonis

School of Biomedical Engineering

In partial fulfillment of the requirements

For the Degree of Doctor of Philosophy

Colorado State University

Fort Collins, Colorado

Fall 2022

Doctoral Committee:

Advisor: Soham Ghosh

Brian Johnstone
Ketul Popat
Steven Dow

ABSTRACT

INVESTIGATION OF ENVIRONMENTAL FACTORS ON THE INTRANUCLEAR LANDSCAPE OF MESENCHYMAL STROMAL CELLS

Mesenchymal stromal cells (MSC), also known as mesenchymal stem cells, are popular candidates for tissue engineering and regenerative medicine. They can differentiate into many tissue types, and they can also help in regeneration through their trophic and immunomodulatory properties. Despite being investigated thoroughly for the last four decades and being under clinical trial in more than a thousand FDA approved studies, their application in clinics is very limited. One of the most important challenges in using MSC is that after harvesting from the patient, they need to be expanded to millions of cells for successful clinical outcomes. During this process, MSCs lose their differentiation potential, and trophic and immunomodulatory properties. In this thesis, I investigated the potential mechanisms of how environmental factors cause the MSC to divert from their phenotype during the expansion process. Subsequently, I intervened these mechanisms to achieve high quality MSCs without compromising the number of cells, i.e., their proliferation potential. Specifically, I investigated how two critical biophysical factors - mechanical stiffness and oxygen concentration of the MSC environment affects the cell phenotype and function through mechanisms involving epigenetic modifiers, transcription factors, and the chromatin architecture.

First, the regulation of mechanics-induced population heterogeneity in MSCs was examined. Plastic culture and fibrotic conditions post-transplantation experienced by the MSC is completely different from the natural biomechanical niche of the MSC. Accordingly, the role of the mechanical environment has been shown to be a critical determinant of MSC gene expression

and function. In this study, we report that human bone marrow-derived primary MSC population becomes phenotypically heterogenous when they experience an abnormal mechanical environment, compared to their native environment. Using a newly developed technique to quantify the heterogeneity, we provide evidence of phenotypical heterogeneity of MSC through high-resolution imaging and image analysis. Additionally, we provide mechanistic insight into the origin of such substrate mechanics-driven heterogeneity, which is further determined by the cell-cell mechanical communication through the substrate.

In the second study, we investigated how the chromatin architecture and epigenetic landscape changes in MSCs by the substrate mechanical stiffness, thus causing a shift from the MSC phenotype. Using high-resolution confocal microscopy and advanced image analysis we identified the key epigenetic drivers in the mechanical stiffness mediated chromatin organization changes. Subsequently, we targeted several components of a proposed mechanobiological pathway to achieve MSCs with higher growth factor secretion without compromising their proliferation. The outcome of these studies might provide mechanism-driven design principles to the molecular, cellular and tissue engineering researchers for the rational design of MSC culture conditions and scaffolds, thus improving their functional outcome.

Finally, the effect of oxygen concentration on MSC proliferation and performance were explored. Culture under physiological oxygen concentration (physioxia) can increase the proliferation of MSCs through a pathway initiated by the stabilization of the hypoxia-inducible factor-1 (HIF-1). Stabilized HIF-1α translocates into the nucleus, triggering the transcription of target genes conducive to MSC activity and proliferation. However, stabilized HIF-1α also triggers the p21 pathway causing cell cycle arrest, decreasing the MSC proliferation thereby limiting the beneficial effect of physioxia. Maintaining low oxygen conditions can be challenging, especially

at a large scale, so rational exploitation and selective manipulation of such pathways through biochemical means has the potential to culture MSCs easily at scale. In this work, we created a mathematical model to predict optimal physioxic culture parameters to achieve the highest MSC proliferation. Through analysis of a gene downstream of the HIF-1 pathway, we also compared standard physioxic culture (2% O_2) to treatment with deferoxamine mesylate (DFO), a physioxia-mimicking drug. The outcomes of this study might provide the rationale for MSC culture under standard hyperoxic conditions with only a simple addition of a combination of drugs to the culture medium to improve the scalability of MSC culture.

Together, the results of the work will identify the mechanistic details of culture environment factors that play a role in determining the phenotype of MSCs during *in vitro* expansion process. The combination of these techniques to optimize MSC culture *in vitro* has the potential to resolve the current impediment to the clinical success of MSC therapies.

ACKNOWLEDGEMENTS

There is no doubt in my mind that I would not be writing this body of work without the lovely people that have supported me over the last few years. I am so glad to have a chance to acknowledge them here. I have greatly enjoyed doing this PhD, and that is mainly because of the support I had surrounding me.

I would like to first express my deepest appreciations for my advisor, Dr. Soham Ghosh. With his support and guidance, I was able to complete a very interesting work and learnt how to be a competent researcher. Having constant feedback has helped me to grow so much in scientific communication. It was such a great experience to be able to work in a brand-new lab and watch it grow.

Next, I extend my sincerest thanks to my committee members Dr. Steven Dow, Dr. Brian Johnstone and Dr. Ketul Popat. I am so appreciative of the expertise, knowledge, and time they so generously provided. I also would like to acknowledge the School of Biomedical Engineering and the Translational Medicine Institute for the resources offered that allowed me to complete my research. I am also so very grateful for my classmates and lab members, especially our stellar undergraduate students. The time they dedicated and attention to detail were instrumental to completing my projects.

Lastly, I couldn't have done this without my friends and family's support. A special shoutout to Kyle for being my main motivator and picking up my slack when things became overwhelming. To my friends and family, thank you for all of the trips and phone calls, it really kept me going being so far away. I cannot reiterate enough how happy I am to have accomplished this thanks to you all.

TABLE OF CONTENTS

ABSTRACT ii
ACKNOWLEDGEMENTS v
CHAPTER 1: INTRODUCTION 1
Potential of MSCs in Clinical Therapies 1
Characterization of MSCs 2
Differentiation and Proliferation Properties 4
Immunomodulatory Properties 6
MSC Culture Environment 8
Thesis Outline and Goals 9
REFERENCES 10
CHAPTER 2: CHARACTERIZATION OF MECHANICS-DRIVEN HETEROGENEITY IN MESENCHYMAL STROMAL CELLS 16
Background 16
Heterogeneity in MSC Phenotype 17
Donor Specific Variability in MSC 18
Tissue-Specific Variability in MSC 20
MSC Mechanosensing Effects on Heterogeneity 22
The Role of YAP/TAZ in MSC Mechanosensing 22
Materials and Methods 25
MSC culture 25
MSC culture on substrates with varying mechanical stiffness and cell density 25
Preparation of thin PDMS substrate 26
Cell Staining for immunofluorescence, actin, and DNA 27
Quantification of cell and nuclear morphology and stress fiber formation 27
Quantification of chromatin architecture 28
Quantification of immunofluorescence images 29
Quantification of heterogeneity 29
Cell treatments with cytoskeleton, YAP, and Runx2 modifying drugs 30
Statistical Analysis 30
Results 31

Soft substrates promote a more homogeneous population of cell phenotype over passaging 31
Soft substrates promote a more homogeneous nuclear phenotype over passaging 32
Seeding density has little impact on nucleus phenotype, but significantly affects chromatin organization 35
Functional indications of substrate mechanics-driven heterogeneity 37
Cytoskeletal tension significantly affects cell and nuclear phenotype but not the heterogeneity in passage 5 38
Mechanobiological pathway inhibiting drugs can increase stemness markers and decrease the heterogeneity in Passage 4 40
Cytoskeletal tension is reinforced by the perinuclear actin cap 40
Emergent stress field of a cell community lowers intracellular strain 43
Discussion 44
REFERENCES 47
CHAPTER 3: MECHANICAL STIFFNESS REGULATES CHROMATIN REMODELING IN MESENCHYMAL STROMAL CELLS DURING MONOLAYER CULTURE 55
Background 55
Epigenetics 55
Effects of Substrate Stiffness on MSC 56
Chromatin Remodeling 59
Materials and Methods 63
MSC culture 63
MSC culture on substrates with varying mechanical stiffness and cell density 64
Preparation of thin PDMS substrate 65
Live imaging of cell nucleus during cell attachment 66
Cell Staining for immunofluorescence, actin, and DNA 66
Quantification of cell and nuclear morphology and stress fiber formation 67
Quantification of chromatin architecture 67
Quantification of immunofluorescence images 68
Cell treatments with drugs 68
Cell counting and gene expression analysis 69
Statistical Analysis 69
Results 69

Serial passaging on a soft substrate increases a stemness marker but decreases the chromatin segregation 69
Serial passaging leads to a flatter cell shape and more rounded nucleus on the stiff substrate 71
Soft substrate affects the localization and expression of the facultative repressive marker H3K9me3 but not the constitutive repressive marker H3K27me3 73
Soft substrate promotes a higher localization of active epigenetic markers in the nucleus 76
Soft substrate promotes the increased activity of SWI/SNF chromatin remodeling complex 78
Chromatin segregation has slowed temporal dynamics 79
Targeting the mechanobiological and epigenetic pathways is a potential strategy to maintain MSC stemness 81
Discussion 82
REFERENCES 85
CHAPTER 4: INVESTIGATION OF THE PHYSIOXIA RELATED PATHWAYS IN MSC PROLIFERATION 90
Background 90
MSC Performance Under Physioxia: Multiple Pathways Intersect 91
Role of HIF-1α During Physioxia 94
Role of p21 in Cell Survival 95
Physioxia Induction in Vitro 96
Stem Cell-Specific Growth Models 97
Project Goals 99
Materials and Methods 99
Predictive mathematical model 99
MSC Culture 100
Cell treatments with physioxia-mimetic drugs 101
RNA Extraction and Reverse Transcription 102
Quantitative Real-Time PCR 102
Statistics 103
Results 103
Mathematical model determines optimal parameters in physioxia-dependent cell proliferation 103
DFO treatment can similarly induce a physioxic response at the gene expression level 106

Discussion 107
REFERENCES 110
CHAPTER 5: FUTURE DIRECTIONS AND POTENTIAL IMPACT 114
Mechanical stiffness-driven heterogeneity through the Runx2 pathway 114
Mechanics-induced epigenetic pathways as a potential strategy to maintain MSC stemness 115
Drug-mediated HIF-1α stabilization to increase MSC proliferation 116
APPENDIX A 117
Supplementary Figures 117
Quantification of stress fiber formation 121
APPENDIX B 122
Significance Tables 122
APPENDIX C 125
Hypoxia Model Intermediate Equations 125

CHAPTER 1: INTRODUCTION

Mesenchymal stromal cells (MSCs) have been widely investigated for more than three decades because of their elusive biological function, broad clinical potential, and as a central building block in the tissue engineering and regenerative medicine field. They can be expanded *in vitro* for differentiation into many cell types, and they can produce an abundance of useful growth factors and cytokines [1] because of their immunomodulatory and trophic properties. Theoretically, these traits allow MSCs to regenerate a variety of tissue types as elucidated through numerous *in vitro* and preclinical *in vivo* studies with potential applications in many tissue types. However, there are significant hurdles that need to be overcome to bring MSCs to the clinic in a scalable manner. Preclinical trials show that the outcome of MSC administration often fails, or the results are highly variable. Such variability and the cost associated with *in vitro* MSC expansion are the key limiting factors for MSCs not reaching the clinical approval stage for widespread applications. My thesis attempts to address these challenges to some degree so that MSCs can be brought to clinics in the future.

Potential of MSCs in Clinical Therapies

The potential for MSC proliferation and differentiation may vary considerably depending on the source of MSC, which is a direct reflection of the specific microenvironments in which they reside [2]. The complexity of studying and characterizing MSC *in vivo* has led to little knowledge regarding their functions in the physiological setting. The function of MSCs *in vivo* is difficult to evaluate, but *in vitro* experiments can provide some mechanistic insight on their functions. MSCs can act directly in regeneration through differentiation and indirectly by producing and secreting

factors that enhance the endogenous regeneration of injured tissue and decrease inflammation. These attributes make MSCs a promising tool for cell therapies and tissue engineering. However, the expansion of MSCs *in vitro* to obtain a sufficient number of cells has been challenging for a multitude of reasons. The artificial *in vitro* expansion condition is significantly different from their *in vivo* niche, and such differences most likely lead to the deviation in MSCs phenotype during the *in vitro* expansion culture.

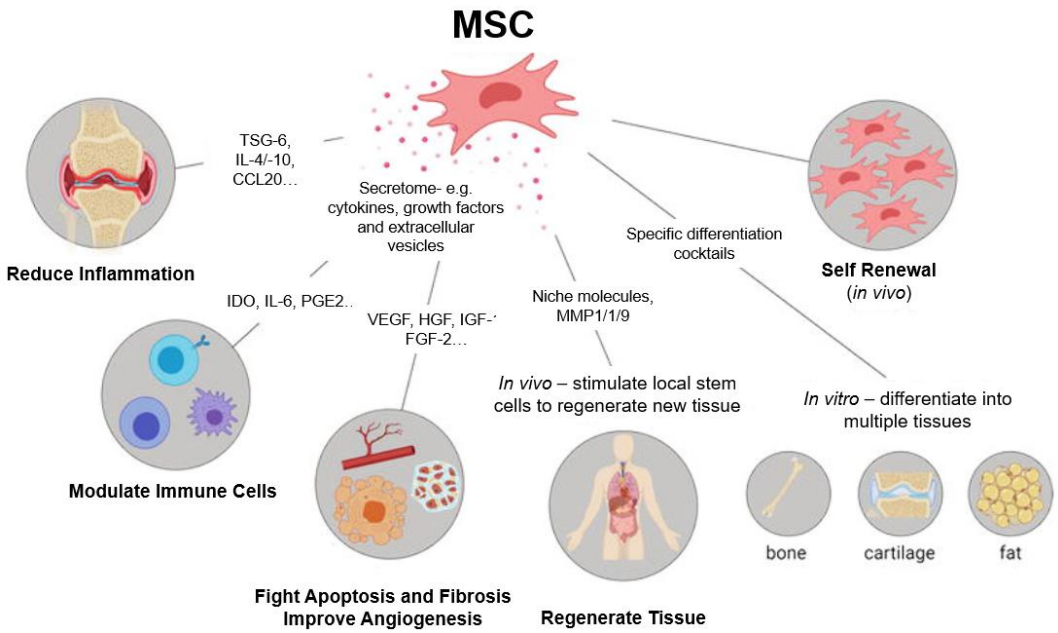

Figure 1. Different modes of action of MSCs. MSCs modulate the host immune systems, e.g., by secreting various trophic factors. Thereby, they reduce inflammation, promote neo-angiogenesis, and prevent apoptosis and fibrosis. Further, they stimulate local stem cells to develop new tissue. TSG-6, tumor necrosis factor-inducible gene 6 protein also known as TNF-stimulated gene 6 protein; IL-4/6/10, interleukins 4, 6, and 10; IDO, indoleamine 2,3-dioxygenase; PGE2, prostaglandin E2; VEGF, vascular endothelial growth factor; FGF-2, basic fibroblast growth factor; HGF, hepatocyte growth factor; IGF-1, insulin-like growth factor 1; MMP1/2/9, matrix metalloproteinase-1/2/9. Adapted from Barekzai et al. (2019).

Characterization of MSCs

Multipotent mesenchymal stromal cells (MSCs) from different sources such as bone marrow and adipose tissue are used in a variety of applications for tissue engineering and regenerative medicine [1, 3–5]. In 2006, the International Society of Cellular Therapy (ISCT) proposed basic criteria for

defining MSCs. They determined cell populations are considered MSCs if they show plastic adherent properties under specific culture conditions, are capable of trilineage differentiation into osteoblasts, chondrocytes, and adipocytes [5, 6]; and if they express various cell surface markers such as CD73, CD90, and CD105 while lacking CD34 (hematopoietic and endothelial cells), CD45 (pan-leukocyte), CD14 or CD11b (monocytes and macrophages), CD79⟨ or CD19 (B cells), and HLA-DR expression [4]. We now know that MSCs also express other surface markers, but the expression of specific combinations of the markers appear to be host tissue-dependent (Table 1), with no single marker being indicated as specific for MSCs [2]. There are controversies arising regarding the proper identification of MSCs, with the criteria proposed by the ISCT not being sufficient since MSCs isolated from different tissues represent a relatively heterogeneous group of cells. However, for any MSC-based regenerative medicine application, the ISCT criteria should be used as a minimum requirement. The most recent literature points to a pericyte origin of MSCs which explains their presence in virtually all tissues that contain blood vessels, including the heart and brain, outside of the traditional MSCs sources such as bone marrow, adipose, and dental pulp.

Table 1. Comparison of MSCs from different sources in reference to different parameters: bone marrow-derived MSCs (BM-MSC), adipose tissue-derived MSCs (AT-MSC), umbilical cord-derived MSCs (UC-MSC), dental pulp stem cells (DPSC), and endometrial MSCs (eMSC). Adapted from from Mastrolia et al (2019).

	BM-MSC	AT-MSC	UC-MSC	DPSC	eMSC
Tissue availability	✓✓	✓✓✓	✓✓✓	✓	✓✓✓
Cell yield	✓	✓✓	✓✓	✓✓	✓✓
Cell shape uniformity	✓	✓✓	✓✓✓	✓✓	✓✓✓
Proliferation	✓✓	✓✓	✓✓✓	✓✓✓	✓✓✓
In vitro senescence	✓✓✓	✓✓	✓	✓✓	✓
Differentiation ability	✓✓✓	✓✓	✓✓	✓✓	✓✓
Stromal function	✓✓✓	✓✓✓	✓✓	✓✓	✓✓
Autologous use	✓✓✓	✓✓✓	✓	✓	✓✓
Allogenic use	✓✓✓	✓✓✓	✓✓✓	✓✓✓	✓✓✓

✓ low; ✓✓, medium; ✓✓✓, high.

To assess the functionality of MSCs in this study, the surface protein CD73 was examined. CD73 is a well-known marker for cultured MSCs in mice and humans, whereas it exhibits only moderate expression in mesodermal cells. There are two main mechanisms of CD73: enzymatic and non-enzymatic functions [7]. CD73 as an enzyme catalyzes the AMP breakdown into adenosine, a signaling molecule in the pathway of MSC-mediated immunosuppression [8]. A specific example is provided from Zhai et al as follows. [9]. They engineered human umbilical cord MSCs CD73+ extracellular vesicles, mitigating inflammation from spinal cord injuries through increased levels of adenosine. The non-enzymatic function of CD73 is as a regulatory molecule for roles such as stemness, epithelial-mesenchymal transition [10, 11], or tissue homeostasis [12]. CD73-positive MSCs have vascular and perivascular expression but can occasionally be found in fibroblasts. Quantification of CD73 in conjunction with a more MSC-specific marker such as Stro-1, NG2, CD146, or 3G5 would increase the confidence of cells being "true MSCs" [13]. The immunofluorescent studies reported here only examine the CD73 marker as a baseline so that other proteins can be analyzed concurrently. This is a satisfactory preliminary marker of stemness, though, since it is seen that bone marrow MSCs that are positive for CD73 display increased stemness [10] *in vitro* and promote fracture healing *in vivo* [14]. In studies of CD73-positive adipose-derived MSCs, macrophage infiltration was reduced, and fibrosis development was subdued [15], with structural and functional repair of myocardial infarction in murine hearts [16]. These studies support the use of CD73 as a functional indicator in my thesis.

Differentiation and Proliferation Properties

Different tissue-derived MSCs exhibit tendencies to differentiate into different end-differentiated cells by varying degrees, therefore such differentiation and regeneration ability

contribute to the variable clinical efficacy. To provide a large enough number of MSCs for clinical applications, the cells need to be amplified on a large scale through long-term culture. A large enough cell population is achieved through serial passaging, but this inevitably leads to MSC senescence followed by subsequent gene expression changes deviating from the MSC phenotype. Proteomic analysis reveals that stemness and proliferation-related genes [17, 18] are highly expressed in undifferentiated MSCs [18]. Throughout long-term passaging, MSCs start to differentiate gradually, losing their differentiation ability and stemness. Figure 2 demonstrates the changes that MSCs experience over serial passaging. The capacity for the specific differentiation into osteoblasts, chondrocytes, or adipocytes significantly decreased as passaging continued (Figure 2A). Stemness related gene expression also decreases, accompanied by an increase in senescence-related proteins (Figure 2 B, C) [19, 20]. Having the ability to maintain stem cell-specific properties through passaging is essential for MSCs to be translated into the clinic.

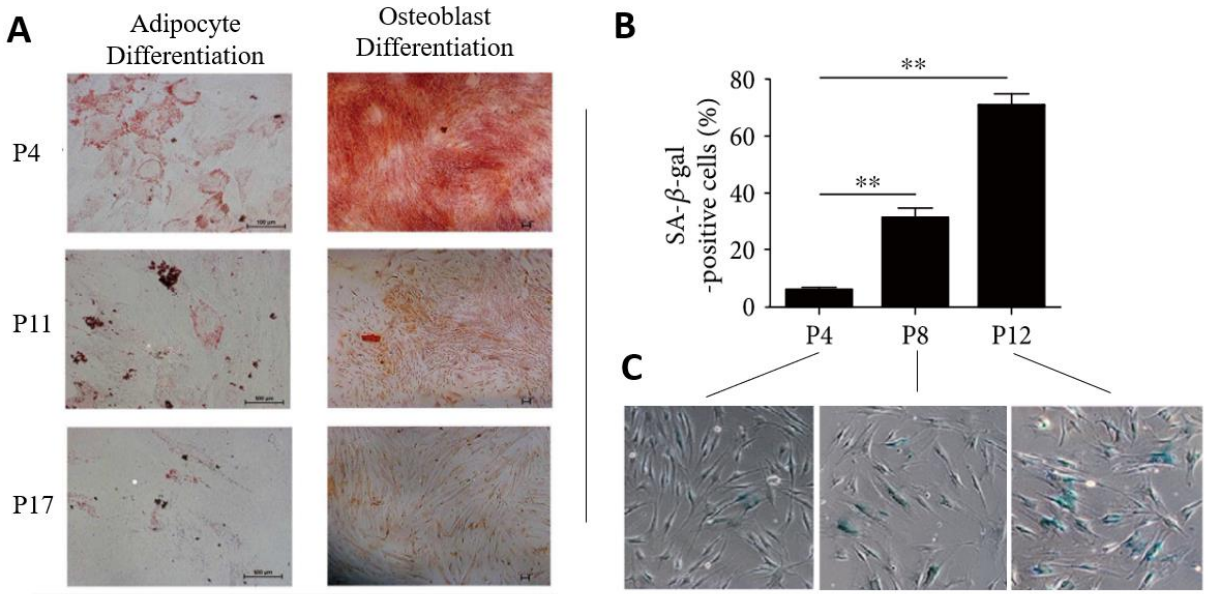

Figure 2. Over long-term passaging, differentiation potential decreases while senescence increases in MSC. (A). human umbilical cord MSCs were differentiated into adipocytes for 21 days and osteoblasts for 14 days. Fat accumulation was visualized by Oil Red-O staining and osteogenic differentiation was visualized with Alizarin Red staining. Adapted from Gu et al. Senescence significantly increases (B, C) after culture under standard conditions for multiple passages. Stained for senescence-associated β-galactosidase. Adapted from Li, X. et al.

Immunomodulatory Properties

Preclinical and clinical studies have shown that MSCs demonstrate immune response attributes and they have anti-inflammatory properties [21]. Paracrine signaling is primarily responsible for the involvement of MSCs in the modulation of immune responses and they are correlated with the therapeutic benefits of these cells. These immunomodulatory features are most likely due to several cytokines and regulatory factors, such as TGFβ and IL10, as well as extracellular vesicles e.g., exosomes that convey regulatory messages to recipient immune cells in the microenvironment [22]. Secreting various types of proteins allows MSCs to contribute to cell migration, angiogenesis, and anti-apoptotic processes. Specifically, it has recently been demonstrated that MSCs play a critical role in regulating the inflammatory micro-environment and immune cell interactions with T cells, B cells, and natural killer cells. The MSC secretome, similar to other MSC attributes, is majorly influenced by donor variability as well as different culture conditions [22], and these factors need to be better understood for clinical success.

MSC-derived extracellular vesicles, which include exosomes (~50 - 200 μm size range) and microvesicles (>200 μm) are being examined for their use in cell-free therapies. These exosomes can influence the body's response to injury, infection, and disease through their contents which can include cytokines, growth factors, or regulatory miRNAs. The miRNAs contained within MSC-derived exosomes have been shown to inhibit tumor growth, reduce cardiac fibrosis following myocardial infarction, and stimulate endothelial cell angiogenesis [23–25]. The quality and potency of MSC exosome production are dictated by their microenvironment in the same manner as cell-based MSC therapies. This explains why although great effort that has been made to determine whether MSCs or MSC-derived exosomes are better for therapeutic applications, a clear conclusion has yet to be made [26].

Clinical Trials

Many studies focus on the use of MSCs in cell therapies and accordingly, they are being used as a potential technique to treat degenerative diseases of musculoskeletal, cardiovascular and respiratory systems to name a few. The preclinical data promotes the expectation of the use of MSCs in human clinical trial applications, however, the clinical outcomes of advanced trials have fallen short of expectations compared to the outcomes in animal models. This is due to the many challenges that remain to be overcome before the efficient clinical application of MSC-based therapy.

The lack of FDA approval despite MSC treatments being used in a multitude of patients in over thousands of clinical trials, leading to variable outcomes [1, 2, 5] is a huge discrepancy that needs to be addressed soon if we want to leverage on the MSC related knowledge generated over decades. Several issues, including finding a suitable source and isolating a well-characterized, homogeneous population are critical to overcome in order to achieve the appropriate therapeutic effects.

To address the safety profile of MSC, Musiał -Wysocka et al. [2] compiled a comprehensive review of BM-MSC clinical trials and it was found that there was no relationship between the use of MSCs and tumorigenic potential - therefore no serious side effects were reported in terms of oncogenic potential. Safety and impact of MSCs were also evaluated in several clinical trials with longer durations and no serious adverse effects resulting from the therapy were observed, even one year after the trial had ended, though longer-term (>5 years) studies for MSC therapies are still required [2]. The success of MSC depends on many variables including the cell model, method of culture, cell heterogeneity, secreted molecules, and many other factors that are still being uncovered. To summarize, MSC therapies have been designated safe by the FDA [27]

through clinical trials. Overall, they have shown promising outcomes [28–31], as reported by clinical studies. A prevalent limitation of these clinical trials is the complexity and cost involved in cell expansion [30, 31]. Over 100 million cells is the typical quantity required for large defects. This has been deemed hard to achieve, with a reported fibroblast-like phenotype through expansion. Besides, dose dependence of MSCs also reveals that abundant MSCs should be ready for any clinical trial to be started. In some smaller clinical trials, no advantage of MSC therapies was observed [32], possibly due to the effects of MSC population heterogeneity. Overall, these clinical trial results grow the confidence in the use of MSCs for therapies but achieving a high enough number of real MSCs is hindering their progress for clinical use.

MSC Culture Environment

To become proliferative and maintain their true phenotype, MSCs need a permissive and instructive environment. Hence, the desired phenotype is dependent on the cellular environment and the temporal application of instructive external agents, and their duration [1]. *In vitro* expansion of MSCs is usually performed in a standard 2D petri dish culture, but this culture method does not allow the cells to experience the natural *in vivo* environment, e.g., the extracellular mechanical microenvironment/signaling cues that help maintain the MSC phenotype. This altered cell-extracellular matrix (ECM) interaction leads to a decrease in stemness in adult stem cells and lowers their therapeutic potential. As an example, a chemokine receptor CXCR4 is involved in the migration of MSCs *in vivo*. Expression of CXCR4 is lost during *in vitro* culture on flasks, whereas the presence of cytokines like HGF or physioxic conditions restores its expression [2]. Certainly, there are many complex factors to be considered though when considering engineering the MSC environment. A lack of the knowledge of native MSC environment is a hindrance to creating a

similar environment *in vitro*. There have been many reports that MSCs cultured in a 3D system such as spheroids have properties that are far superior to those of 2D culture. Such benefits include enhanced differentiation capacity, increased migration and homing efficiency to a damaged site, and an increase in regenerative and anti-inflammatory properties [33–38]. However, these benefits of 3D culture are accompanied by a slow rate of proliferation as cells do not have enough space to proliferate. Overall, elucidation of environmental factors and optimizing them for optimal MSC performance is a timely topic and this thesis will address that issue.

Thesis Outline and Goals

The overall goal for MSC *in vitro* expansion culture is to obtain a large, homogeneous, true MSC population that can be used in a variety of tissue engineering applications. When MSCs turn into a heterogeneous population during expansion, they lose their stemness and could cause unintended detrimental and suboptimal therapeutic effects due to the mixed cell population. Our goal is to gain an understanding of the underlying mechanisms inside the nucleus and modulate them to obtain (1) a phenotypically homogeneous MSC population (2) that retains stemness by intervening in the mechanosensitive pathways, (3) while maintaining high proliferation capacity through the physioxia related pathways.

REFERENCES

1. Pittenger, M. F., Discher, D. E., Péault, B. M., Phinney, D. G., Hare, J. M., & Caplan, A. I. (2019, December 1). Mesenchymal stem cell perspective: cell biology to clinical progress. *Nature Partner Journals - Regenerative Medicine*. Nature Research. https://doi.org/10.1038/s41536-019-0083-6

2. Musiał-Wysocka, A., Kot, M., & Majka, M. (2019, July 1). The Pros and Cons of Mesenchymal Stem Cell-Based Therapies. *Cell Transplantation*. SAGE Publications Ltd. https://doi.org/10.1177/0963689719837897

3. Cao, X., Frenette, P. S., Mao, J. J., Robey, P. G., Simmons, P. J., Wang, C.-Y., & Bianco, P. (2013). The meaning, the sense and the significance: translating the science of mesenchymal stem cells into medicine. *Nature Medicine*, *19*(1). https://doi.org/10.1038/nm.3028

4. Kobolak, J., Dinnyes, A., Memic, A., Khademhosseini, A., & Mobasheri, A. (2016, April 15). Mesenchymal stem cells: Identification, phenotypic characterization, biological properties and potential for regenerative medicine through biomaterial micro-engineering of their niche. *Methods*. Academic Press Inc. https://doi.org/10.1016/j.ymeth.2015.09.016

5. Gomez-Salazar, M., Gonzalez-Galofre, Z. N., Casamitjana, J., Crisan, M., James, A. W., & Péault, B. (2020, February 28). Five Decades Later, Are Mesenchymal Stem Cells Still Relevant? *Frontiers in Bioengineering and Biotechnology*. Frontiers Media S.A. https://doi.org/10.3389/fbioe.2020.00148

6. Rennerfeldt, D. A., & Van Vliet, K. J. (2016). Concise Review: When Colonies Are Not Clones: Evidence and Implications of Intracolony Heterogeneity in Mesenchymal Stem Cells. *Stem Cells*, *34*(5), 1135–1141. https://doi.org/10.1002/stem.2296

7. Gao, Z.-W., Wang, H.-P., Lin, F., Wang, X., Long, M., Zhang, H.-Z., & Dong, K. (n.d.). CD73 promotes proliferation and migration of human cervical cancer cells independent of its enzyme activity. https://doi.org/10.1186/s12885-017-3128-5

8. de Oliveira Bravo, M., Carvalho, J. L., & Saldanha-Araujo, F. (n.d.). Adenosine production: a common path for mesenchymal stem-cell and regulatory T-cell-mediated immunosuppression. *Purinergic Signalling*. https://doi.org/10.1007/s11302-016-9529-0

9. Zhai, X., Chen, K., Yang, H., Li, B., Zhou, T., Wang, H., … Li, M. (2021). Extracellular vesicles derived from CD73 modified human umbilical cord mesenchymal stem cells ameliorate inflammation after spinal cord injury. *Journal of Nanobiotechnology*, *19*(1), 1–20. https://doi.org/10.1186/S12951-021-01022-Z/FIGURES/8

10. Lupia, M., Angiolini, F., Bertalot, G., Freddi, S., Sachsenmeier, K. F., Chisci, E., … Cavallaro, U. (2018). Stem Cell Reports Article CD73 Regulates Stemness and Epithelial-Mesenchymal Transition in Ovarian Cancer-Initiating Cells. https://doi.org/10.1016/j.stemcr.2018.02.009

11. Hu, Y., Kong, D., Qin, Y., Yu, D., Jin, W., Li, X., … Wang, H. (2021). CD73 expression is critical to therapeutic effects of human endometrial regenerative cells in inhibition of cardiac allograft rejection in mice. *STEM CELLS Translational Medicine*, *10*(3), 465–478. https://doi.org/10.1002/SCTM.20-0154

12. Minor, M., Alcedo, K. P., Battaglia, R. A., & Snider, N. T. (2019). Cell type- And tissue-specific functions of ecto-5=-nucleotidase (CD73). *American Journal of Physiology - Cell Physiology*, *317*(6), C1079–C1092. https://doi.org/10.1152/AJPCELL.00285.2019

13. Lv, F. J., Tuan, R. S., Cheung, K. M. C., & Leung, V. Y. L. (2014). Concise Review: The Surface Markers and Identity of Human Mesenchymal Stem Cells. *STEM CELLS*, *32*(6), 1408–1419. https://doi.org/10.1002/STEM.1681

14. Kimura, K., Breitbach, M., Schildberg, F. A., Hesse, M., & Fleischmann, B. K. (2021). Bone marrow CD73+ mesenchymal stem cells display increased stemness in vitro and promote fracture healing in vivo. *Bone Reports*, *15*, 101133. https://doi.org/10.1016/J.BONR.2021.101133

15. Suto, E. G., Mabuchi, Y., Toyota, S., Taguchi, M., Naraoka, Y., Itakura, N., … Akazawa, C. (2020). Advantage of fat-derived CD73 positive cells from multiple human tissues, prospective isolated mesenchymal stromal cells. *Scientific Reports 2020 10:1*, *10*(1), 1–9. https://doi.org/10.1038/s41598-020-72012-8

16. Tan, K., Zhu, H., Zhang, J., Ouyang, W., Tang, J., Zhang, Y., … Deng, X. (2019). CD73 expression on mesenchymal stem cells dictates the reparative properties via its anti-inflammatory activity. *Stem Cells International*, *2019*. https://doi.org/10.1155/2019/8717694

17. Ohnishi, S., Yasuda, T., Kitamura, S., & Nagaya, N. (2007). Effect of Hypoxia on Gene Expression of Bone Marrow-Derived Mesenchymal Stem Cells and Mononuclear Cells. *Stem Cells*, *25*(5), 1166–1177. https://doi.org/10.1634/stemcells.2006-0347

18. Zhou, T., Yuan, Z., Weng, J., Pei, D., Du, X., He, C., & Lai, P. (2021). Challenges and advances in clinical applications of mesenchymal stromal cells. *Journal of Hematology & Oncology 2021 14:1*, *14*(1), 1–24. https://doi.org/10.1186/S13045-021-01037-X

19. Gu, Y., Li, T., Ding, Y., Sun, L., Tu, T., Zhu, W., … Sun, X. (2016). Changes in mesenchymal stem cells following long-term culture in vitro. *Molecular Medicine Reports*, *13*(6), 5207–5215. https://doi.org/10.3892/mmr.2016.5169

20. Cicione, C., Muiños-López, E., Hermida-Gómez, T., Fuentes-Boquete, I., Díaz-Prado, S., & Blanco, F. J. (2013). Effects of Severe Hypoxia on Bone Marrow Mesenchymal Stem Cells Differentiation Potential. *Stem Cells International*, *2013*. https://doi.org/10.1155/2013/232896

21. Gao, F., Chiu, S. M., Motan, D. A. L., Zhang, Z., Chen, L., Ji, H.-L., … Lian, Q. (2016). Mesenchymal stem cells and immunomodulation: current status and future prospects. *Cell Death & Disease*, *7*(1), e2062. https://doi.org/10.1038/CDDIS.2015.327

22. Zhou, Y., Yamamoto, Y., Xiao, Z., & Ochiya, T. (2019). The Immunomodulatory Functions of Mesenchymal Stromal/Stem Cells Mediated via Paracrine Activity. *Journal of Clinical Medicine*, *8*(7), 1025. https://doi.org/10.3390/JCM8071025

23. Luo, T., von der Ohe, J., & Hass, R. (2021). MSC-Derived Extracellular Vesicles in Tumors and Therapy. *Cancers*, *13*(20). https://doi.org/10.3390/CANCERS13205212

24. Sun, S. J., Wei, R., Li, F., Liao, S. Y., & Tse, H. F. (2021). Mesenchymal stromal cell-derived exosomes in cardiac regeneration and repair. *Stem Cell Reports*, *16*(7), 1662–1673. https://doi.org/10.1016/J.STEMCR.2021.05.003

25. Xue, C., Li, X., Ba, L., Zhang, M., Yang, Y., Gao, Y., … Zhao, R. C. (2021). MSC-Derived Exosomes can Enhance the Angiogenesis of Human Brain MECs and Show Therapeutic Potential in a Mouse Model of Parkinson's Disease. *Aging and Disease*, *12*(5), 1211. https://doi.org/10.14336/AD.2020.1221

26. Phinney, D. G., & Pittenger, M. F. (2017). Concise Review: MSC-Derived Exosomes for Cell-Free Therapy. *STEM CELLS*, *35*(4), 851–858. https://doi.org/10.1002/STEM.2575

27. Parekkadan, B., & Milwid, J. M. (2010). Mesenchymal Stem Cells as Therapeutics. *Annual review of biomedical engineering*, *12*, 87. https://doi.org/10.1146/ANNUREV-BIOENG-070909-105309

28. Hare, J. M., Fishman, J. E., Gerstenblith, G., Velazquez, D. L. D., Zambrano, J. P., Suncion, V. Y., … Heldman, A. W. (2012). Comparison of Allogeneic vs Autologous Bone Marrow–Derived Mesenchymal Stem Cells Delivered by Transendocardial Injection in Patients With Ischemic Cardiomyopathy: The POSEIDON Randomized Trial. *JAMA*, *308*(22), 2369. https://doi.org/10.1001/JAMA.2012.25321

29. Butler, J., Epstein, S. E., Greene, S. J., Quyyumi, A. A., Sikora, S., Kim, R. J., … Gheorghiade, M. (2017). Intravenous Allogeneic Mesenchymal Stem Cells for Nonischemic Cardiomyopathy. *Circulation Research*, *120*(2), 332–340. https://doi.org/10.1161/CIRCRESAHA.116.309717

30. Bolli, R., Mitrani, R. D., Hare, J. M., Pepine, C. J., Perin, E. C., Willerson, J. T., … Simari, R. D. (2021). A Phase II study of autologous mesenchymal stromal cells and c-kit positive cardiac cells, alone or in combination, in patients with ischaemic heart failure: the CCTRN CONCERT-HF trial HHS Public Access. *Eur J Heart Fail*, *23*(4), 661–674. https://doi.org/10.1002/ejhf.2178

31. Orozco, L., Munar, A., Soler, R., Alberca, M., Soler, F., Huguet, M., … García-Sancho, J. (2014). Treatment of knee osteoarthritis with autologous mesenchymal stem cells: Two-year follow-up results. *Transplantation*, *97*(11). https://doi.org/10.1097/TP.0000000000000167

32. Vilela, C. A. P., Messias, A., Calado, R. T., Siqueira, R. C., Silva, M. J. L., Covas, D. T., & Paula, J. S. (2021). Retinal function after intravitreal injection of autologous bone marrow-derived mesenchymal stromal cells in advanced glaucoma. *Documenta Ophthalmologica 2021 143:1*, *143*(1), 33–38. https://doi.org/10.1007/S10633-021-09817-Z

33. Costa, L. A., Eiro, N., María Fraile, ·, Luis, ·, Gonzalez, O., Saá, J., … Vizoso, F. J. (2021). Functional heterogeneity of mesenchymal stem cells from natural niches to culture conditions:

implications for further clinical uses. *Cellular and Molecular Life Sciences*, *78*, 447–467. https://doi.org/10.1007/s00018-020-03600-0

34. Zhou, Y., Chen, H., Li, H., & Wu, Y. (2017). 3D culture increases pluripotent gene expression in mesenchymal stem cells through relaxation of cytoskeleton tension. *Journal of Cellular and Molecular Medicine*, *21*(6), 1073–1084. https://doi.org/10.1111/jcmm.12946

35. Marshall, J., Barnes, A., & Genever, P. (2018). Analysis of the intrinsic self-organising properties of mesenchymal stromal cells in three-dimensional co-culture models with endothelial cells. *Bioengineering*, *5*(4). https://doi.org/10.3390/bioengineering5040092

36. Kudva, A. K., Luyten, F. P., & Patterson, J. (2017). Initiating human articular chondrocyte re-differentiation in a 3D system after 2D expansion. *Journal of materials science. Materials in medicine*, *28*(10), 156. https://doi.org/10.1007/s10856-017-5968-6

37. Foster, N. C., Henstock, J. R., Reinwald, Y., & El Haj, A. J. (2015). Dynamic 3D culture: Models of chondrogenesis and endochondral ossification. *Birth Defects Research Part C: Embryo Today: Reviews*, *105*(1), 19–33. https://doi.org/10.1002/bdrc.21088

38. Caires, H. R., Barros da Silva, P., Barbosa, M. A., & Almeida, C. R. (2018). A co-culture system with three different primary human cell populations reveals that biomaterials and MSC modulate macrophage-driven fibroblast recruitment. *Journal of Tissue Engineering and Regenerative Medicine*, *12*(3), e1433–e1440. https://doi.org/10.1002/term.2560

CHAPTER 2: CHARACTERIZATION OF MECHANICS-DRIVEN HETEROGENEITY IN MESENCHYMAL STROMAL CELLS

Background

Autologous MSC therapies require a bone marrow aspirate from the patient. However, of the bone marrow mononuclear cells harvested, only 0.001% to 0.01% of the cell population comprises true MSCs [1]. To enrich the MSC content of the bone marrow aspirate, the cells are processed through density gradient centrifugation followed by direct plating [2]. Cells are deemed as MSC when they form the fibroblast colony-forming units (CFU-F) after plastic adherence [3]. Under these practices, only around 700 CFU-F/ml bone marrow aspirate can be collected [4], which is too small in comparison to the number of cells needed for therapeutic purposes, so expansion to millions of cells is required. For reference, between 8 and 20 million cells are required in the treatment of chondral defects using matrix-induced autologous implantation with MSCs [5, 6], and for MSC therapies a dose of roughly about 100 million cells/70 kg are required to treat a patient if injected directly in the bloodstream [7].

The release criteria for MSCs are variable in clinical trial reports and is not standardized or required by regulatory agencies such as FDA. It was reported that only 53.6% of clinical trials examined the specific cell markers in the cell population, with the assessment of functionality being very limited, sometimes falling short of the minimum suggestions by the International Society of Cell Therapy to ensure a population of MSCs [8, 9]. Due to these inconsistencies, the cell population is not homogeneous at the outset of *in vitro* expansion, where other factors, such as seeding density, start to have an impact on the cells' functional potential [10]. Subsequently, the *in vitro* expansion process to obtain such large numbers of cells becomes compromised by the

gradual differentiation of MSC into an increasingly larger population of osteoprogenitor-like cells (non-MSC) that do not retain the MSC-specific attributes, thus making the population heterogeneous. Even a small subpopulation of these "non-MSCs", straying from the spindle-shaped population that generally represents multipotent cells [10], affects the population level functionality, limiting the therapeutic benefits at the clinical endpoint. Even when a cell population is established from a single MSC clone isolated in the culture, these cultures still become heterogeneous [11]. This reduced potential and increased heterogeneity can be attributed to the *in vitro* expansion on plastic as well as their response to the post-transplantation fibrotic environment. In the context of MSC culture, expansion, and delivery in tissues, a key notable factor is that the mechanical environment on plastic or inside the fibrotic tissues is quite different from the natural soft niche experienced by MSC in vivo [12].

Heterogeneity in MSC Phenotype

The heterogeneity of MSCs refers to various aspects such as proliferation rate, cell morphology (Figure 3) [13], and cellular aging markers [14, 15]. MSCs are composed of slow and fast dividing subpopulations, which is demonstrated by different colony sizes from an individual clone. Even within a colony, MSCs usually have a heterogeneous cellular morphology and growth pattern within a colony, i.e. spindle shape, round, tightly packed, or dispersed. The number of cell divisions is limited for all somatic cells in culture, with the cell division history being

heterogeneous since cell divisions are not synchronized. This is just one component that influences the increased cell population heterogeneity during *in vitro* culture expansion.

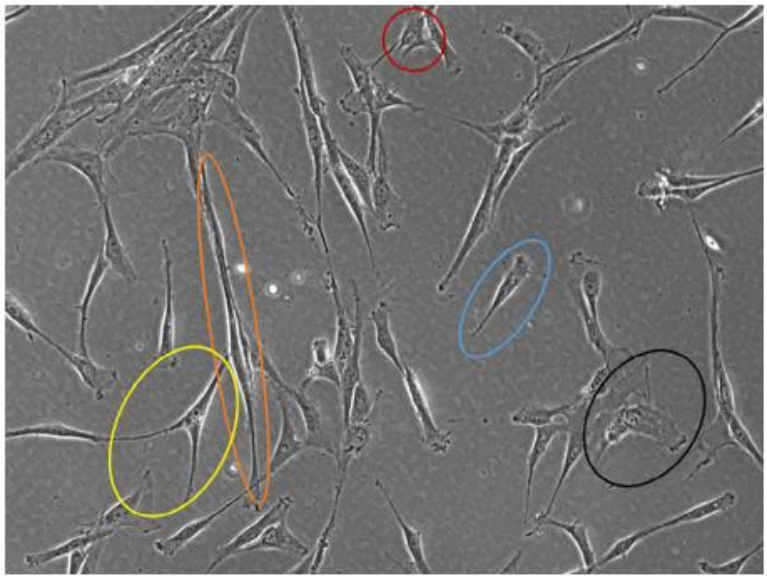

Figure 3. Heterogeneity of the MSC phenotype. There are tri-polar shapes (yellow), long spindle-shaped cells (orange), small round cells (red), short spindle-shaped cells (blue), and flattened enlarged cells (black). Contrast Ph1 ×100 magnification, observer A1 (Zeiss). Adapted from Mastrolia et al.

Donor Specific Variability in MSC

MSC can also have variability based on their donor. Mastrolia et al. summarized a study performed in a rat model that revealed the superiority of female MSCs in reducing lung inflammation compared to male MSCs. This gender variability was confirmed in another study for adipose-derived MSCs which showed increased adipogenic differentiation in cells harvested from female mice compared to male mice [13]. In addition, age is also a factor, with MSCs isolated from older donors showing altered compositions and functions of membrane glycerophospholipids, which affect MSCs' ability to migrate, home, and engraft into a site of injury [16].

C. Sun et al (2020) [17] investigate the gene expression profile of human primary Wharton's jelly MSCs from three donors cultured *in vitro* using single-cell RNA sequencing.

Figure 4A shows that the cells from all three donors were mostly proliferative. Upon principle component analysis (Figure 4B) it was shown that PC1, cell cycle effect, accounted for most of the variance compared to PC2, donor-to-donor variation. To remove these effects, the group performed cell cluster analysis and identified six candidate clusters (C0-C5). Differentially expressed gene analysis was performed amongst those clusters. The results across clusters varied greatly demonstrating just how heterogeneous a population of MSCs can be even upon selective clustering into subpopulations [17].

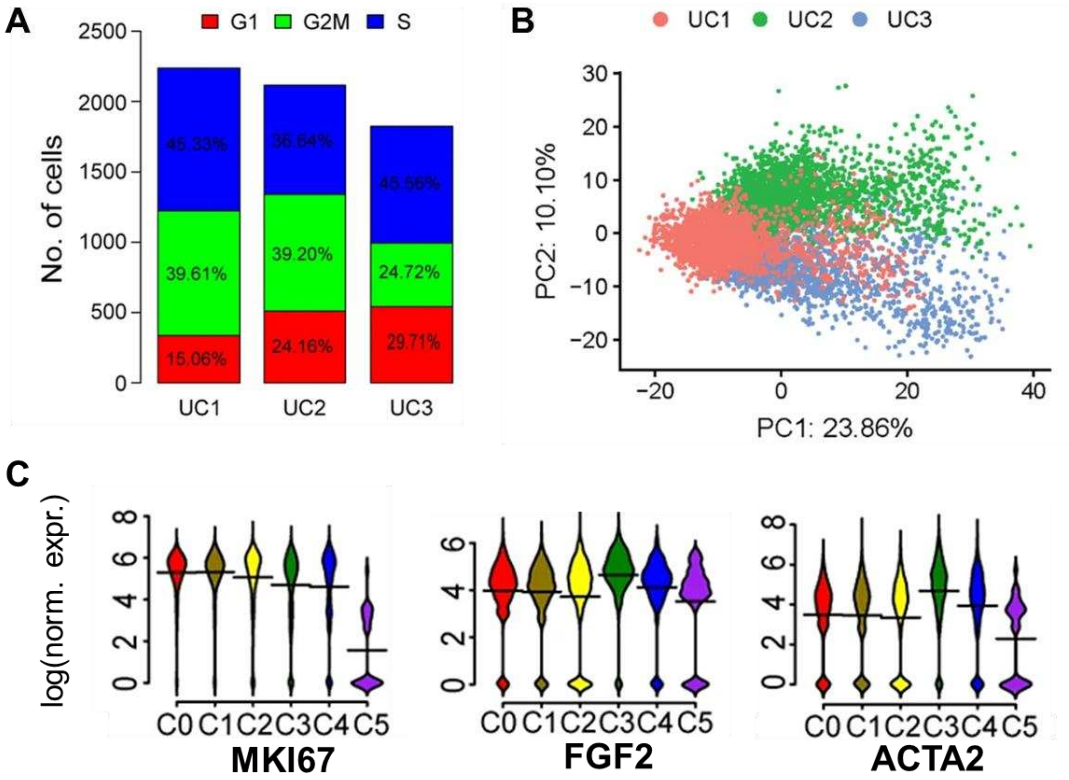

Figure 4. Single cell RNA-seq data reveals significant heterogeneity from a single tissue source across donors. (A) The percent of cells assigned to each cell cycle phase was varied for each of the three umbilical cord (UC) samples. (B) Cell cycle effects represent the dominant source of heterogeneity in primary cultured Wharton's jelly MSC population. (C) Bean plots showing the expression of three representative DEGs among the six subpopulations. MKI67 is associated with proliferation, FGF2 is critical for stem cell maintenance, and ACTA2 is involved in stem cell migration. Adapted from C. Sun et al (2020).

Tissue-Specific Variability in MSC

Nguyen et al. [18] characterized and compared MSCs collected from the bone marrow, acetabular subchondral bone, and trabecular bone on the femoral head. The cells from the three sources showed a fibroblast-like phenotype and were able to differentiate into osteoblasts, chondrocytes, and adipocytes. However, the cells from the different sources displayed varied differentiation potentials (Figure 5A). Under osteogenic differentiation conditions, the cells from the acetabulum had the lowest accumulation of calcium deposit while cells from the bone marrow and femur showed a significantly increased amount of calcium deposit. In chondrogenic and adipogenic conditions, bone marrow cells possessed a predominant differentiation capacity compared with the other cell types [18]. Interestingly, cells from acetabulum had significantly higher proliferation comparatively, yet differentiation capacity was moderate (Figure 5B, C). Conversely, bone marrow-derived MSCs had the highest differentiation capacity yet the lowest proliferation. The final results clearly demonstrated that the anatomical site from the same donor influences the multipotent potential of MSCs.

Wagner et al. [19] analyzed global gene expression profiles of human MSCs isolated from different tissues, bone marrow, adipose, and umbilical cord, and compared them to terminally differentiated human fibroblasts. No phenotypic differences were observed by flow cytometry and, interestingly, MSCs derived from different donors using the same procedure resulted in a consistent and reproducible gene expression profile. Yet, MSCs from various sources or using different culture conditions yielded genes that were differentially expressed [19]. The MSCs from the same tissue type, just different locations showed heterogeneity and differences in cell lineage differentiation that may indicate variations in cell commitment [18].

MSC heterogeneity reduces clinical effectiveness and translation because the maximum effectiveness is reduced [20], and could also partially explain the lack of reproducibility of some initial reports [19]. Establishing standards or methods to bring the MSC population to a homogeneous state and maintain that homogeneity could have significant impacts on the success of MSC therapies and clinical trials.

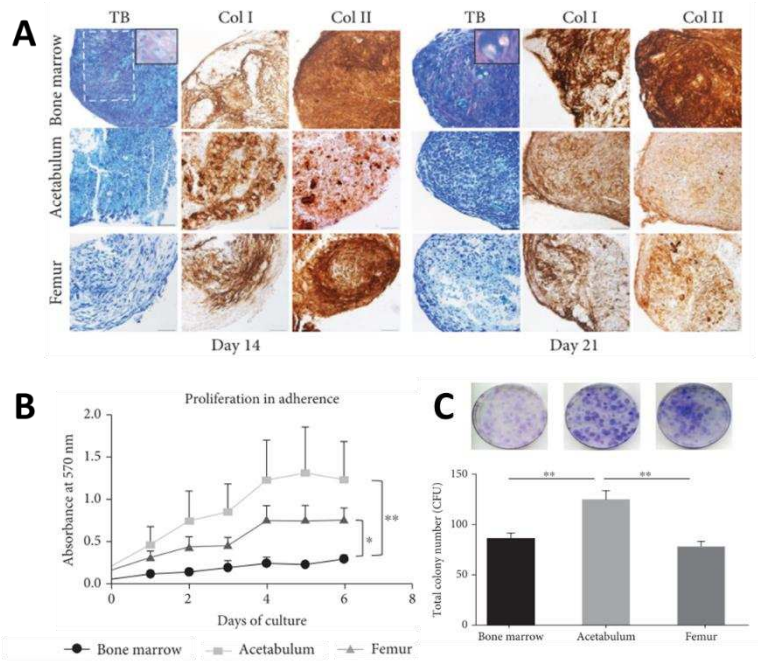

Figure 5. Source variability is a significant factor to consider. Each source has significantly different differentiation capability, proliferation, and colony formation. (A) Images of toluidine blue O (TB) stain and immunohistochemistry for collagen type I (Col I) and collagen type II (Col II). The white dash line covers the most violet zone on the photo, showing the coloration of the more intensified cartilage matrix. The brown color indicates the expression of Col I and II. Scale bar: insets 5 µm, others 25 µm. (B) Proliferation curve of the cells in adherent culture was determined by measuring the absorbance of cells stained with crystal violet at 570 nm wavelength. *p = 0.0146, **p = 0.0076. (C) Cell colonies stained with crystal violet solution after plating for 14 days, showing a 1.5- and 1.6-fold increase in the cells derived from the acetabulum compared with cells from the bone marrow and femur respectively. **p<0.006. Adapted from Nguyen et al. (2019).

MSC Mechanosensing Effects on Heterogeneity

The substrate or the extracellular matrix mechanics of the cell affect the structure and mechanics of the cytoskeleton and the nucleus [21], which can have far-reaching impacts through gene expression and cell function, as shown in many cell types including MSC. Cells exert contractile forces on their culture substrate and the substrate elasticity can alter the migration behavior of endothelial cells, promoting the formation of cell-cell interactions [22] through integrins that transmit these mechanical signals via actin stress fibers and associated pathways [23]. Smith et al. reports that MSCs cultured on substrates that mimic the elasticity of their respective environment expressed those corresponding markers, and subsequently when their myosin-II- based mechanical interactions with the matrix were inhibited, genes that indicated lineage specification were no longer expressed. The mechanical signal from the substrate elasticity can be relayed through the LINC (Link of Nucleoskeleton and Cytoskeleton) complex to the nucleus to trigger differential gene regulation pathways through epigenetic regulations [24] or the engagement of transcriptional coactivators such as YAP (Yes-associated protein) and Transcriptional Co-Activator TAZ [23, 25].

The Role of YAP/TAZ in MSC Mechanosensing

Recent studies have expanded the understanding of a cell's ability to sense its physical surroundings and respond to these stimuli to initiate the activation of intracellular signaling pathways that trigger downstream events. One of the most extensively studied mechanosensors in mammals is YAP and TAZ. YAP/TAZ regulates key biological processes such as cell proliferation and migration, differentiation, and cell morphology [26] requiring Rho GTPase activity and tension exerted by the actomyosin contraction [27]. They shuttle between the cytosol and nucleus

to regulate the target gene expression, being key mediators of cellular response to mechanical stimuli such as cell density, cell attachment area, shear forces, and substrate stiffness [28–30]. During the specification of MSC fate, YAP/TAZ can act as a molecular rheostat that modulates MSC differentiation [31]. On stiff substrates where the cells experience higher intracellular strain, YAP localizes to the nucleus and interacts with the transcription factor Runt-related transcription factor 2 (Runx2). Runx2 is the master gene of osteogenic differentiation [32], instructing the cells to follow an osteogenic lineage which may potentially cause a heterogeneous shape and size distribution due to the deviation of the population away from the MSC phenotype. Conversely, on soft substrates, there is lower intracellular strain and cytoskeletal F-actin formation, and accordingly, MSCs favor MSC homeostasis, accompanied by down-regulation of Runx2 [33] and a more uniform cell shape and size [21]. This ability of MSCs to perceive stiffness and subsequently alter their phenotype can be influenced by cell seeding density as well. Contracting cells are known to transmit stress to neighboring cells over distances of tens of micrometers away, with substrate stiffness being a key determinant in the ability of cells to mechanically communicate [34]. Cell seeding density can have a key role in the ability to transmit stresses through the substrate and cause changes in cell morphology, as shown in the migration of endothelial cells [22]. Cells that are seeded at a low density are known to show impaired proliferation or accelerated senescence in MSC. Therefore, understanding the mechanical interaction of cell clusters through substrate could be relevant to the MSC mechanosensitive response, population heterogeneity and function. As cells replicate, differentiate, or senesce; measurable changes occur in the cell phenotype such as their size or the mechanical stiffness and these characteristics may serve as indicators of cell fate. Lee et al. (2014) examined multivariate biophysical markers and their potential to predict MSC multipotency and determined that a combination of small nucleus diameter, low cell

stiffness, low F-actin content, and high nuclear fluctuations suggestive of an open chromatin architecture, are indicative of undifferentiated subpopulations in culture-expanded MSCs [35]. During longer *in vitro* expansion, MSC nuclei became larger and the cell shape becomes wider and flatter with increasing morphological alterations [36, 37]. These phenotype changes are indicative of an osteoprogenitor population, rather than a population of MSCs. Understanding the mechanisms of how the non-MSC subpopulation originates throughout *in vitro* culture can provide us with the 'pre-treatment' strategies to intervene in the mechanisms to obtain a high-quality, homogeneous MSC population suitable for MSC-based tissue engineering/ regenerative medicine applications.

In this study, we developed a technique to quantify the MSC population heterogeneity for investigating the mechanism of how the mechanical stiffness of the environment and the cell-cell mechanical communication through the growth substrate leads to a more heterogeneous population from undifferentiated MSCs. We hypothesize that neighboring cells communicate through the compliant substrate, promoting a homogeneous population of cells with the MSC phenotype. To test this hypothesis, using human bone marrow-derived primary MSC, we examined how substrate mechanics in combination with seeding density determines the MSC cell and nuclear phenotype over multiple passages, through high-resolution imaging of the nucleus and the cytoskeleton. The functional meaning of population-level MSC heterogeneity was assessed through the imaging of a stemness marker and Runx2. Knowledge of the mechanisms to maintain a homogeneous MSC population in two-dimensional culture can provide future intervention strategies to gain more control over MSC during their longer-term expansion in the clinical setting without requiring a specialized bioreactor system.

Materials and Methods

MSC culture

Passage 2 primary human bone marrow-derived MSC (PT-2501) were purchased from Lonza for all the experiments. These cells are a mixed population of cells derived from the bone marrow of healthy adult individuals. Cells were maintained in bulletkit (Lonza) growth medium kit consisting of the MSC Basal medium (PT-3238) and the supplemental kit (PT-4105) as stated in the manufacturer's protocol. The culture condition was 5% CO2, 37°C temperature and 90% relative humidity. For all the experiments, cells were seeded in a 75 cm^2 T-flask and passaged at 90% confluency at 5000 cells/ cm^2, unless stated otherwise whereas in some cases cells were seeded at a higher or lower density. Trypsin-EDTA (0.05%) was used for subculturing. The medium was replenished every 3 days. Subsequently, passage 3 and 4 cells were used for all the experiments except for the cell treatment with the cytoskeleton modifying drug group where passage 5 cells were used. For all experiments, cells were directly seeded on the substrate after thawing the cells previously stored in a liquid nitrogen tank.

MSC culture on substrates with varying mechanical stiffness and cell density

Three substrate stiffness groups were prepared for cell culture. Soft: Sylgard 527 PDMS (*E*~5 kPa), medium stiffness: Sylgard 184 PDMS (*E*~1 MPa) ,and stiff: polymer resembling cell culture plastic (*E*~1 GPa). Those mechanical stiffness conditions represent the physiological bone marrow stiffness, pathological fibrotic condition, and the standard T flask cell culture condition respectively. Cells were cultured on 8 well chamber slides (ibidi, 80821) with thin bottom for high-resolution imaging using a confocal microscope. For the stiff group, untreated polymer bottom slides were used followed by bovine Type 1 collagen coating (50 µg/ml, A10644-01, Gibco). For

the soft and medium stiffness groups, the bottom polymer coverslip was removed, and custom-made chamber slides were refabricated with a thin PDMS substrate as described in the next section. For the baseline cases, 5000 cells/cm^2 cell density was used. To understand the effect of cell density on the MSC heterogeneity 100, 1000, and 10000 cells/ cm^2 were used in addition to the 5000 cells/ cm^2 group.

Preparation of thin PDMS substrate

Polydimethylsiloxane (PDMS) substrates were prepared using Sylgard 527 and Sylgard 184 (Dow Corning). To fabricate the thin soft PDMS substrate (~ 5 kPa), Sylgard 527 was mixed at a 1:1 ratio of each solution provided by the manufacturer. The mixture was then placed in a water bath at 37°C for 20-30 minutes to begin the curing process. Sylgard 184 thin PDMS sample was prepared by mixing ten parts of base with one part of curing agent and vigorous mixing. A small amount of each mixture (~70 µl) was distributed across a glass coverslip (24x60 mm). The glass coverslips were then placed in a vacuum chamber for 20 minutes to remove any bubbles. For attachment of the coverslip to the bottomless chamber slide (ibidi, 80821), the coverslip was partially cured for 2 hours at 75°C and Sylgard 184 (10:1 mixture) was used to mount the coverslip to the chamber slide. To completely cure, it was placed in a 75°C oven overnight. Cured PDMS was then plasma treated (BD-20AC, Electro-Technic) to facilitate the collagen coating. Then they were sterilized in the cell culture cabinet with a 70% ethanol soak under UV light for 20 minutes, followed by incubation in a type I collagen coating (50 µg/ml, A10644-01, Gibco) for 1 hour to improve cell attachment and proliferation. The stiff group with polymer bottom was also treated with the plasma and the same type I collagen solution to maintain the same biochemical treatment

between the groups. Cells were seeded on these prepared substrates and cultured with the previously stated culture condition.

Cell Staining for immunofluorescence, actin, and DNA

For all imaging tasks, cells were fixed with 4% PFA (in 1X PBS: Phosphate Buffer Solution) for 10 minutes at room temperature. Cells were permeabilized with 0.1% Triton X-100 in 1X PBS, washed with 1X PBS, and blocked for the non-specific binding sites with bovine serum albumin and normal goat serum. Primary antibodies for CD73 (41-0200) and Runx2 (PA5-82787) were then diluted at 1:100 in antibody dilution buffer and incubated overnight at 4°C. Next, secondary antibodies (A32731, A32727) were applied at 1:200 dilution at room temperature for 2 hours. All antibodies were purchased from ThermoFisher Scientific. Then, cells were stained for the DNA using DAPI (ThermoFisher Scientific) and for the F-actin, using phalloidin conjugated with a fluorescent protein (ThermoFisher Scientific). Cells were imaged across their midsection using a confocal microscope (Zeiss LSM 980). Cells were imaged either at high resolution with 20X air objective or at low resolution with 10X air objective for all subsequent analyses. For all imaging, the imaging setting (laser power, gain, etc.) was maintained constant between the groups. For the low-resolution imaging, the tile mode of imaging was used to image the complete surface area so that analysis could be performed to derive population-level parameters in order to obtain a robust quantification of heterogeneity.

Quantification of cell and nuclear morphology and stress fiber formation

Cell area and actin stress fiber quantification: To assess the amount of stress fiber in the cytoskeleton, the high-resolution GFP-phalloidin stained images were used. Stress fiber intensity

quantification was performed using a custom MATLAB code (Figure S1). Briefly, the code finds the local maximum and minimum of the actin intensity and calculate that ratio as a measure of stress fiber formation. The same code was used to calculate the cell area. The cytoskeleton phenotype was not analyzed as a function of cell density effect due to technical limitations in identifying individual cells at the high seeding density.

Nuclear area and other geometrical parameters calculation: nuclear morphology quantification was performed on the tiled images of the entire growth surface for robust image analysis. Images were binarized and watershed separation was applied to separate cells that were touching or very close using ImageJ. These images were then imported into MATLAB. Subsequently, disk structuring elements were created through the strel() function, to create masks over each identified nucleus, which were then smoothed and filled to create a solid element. The size filtering for the nucleus images was critical to avoid any small background particles that may remain or any nuclei that were not separated by the watershed function. The final allowable elements were labeled for later reference and then measured with the regionprops() function to calculate the nucleus area and circularity.

Quantification of chromatin architecture

To calculate chromatin segregation from the DAPI stained nucleus images, a technique was adapted from a previous approach described by Irianto et al. [38]. The high-resolution images of nuclei were cropped and apportioned into images of individual nuclei. To calculate the chromatin segregation index based on the DAPI stain, the gradient-based Sobel edge detection algorithm produced an edge map, then a thinning algorithm reduced strong border edge lines so they could

be excluded. Next, the edge areas were measured, and this value was divided by the cross-sectional area of the nucleus.

Quantification of immunofluorescence images

For quantification of CD73 and Runx2 protein fluorescence, 20x images of cells stained for DAPI, actin, CD73, and Runx2 were imaged together. ImageJ was used for measuring the intensity values for each channel. Briefly, in the Runx2 channel, cells were randomly chosen throughout the well, and the cell and nucleus shapes were outlined and added as a region of interest (ROI). The mean intensity was then calculated by Image J for the nucleus in the Runx2 channel and the cell shape ROI was added to the CD73 channel where that mean intensity was measured. Then, the nucleus image was subtracted from the cell image to obtain an ROI of the cell excluding the nucleus area. This new ROI was opened in the Runx2 channel where the cytoplasmic Runx2 mean intensity was calculated. The Runx2 mean intensity within the nucleus and the cytoplasm respectively were divided to obtain a ratio of nuclear Runx2 over cytoplasmic Runx2 mean intensity.

Quantification of heterogeneity

Heterogeneity of the quantified parameters such as cell and nuclear geometrical phenotype was evaluated using a common measure of dispersion, the interquartile range (IQR) (quartile 3 - quartile 1). IQR as a measure of dispersion can be beneficial for quantifying the biological data specifically due to the irregularity that can occur between biological replicates. The usual drawback for IQR is that only a subset of the data points is accounted for. However, performing regression deletion diagnostics revealed that each linear model, even after a log transform, contains several influential outliers within our datasets. Using IQR as a measure of data dispersion reduces

the effects of these extreme values [39]. Concurrently, a large consideration for other measures of dispersion is the distribution of the data, with a normal distribution being a prerequisite for proper representation. Visualization of the density plots of the data (Figure S2-5) revealed that our data has a variety of skewed distributions, however, IQR is not tied to the symmetry or distribution of the data, unlike standard deviation which would lose its effectiveness [40].

Cell treatments with cytoskeleton, YAP, and Runx2 modifying drugs

To understand the role of mechanical integrity of the cytoskeleton on the chromatin architecture and the nuclear phenotype, cytochalasin D (ThermoFisher Scientific) at a concentration of 0.02 µM or 0.05 µM and Y27632 (Tocris Biosciences) at concentrations of 2 µM or 10 µM were applied to P5 cells 24 hours after seeding. All the control groups for these experiments were vehicle-treated (DMSO). Cells were then fixed after 2 days of treatment, for subsequent staining and imaging. The combination drug treatments combine the two lowest concentrations of Cytochalasin D (0.02 µM) and Y27632 (2 µM) together. Separately, P4 cells were treated with either Y27632 (4 µM) or Verteporfin (2 µM) to inhibit cytoplasmic YAP or CADD522 (2 µM) to inhibit Runx2.

Statistical Analysis

Statistical analysis was performed using Student's t-test (RStudio [41–43]). Results are expressed as mean ± standard deviation, with differences considered statistically significant at $p < 0.05$ or $p < 0.01$, as specified in the figure legends. Sample and replicate numbers are provided in the figure legends.

Results

Soft substrates promote a more homogeneous population of cell phenotype over passaging

MSC phenotype is known to be affected by the substrate mechanical stiffness. We investigated how the quantitative measures of the cell phenotype and their heterogeneity are affected by a wide range of stiffness representing the physiologically healthy bone marrow (soft), pathological fibrotic tissue (medium), and tissue culture substrate (stiff) (Figure 6, Figure A2.A). Passage 3 (P3) MSCs were cultured to 90% confluency and subcultured to passage 4 (P4) to quantify how the mechanics of the substrate affects the heterogeneity in the cell area and the F-actin intensity over one passaging. It was observed that on stiff substrates, the cell area was higher, and the cells were flatter, whereas the cells grown on the medium and soft substrates better maintained a smaller cell area and spindle-like shape, characteristics of MSC (Figure 6A).

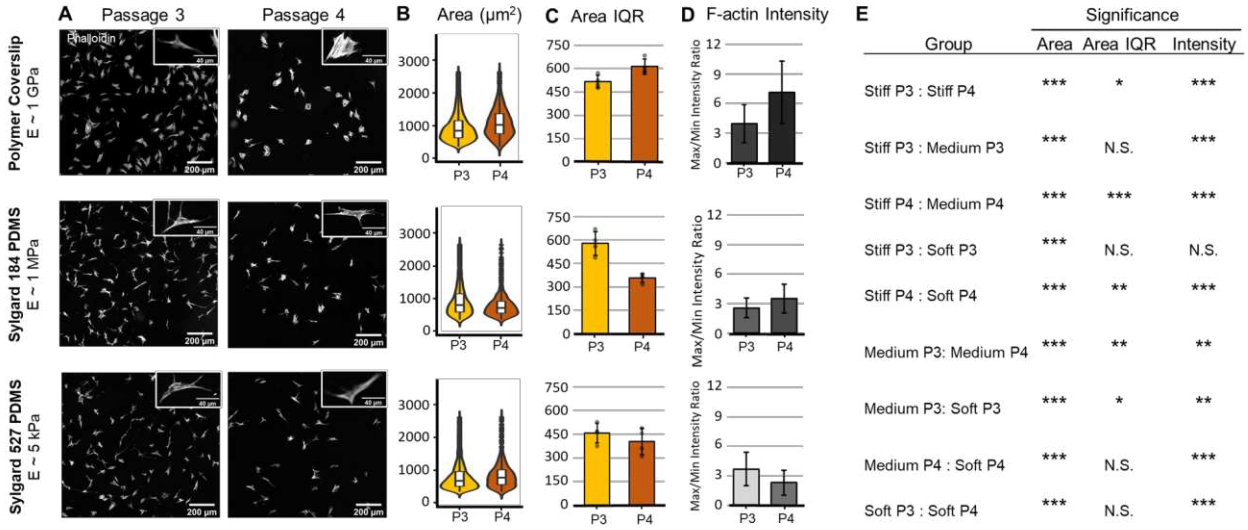

Figure 6. Effect of substrate stiffness on human BM-MSC cytoskeleton phenotype over one passage. (A) Representative images of F-actin staining over one passage on substrates with varying stiffnesses. (B) Violin plots to show the complete distribution of the data with embedded boxplot (n = 1000 cells) for cell area. (C) Quantification of the interquartile range (IQR) of the parameter cell area from 4 technical replicates to represent the heterogeneity of the MSC population. (D) F-actin intensity quantification of MSCs cultured on PDMS substrates in passage 3 (P3) and passage 4 (P4) (n ~ 30 cells). (E) Table of p-values for various comparisons in each quantity. Stiff = 1 GPa,

medium = 1 MPa, soft = 5 kPa. Error bars represent ± SD. N.S. (Not Significant): $p>0.05$, *$p<0.05$, **$p<0.01$, ***$p<0.001$.

Quantification of these observations revealed that there was significant spreading on the stiff substrate over one passage, with the cells on the soft and medium substrates remaining significantly smaller than the cells on the stiff substrate even after one passage (Figure 6 B, E). As an indicator of MSC population heterogeneity, the interquartile range (IQR) of the area measurements was calculated (Figure 6C). The IQR values indicated that the soft and medium substrate significantly reduced the variation of cell area over one passage when compared to cells grown on stiff substrates (Figure 6C, E). The IQR values further revealed that the medium substrate homogenized the cell area over one passage, while the stiff substrate cell area became more heterogeneous, whereas on the soft substrate the heterogeneity remained low over one passage. Another observation from high-resolution imaging was the increasing intensity of the phalloidin (F-actin) stain over passaging on stiff substrates (Figure 6A, *top right inset image*). The intensity ratio of the F-actin significantly increased from P3 to P4 in the stiff and medium groups, but significantly decreased on the soft substrate (Figure 6D, E). Collectively, the IQR of cell area and the relative F-actin intensity indicate that the MSC phenotype was less heterogeneous on the softer substrate over one passaging.

Soft substrates promote a more homogeneous nuclear phenotype over passaging

After the investigation of cell area and cytoskeleton structure, we examined the effect of substrate stiffness on the nucleus phenotype over passaging (Figure 7, Figure A2.B). Differences in size and shape were observed from P3 to P4 on the various substrates (Figure 7A). Upon quantification of nuclear area and circularity (Figure 7B, F), we found that the nuclei for cells on the medium and stiff substrates became significantly larger in area and more rounded (circularity values closer to

1) after one passage thus indicating a deviation from MSC phenotype. On the soft substrate in P3, nuclei were significantly smaller and more elongated, which was maintained in P4 (Figure 7B, F). Subsequently, the IQR of nucleus area and circularity was examined, again, as an indicator of the heterogeneity of the MSC population phenotype at the nuclear level. IQR values increased for nucleus area and circularity on the medium and stiff substrate but decreased on the soft substrate (Figure 7D, F) over one passage. Therefore, the MSC nuclear phenotype was maintained on the soft substrate over one passage.

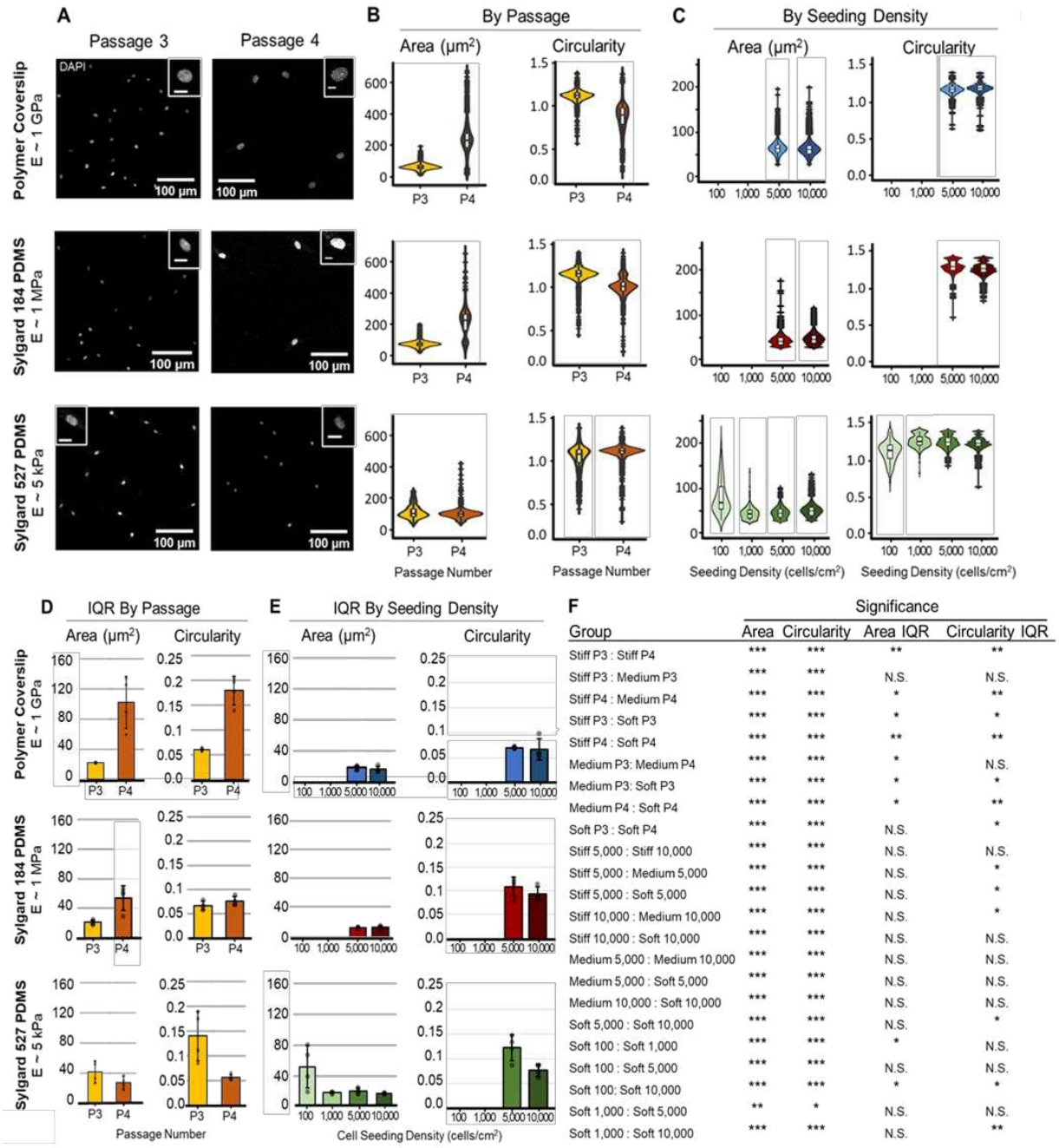

Figure 7. Effect of substrate stiffness and cell seeding density on human BM-MSC nucleus phenotype. (A) Representative images of DAPI stained MSCs over a single passage seeded at 5,000 cells/cm^2. Inset scale bar: 10 µm. (B) Nucleus area and circularity quantification over one passage seeded at 5,000 cells/cm^2, visualized with violin plots to show the complete distribution of the data with embedded boxplot (n = 1000 cells). Circularity is a measure of elongation with 1 representing a perfect circle and an increasing deviation from 1 representing a more elongated shape. (C) Nucleus area and circularity quantification in passage 4 cells with varied seeding densities (n = 1000). (D, E) Quantification of the interquartile range (IQR) of the nucleus area and circularity based on 4 technical replicates to represent the heterogeneity of the MSC population.

(F) Table of comparisons and the corresponding p-value. Error bars represent ± SD. N.S. (Not Significant): $p>0.05$, $*p<0.05$, $**p<0.01$, $***p<0.001$.

Seeding density has little impact on nucleus phenotype, but significantly affects chromatin organization

After determining the effect of substrate stiffness and passaging on MSC cell and nuclear phenotype, we wanted to examine their influence in conjunction with seeding density to explore the effect of substrate-mediated cell communication on the nucleus phenotype (Figure 7, A3). P4 cells were seeded on the stiff, medium, or soft substrates at increasing seeding densities, and the nucleus phenotype was analyzed. Cells grown at 5,000 and 10,000 cells/cm^2 had the smallest area on the soft substrate and were more elongated on the soft and medium substrates compared to the stiff substrate (Figure 7C, F). The IQR values at these higher seeding densities for nucleus area and circularity were largely unaffected by differences in seeding density. A wider array of seeding densities was tested on the soft substrate to explore the limits of cell communication through the compliant substrate. At the sparse seeding density of 100 cells/cm^2, the shape of the nucleus varied widely in area and circularity (Figure 7C). This was corroborated by the significantly large IQR values for this low seeding density, representing higher phenotypic heterogeneity (Figure 7E, F). Taken together, these results indicate that substrate stiffness and not the seeding density is the most influential factor in maintaining a homogeneous MSC population.

Chromatin architecture and organization are closely correlated to the MSC phenotype and function, as demonstrated in previous studies [44]. To understand the effect of substrate stiffness and cell seeding density on chromatin organization, we quantified the percentage of chromatin segregation. A larger percentage of segregated chromatin represents an open chromatin architecture – a hallmark of MSC. As the substrate became softer, the chromatin became

significantly more segregated (Figure 8A), with a similarly significant effect seen as the seeding density became higher. Of note, the stiff substrate, as well as low seeding densities on soft substrate, resulted in a diffused chromatin architecture with low chromatin segregation (Figure 8C). Concurrently, examining the IQR values of the chromatin segregation index showed a foreseeable pattern, that more chromatin segregation led to a larger IQR value (Figure 8B), representing a population of MSC with higher differentiation potential. These findings show that cell communication along with a higher seeding density through a soft substrate leads to a significantly open chromatin architecture.

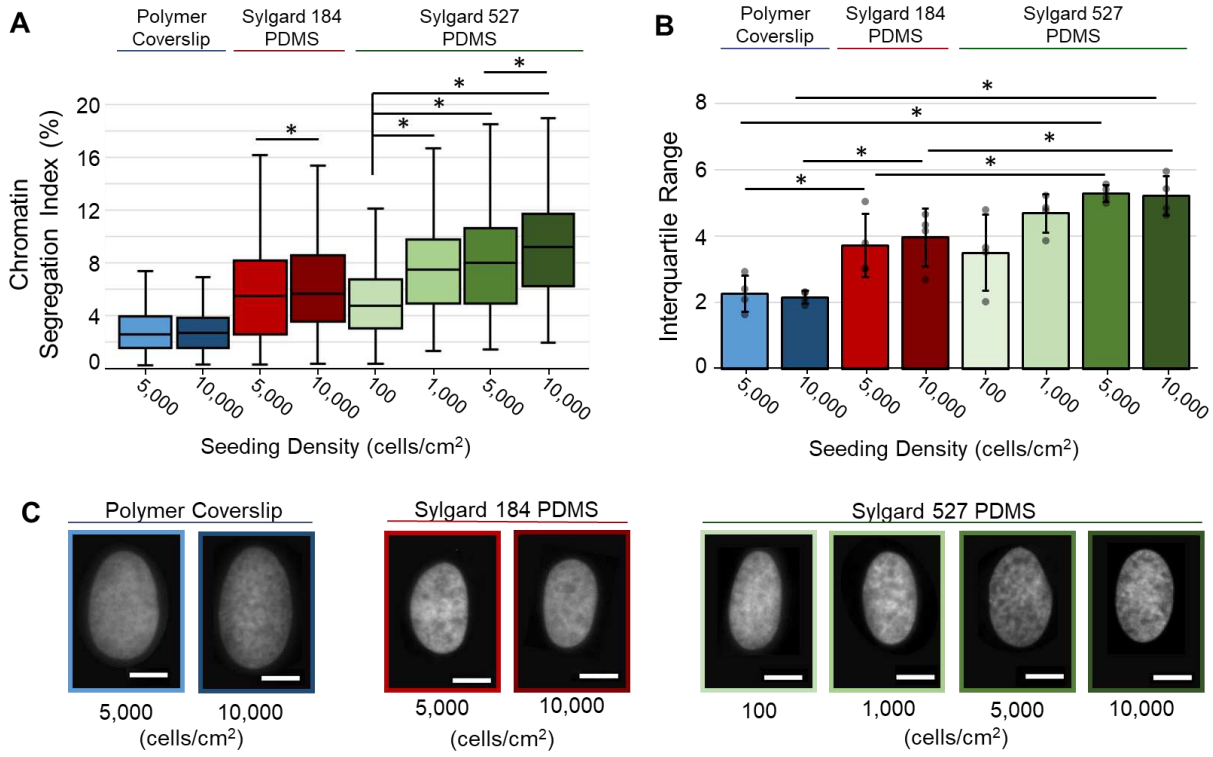

Figure 8. Effect of cell seeding density in combination with substrate stiffness on the chromatin architecture of hMSCs. (A) Quantification of the percent chromatin segregation in passage 4 cells (n = 40). (B) Quantification of the interquartile range (IQR) of the percent chromatin segregation from 4 technical replicates to represent the heterogeneity of the MSC population. (C) Representative images of DAPI stained MSC nuclei. Scale bar:10 µm. Error bars represent ± SD. *p<0.05, ***p<0.001.

Functional indications of substrate mechanics-driven heterogeneity

To examine the functionality of MSCs on the varying substrates in more detail, Passage 4 MSCs were stained for the stemness marker, CD73, and the osteogenesis precursor protein, Runx2. We found a strong relationship between the level of CD73 and the level of Runx2 on the stiff and soft substrates, but no relationship on the medium stiffness substrate (Figure 9A). On soft substrates, cells showed a higher CD73 intensity and lower localization of Runx2 to the nucleus. Stiff substrates, however, showed low CD73 intensity with a high ratio of Runx2 in the nucleus. Localization of Runx2 to the nucleus is an indicator that the cells begin to commit to an osteoprogenitor lineage. Soft substrates showed significantly higher CD73 intensity (Figure 9B, A4.A) and significantly lower Runx2 nuclear localization (Figure 9D, A4.B) compared to the stiff and medium substrates. When examining the heterogeneity of CD73, we saw a significant increase in the medium and soft substrates compared to the stiff substrate (Figure 9C), similar to the trend of chromatin segregation heterogeneity. CD73 is a marker that indicates stemness, an MSC property, which exhibits differentiation potential and this high IQR value represents various lineage opportunities. There were no significant differences in IQR for the Runx2 nucleus localization (Figure 9E). Overall, we found that soft substrate had a higher population of cells exhibiting MSC indicators, with Runx2 that was less localized to the nucleus than cells on stiff and medium stiffness substrates.

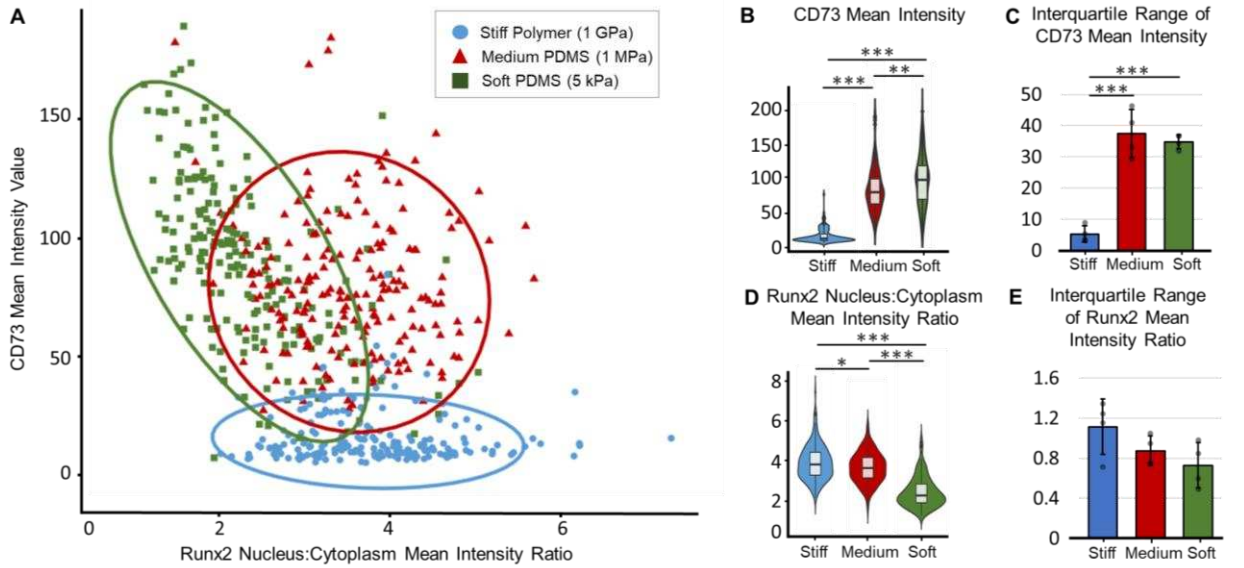

Figure 9. Mean fluorescent intensity analysis and heterogeneity quantification of P4 MSCs seeded at 5,000 cells/cm^2. (A) Scatter plot of CD73 mean intensity and Runx2 nucleus to cytoplasm mean intensity ratio for cells cultured on varied substrate stiffnesses. Each data point represents one cell. 95% confidence level ellipses for a multivariate t-distribution were included as a visual indicator of correlation. (B) Mean intensity values of CD73 visualized with violin plots to show the full distribution of the data with an embedded boxplot (n = 200 cells). (C) Quantification of the interquartile range (IQR) of the CD73 mean intensity values from 4 technical replicates to represent the heterogeneity of the MSC population. (D) Ratio of the mean intensity value of Runx2 in the nucleus divided by the mean intensity value of Runx2 in the cytoplasm (n = 200 cells). (E) Quantification of the interquartile range (IQR) of the Runx2 nucleus to cytoplasm mean intensity ratio from 4 technical replicates to represent the heterogeneity of the MSC population. Error bars represent ± SD. *p<0.05, **p<0.01, ***p<0.001.

Cytoskeletal tension significantly affects cell and nuclear phenotype but not the heterogeneity in passage 5

Now that we have determined that substrate stiffness plays a significant role in the MSC phenotype and the level of phenotype heterogeneity, we attempted to isolate the effects of cytoskeletal tension from cell-cell mechanical communication through the substrate (Figure 10, A5). Passage 5 (P5) cells on stiff substrates were treated either with cytochalasin D (cyto-D), Y27632, or a combination of both drugs. Treatment with cyto-D inhibits the actin polymerization, and treatment with Y27632 inhibits the Rho-associated protein kinase (ROCK), impeding actomyosin contraction. The ROCK

inhibition led to a smaller nuclear area, increased elongated nuclear shape, and an overall smaller cell area (Figure 10A, C), thus recovering the MSC phenotype. However, the analysis of the IQR values, as an indicator of MSC population heterogeneity, revealed that cytoskeletal mechanics inhibitors had no significant effects on IQR (Figure 10B, D), at least in the late passage cells on a stiff substrate. Lastly, we wanted to examine if those cytoskeletal mechanics inhibitors affect the formation of stress fibers. There were no significant changes in the F-actin intensity ratio (Figure 10E) compared to the control group. These results indicate that cytoskeletal tension indeed affects the MSC phenotype but not their phenotypical heterogeneity.

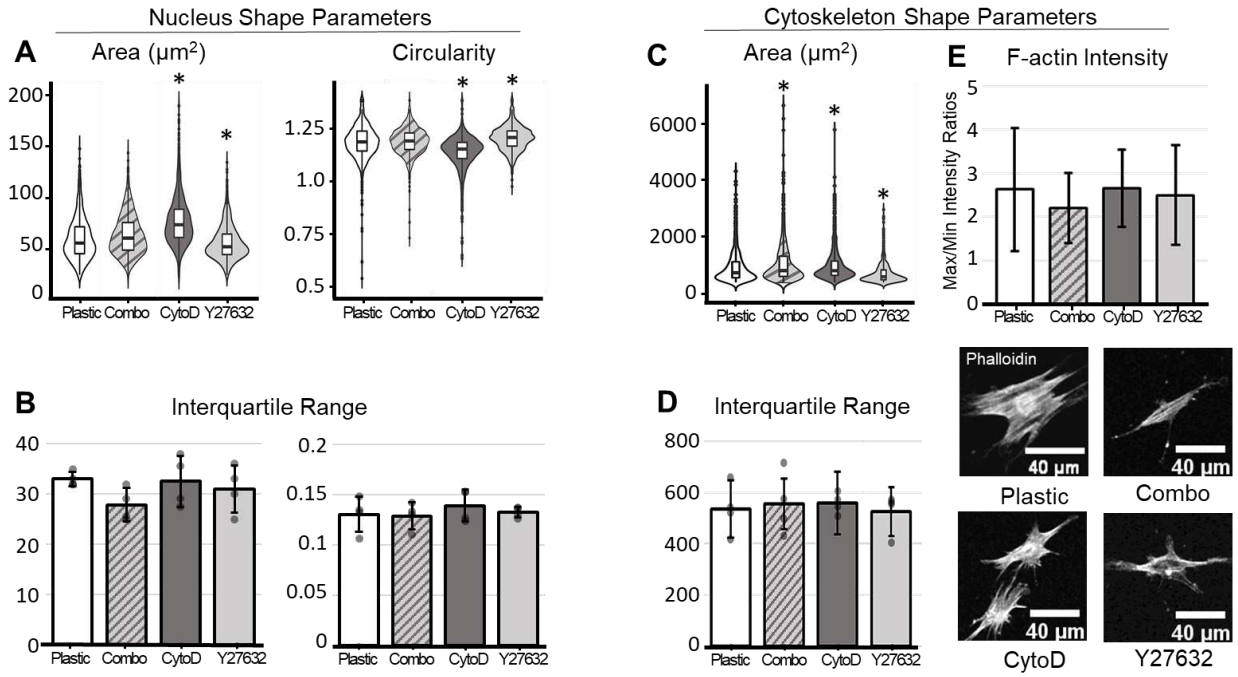

Figure 10. Effect of mechanics inhibitors on the phenotype of hMSCs. Passage 5 cells were cultured on a stiff substrate and were treated with cytochalasin D (cyto-D), the ROCK inhibitor Y27632, or a combination treatment of cyto-D and Y27632. (A) Nucleus area and circularity quantification are visualized through violin plots to show the distribution of the data with embedded boxplots (n = 1000 cells/group). (B) Quantification of the interquartile range (IQR) of the nucleus area and circularity from 4 technical replicates to represent the heterogeneity of the MSC population. (C) Cell area and quantification are visualized through violin plots to show the distribution of the data with embedded boxplots (n = 1000 cells/group). (D) Quantification of the interquartile range (IQR) of the cell area from 4 technical replicates to represent the heterogeneity of the MSC population. (E) F-actin intensity quantification of hMSCs cultured on tissue culture plastic in passage 5 with various mechanics inhibitor treatments (n = ~30 cells/group).

Representative images of the phalloidin stained cells from each treatment group. Error bar: SD. *p<0.05.

Mechanobiological pathway inhibiting drugs can increase stemness markers and decrease the heterogeneity in Passage 4

Next, we investigated if the inhibition mechanobiological pathways can recover stemness or MSC markers in earlier passage cells. On inhibiting Rho-ROCK (by Y27632), Runx2 (by CADD522), and cytoskeletal YAP (by verteporfin) the MSC population showed an increase in CD73 marker, and also lower actin stress fiber formation, even though the cells were culture on a plastic substrate (Figure 11). These results are seen in MSCs cultured on soft substrates.

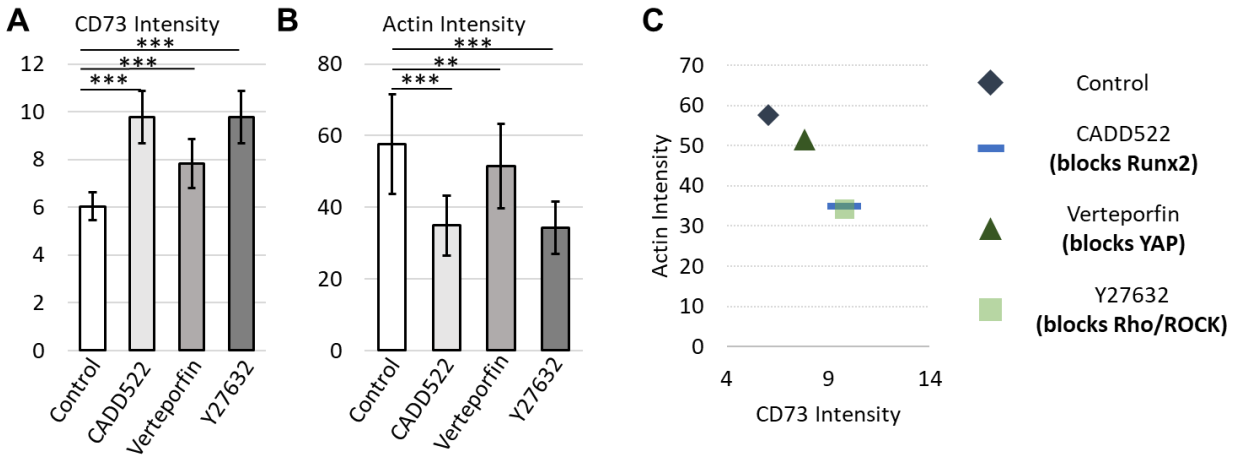

Figure 11. Drug treatment inhibiting Rho-ROCK, cytoplasmic YAP, and Runx2 in the cells maintain the stemness of MSC, thus making the cell population more MSC-like. (A) CD73 mean intensity values (n= ~20 cells/group). (B) Mean F-actin channel intensity values (n = ~70 cells/group). (C) Mean CD73 intensity and actin intensity values plotted for each group to examine the relationship between these measures. Higher CD73 intensity is seen with a low actin intensity. Error bar: SD. **p<0.01, ***p<0.001.

Cytoskeletal tension is reinforced by the perinuclear actin cap

The increased cytoskeletal tension in cells on stiff substrates was also associated with an observed dome of actin filaments at the apical surface of the MSC nucleus, known as the perinuclear actin cap (Figure 12A, B). Quantification of the proportion of cells with perinuclear actin caps revealed

a relationship between substrate stiffness and seeding density and the perinuclear actin formation. The presence of perinuclear actin caps was more frequent in cells at lower cell density and on the stiff substrate, with instances decreasing significantly for cells on the soft substrate and at a higher seeding density (Figure 12C, D). This corresponds with the increased cell and nucleus area and F-actin intensity on stiff substrates quantified earlier (Figure 6B, C and Figure 7B, C). Together,

these results suggest that the perinuclear actin cap formation is involved with cytoskeletal tension-mediated stress fiber formation around the nucleus.

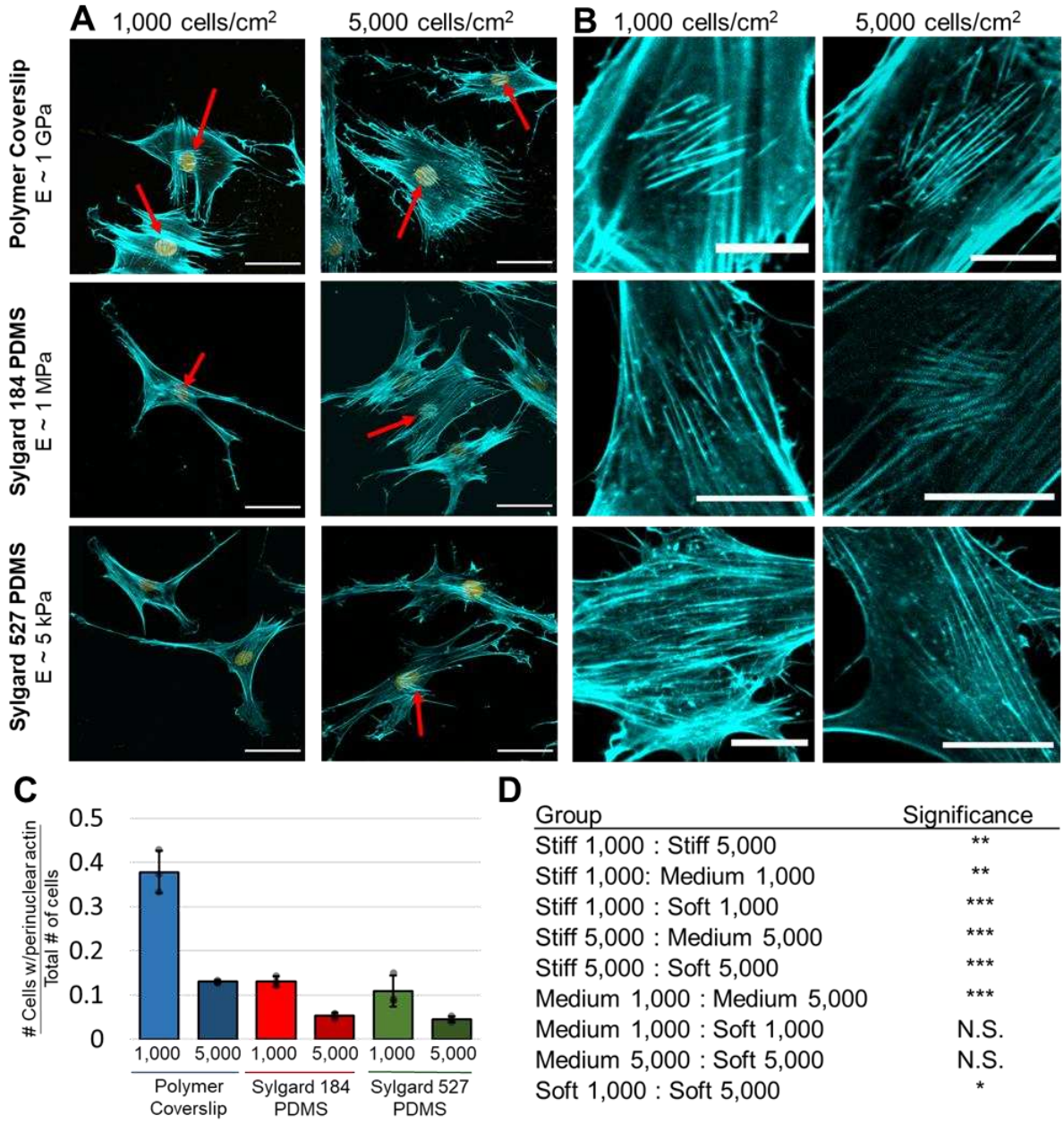

Figure 12. Effect of substrate stiffness and cell seeding density on perinuclear actin formation in BM-MSCs. (A) It was observed that MSCs displayed less perinuclear actin on soft substrates. Red arrows point to cells with visible perinuclear actin. Scale bar: 50 µm. (B) High-resolution imaging of identified perinuclear actin in MSCs shows a clear reduction in perinuclear actin on soft substrates. Scale bar: 20 µm. (C) Ratios were quantified from 3 technical replicates to examine the number of cells that displayed perinuclear actin compared to the total amount of cells in the image (n = 150 for 1,000 cells/cm^2 group, n = 650 for 5,000 cells/cm^2 group). (D) Table of p-values for

various comparisons in each quantity. Stiff = 1 GPa, medium = 1 MPa, soft = 5 kPa. Error bars represent ± SD. N.S. Not Significant: p>0.05, *p<0.05, **p<0.01, ***p<0.001.

Emergent stress field of a cell community lowers intracellular strain

A finite element method-based model (Figure 13) shows that when cells are near each other, they create an emergent stress field on a soft substrate, where mechanical information can pass through one cell from another cell. These stress field from neighboring cells cancels some of the intracellular strain. When they are far, the cells do not interact mechanically, and intracellular strain is higher. On a plastic substrate, such emergent fields do not appear because of the very high stiffness. A lower strain inside the cell not only increases the formation of actin stress fiber by 'actin filament treadmilling', but it can also localize YAP inside the cell nucleus to direct the cell towards a Runx2 pathway. This mechanistic model further explains why the > 5000 cells/ cm^2 had optimal MSC phenotype on the soft substrate.

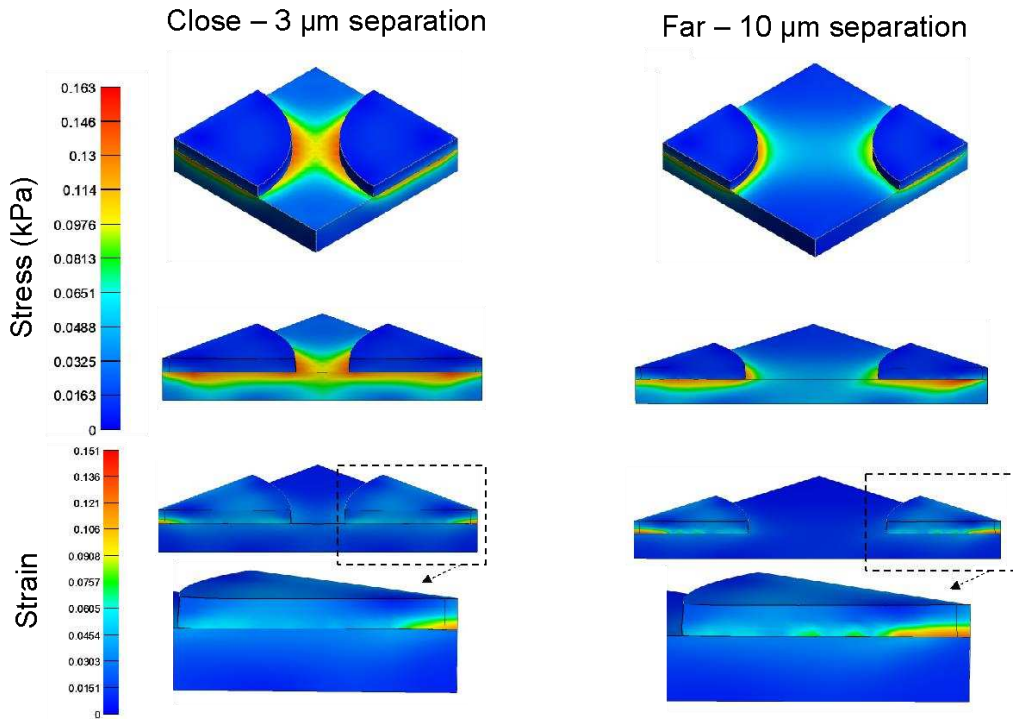

Figure 13. Cells interact with each other through a compliant substrate. Nearby cells create an emergent stress field which lowers the strain in the individual cell. Cells separated from each other experience a lower strain inside the cell.

Discussion

In this study, we provided evidence of phenotypical heterogeneity of MSC during 2D expansion culture. The heterogeneity considered throughout this study was evaluated using a common measure of dispersion, the interquartile range (IQR). Mechanistic insight into the source of substrate mechanics-driven heterogeneity, further influenced by the substrate-mediated cell-cell communication was examined. We found that substrate stiffness plays a key role in the heterogeneity of the MSC phenotype. Soft substrates (~5 kPa) promoted a more homogeneous population of cells with the characteristic MSC cytoskeleton and nuclear phenotype, accompanied by increased expression of CD73, which is associated with a high degree of stemness [45]. Conversely, MSCs grown on the stiff substrate (~1 GPa) not only showed phenotype abnormalities, presence of perinuclear actin caps, and Runx2 nuclear localization, in line with existing reports [46–48] but also, displayed a heterogeneity of phenotype at the population level. These findings are associated with increased cellular senescence [37], decreased proliferation [46], and decreased differentiation potential [10] in MSCs.

It is well-known that MSCs are exposed to biochemical and biophysical signals that can determine lineage commitment [49]. Differentiation via biochemical cues has been extensively studied, while mechanisms of cellular mechanotransduction are becoming increasingly understood. The combination of cell-generated forces and matrix mechanics to coordinate the MSC population needs further investigation to understand these specific interactions. We hypothesized that neighboring cells would communicate through the soft substrate to promote a homogeneous population of MSCs. However, we found that seeding density had little impact on

the heterogeneity of nuclear shape but had a significant effect on the chromatin organization. In the extremely low seeding density case at 100 cells/cm^2, the cells were very far apart, impeding mechanical signaling, resulting in an extremely varied phenotype, spanning from fibroblast-like flat phenotype to MSC-like spindle phenotype with a closed chromatin architecture. An open chromatin architecture, as seen in cells on the softer substrate, is associated with transcriptional activation and is a hallmark of stem cells [50]. These changes in chromatin organization are most likely driven by the mechanical communication to neighboring cells through the substrate because actin fiber intensity was consistent between each seeding density. Accordingly, the increased IQR of chromatin segregation when cells were grown on soft substrates, supports the ability of MSCs to be in varying transcriptional states.

The phenotypic trends towards the MSC-like phenotype and chromatin segregation patterns on soft substrates were substantiated upon CD73 immunofluorescence. CD73 enrichment indicates stemness and the heterogeneous enrichment patterns are associated with reparative properties and anti-inflammatory activity [51]. The nuclear to cytoplasmic ratio of Runx2 was analyzed as an indication of early indication of osteogenic differentiation. When Runx2 is translocated into the nucleus, it induces transcriptional expression of osteogenesis-related genes [52]. The pattern that emerged due to the high nuclear Runx2 in cells on the stiff substrate is consistent with the phenotype of cells on the stiff substrate.

A potential approach to alter the heterogeneity dynamics of a population of MSCs during *in vitro* culture was to disrupt the cytoskeleton tension to impose lower tensile stress inside the cells. Disrupting the cytoskeletal tension with the ROCK inhibitor Y27632 resulted in cells with a significantly restored MSC cell and nucleus phenotype. Cell area was lowered, nucleus became smaller in area and more elongated, representing the MSC phenotype. A contributing factor to this

recovered phenotype after Y27632 treatment is the disruption of the LINC complexes connecting the nucleus to this actin cap, decreasing cellular tension [46]. ROCK inhibition is also known to prevent osteogenic differentiation of MSCs [32]. The phenotype heterogeneity, however, was not significantly affected by inhibiting actin polymerization or actomyosin contraction. Studies have been performed to understand the effects of these cytoskeleton modifying drugs on MSC functionality, but the effects on the population heterogeneity are not specifically explored. Our findings from this study suggest that stiffness-dependent heterogeneity does not rely on actin formation and actomyosin contractions as we hypothesized, and we explain the observation as follows. Cytoplasmic dynamics are faster than intranuclear dynamics. Therefore, during continuous culture to passage 5 on the stiff substrate, the amount of existing F-actin fibers that developed might have outweighed the effects of Y27632, likely leading to irreversible heterogeneity. Overall, this finding might be attributed to the lower plasticity of MSC at later passage because Y27632 treatment on passage 4 cells led to a decrease in heterogeneity values.

Recognizing the natural heterogeneity dynamics of a cell population and understanding its source allows for the minimization of adverse outcomes in efficacy or safety from one patient to the next. This study provides potential targets in the intracellular mechanobiological pathways to control the heterogeneity dynamics of MSCs during *in vitro* expansion. Future studies would involve single cell RNA-sequencing to further quantify the heterogeneity in MSC phenotype and explore the possible pathways to understand the mechanistic origins of heterogeneity.

REFERENCES

1. Crippa, S., & Bernardo, M. E. (2018). Mesenchymal Stromal Cells: Role in the BM Niche and in the Support of Hematopoietic Stem Cell Transplantation. *HemaSphere*, *2*(6). https://doi.org/10.1097/HS9.0000000000000151

2. García-Muñoz, E., & Vives, J. (2021). Towards the standardization of methods of tissue processing for the isolation of mesenchymal stromal cells for clinical use. *Cytotechnology*, *73*(3), 513–522. https://doi.org/10.1007/S10616-021-00474-3/TABLES/2

3. Soleimani, M., & Nadri, S. (2009). A protocol for isolation and culture of mesenchymal stem cells from mouse bone marrow. *Nature Protocols 2009 4:1*, *4*(1), 102–106. https://doi.org/10.1038/nprot.2008.221

4. Li, J., Wong, W. H. S., Chan, S., Chim, J. C. S., Cheung, K. M. C., Lee, T. L., … Chan, G. C. F. (2011). Factors Affecting Mesenchymal Stromal Cells Yield from Bone Marrow Aspiration. *Chinese Journal of Cancer Research*, *23*(1), 43. https://doi.org/10.1007/S11670-011-0043-1

5. Akgun, I., Unlu, M. C., Erdal, O. A., Ogut, T., Erturk, M., Ovali, E., … Akgun, Y. (2015). Matrix-induced autologous mesenchymal stem cell implantation versus matrix-induced autologous chondrocyte implantation in the treatment of chondral defects of the knee: a 2-year randomized study. *Archives of Orthopaedic and Trauma Surgery*, *135*(2), 251–263. https://doi.org/10.1007/S00402-014-2136-Z/FIGURES/3

6. Epanomeritakis, I. E., Lee, E., Lu, V., & Khan, W. (2022). The Use of Autologous Chondrocyte and Mesenchymal Stem Cell Implants for the Treatment of Focal Chondral Defects in Human Knee Joints—A Systematic Review and Meta-Analysis. *International Journal of Molecular Sciences*, *23*(7), 4065. https://doi.org/10.3390/IJMS23074065

7. Ren, G., Chen, X., Dong, F., Li, W., Ren, X., Zhang, Y., & Shi, Y. (2012). Concise Review: Mesenchymal Stem Cells and Translational Medicine: Emerging Issues. *Stem Cells Translational Medicine*, *1*(1), 51–58. https://doi.org/10.5966/SCTM.2011-0019

8. Wilson, A. J., Rand, E., Webster, A. J., & Genever, P. G. (2021). Characterisation of mesenchymal stromal cells in clinical trial reports: analysis of published descriptors. *Stem Cell Research and Therapy*, *12*(1), 1–15. https://doi.org/10.1186/S13287-021-02435-1/FIGURES/6

9. Wright, A., Arthaud-Day, M. L., & Weiss, M. L. (2021). Therapeutic Use of Mesenchymal Stromal Cells: The Need for Inclusive Characterization Guidelines to Accommodate All Tissue Sources and Species. *Frontiers in Cell and Developmental Biology*, *9*, 66. https://doi.org/10.3389/FCELL.2021.632717/BIBTEX

10. Neuhuber, B., Swanger, S. A., Howard, L., Mackay, A., & Fischer, I. (2008). Effects of plating density and culture time on bone marrow stromal cell characteristics. *Experimental Hematology*, *36*, 1176–1185. https://doi.org/10.1016/J.EXPHEM.2008.03.019

11. Wilson, A., Webster, A., & Genever, P. (2019). Nomenclature and heterogeneity: consequences for the use of mesenchymal stem cells in regenerative medicine. *Regenerative Medicine*, *14*(6), 595. https://doi.org/10.2217/RME-2018-0145

12. Kureel, S. K., Mogha, P., Khadpekar, A., Kumar, V., Joshi, R., Das, S., … Majumder, A. (2019). Soft substrate maintains proliferative and adipogenic differentiation potential of human mesenchymal stem cells on long-term expansion by delaying senescence. *Biology Open*, *8*(4). https://doi.org/10.1242/bio.039453

13. Mastrolia, I., Foppiani, E. M., Murgia, A., Candini, O., Samarelli, A. V., Grisendi, G., … Dominici, M. (2019). Challenges in Clinical Development of Mesenchymal Stromal/Stem Cells:

Concise Review. *STEM CELLS Translational Medicine*, *8*(11), 1135–1148. https://doi.org/10.1002/SCTM.19-0044

14. Schellenberg, A., Stiehl, T., Horn, P., Joussen, S., Pallua, N., Ho, A. D., & Wagner, W. (2012). Population dynamics of mesenchymal stromal cells during culture expansion. *Cytotherapy*, *14*(4), 401–411. https://doi.org/10.3109/14653249.2011.640669

15. Heo, S. J., Driscoll, T. P., Thorpe, S. D., Nerurkar, N. L., Baker, B. M., Yang, M. T., … Mauck, R. L. (2016). Differentiation alters stem cell nuclear architecture, mechanics, and mechano-sensitivity. *eLife*, *5*(NOVEMBER2016), 1–21. https://doi.org/10.7554/eLife.18207

16. Musiał-Wysocka, A., Kot, M., & Majka, M. (2019, July 1). The Pros and Cons of Mesenchymal Stem Cell-Based Therapies. *Cell Transplantation*. SAGE Publications Ltd. https://doi.org/10.1177/0963689719837897

17. Sun, C., Wang, L., Wang, H., Huang, T., Yao, W., Li, J., & Zhang, X. (2020). Single-cell RNA-seq highlights heterogeneity in human primary Wharton's jelly mesenchymal stem/stromal cells cultured in vitro. *Stem Cell Research & Therapy 2020 11:1*, *11*(1), 1–16. https://doi.org/10.1186/S13287-020-01660-4

18. Nguyen, V. T., Tessaro, I., Marmotti, A., Sirtori, C., Peretti, G. M., & Mangiavini, L. (2019). Does the harvesting site influence the osteogenic potential of mesenchymal stem cells? *Stem Cells International*. https://doi.org/10.1155/2019/9178436

19. Wagner, W., Wein, F., Seckinger, A., Frankhauser, M., Wirkner, U., Krause, U., … Ho, A. D. (2005). Comparative characteristics of mesenchymal stem cells from human bone marrow, adipose tissue, and umbilical cord blood. *Experimental Hematology*, *33*(11), 1402–1416. https://doi.org/10.1016/j.exphem.2005.07.003

20. Rennerfeldt, D. A., & Van Vliet, K. J. (2016). Concise Review: When Colonies Are Not Clones: Evidence and Implications of Intracolony Heterogeneity in Mesenchymal Stem Cells. *Stem Cells*, *34*(5), 1135–1141. https://doi.org/10.1002/stem.2296

21. Costa, L. A., Eiro, N., María Fraile, ·, Luis, ·, Gonzalez, O., Saá, J., … Vizoso, F. J. (2021). Functional heterogeneity of mesenchymal stem cells from natural niches to culture conditions: implications for further clinical uses. *Cellular and Molecular Life Sciences*, *78*, 447–467. https://doi.org/10.1007/s00018-020-03600-0

22. Reinhart-King, C. A., Dembo, M., & Hammer, D. A. (2008). Cell-cell mechanical communication through compliant substrates. *Biophysical Journal*, *95*(12), 6044–6051. https://doi.org/10.1529/biophysj.107.127662

23. Sun, Y., Wan, B., Wang, R., Zhang, B., Luo, P., Wang, D., … Wu, X. (2022). Mechanical Stimulation on Mesenchymal Stem Cells and Surrounding Microenvironments in Bone Regeneration: Regulations and Applications. *Frontiers in Cell and Developmental Biology*, *10*, 2. https://doi.org/10.3389/FCELL.2022.808303/BIBTEX

24. Seelbinder, B., Ghosh, S., Schneider, S. E., Scott, A. K., Berman, A. G., Goergen, C. J., … Neu, C. P. (2021). Nuclear deformation guides chromatin reorganization in cardiac development and disease. *Nature Biomedical Engineering*, *5*, 1500–1516. https://doi.org/10.1038/s41551-021-00823-9

25. Argentati, C., Morena, F., Tortorella, I., Bazzucchi, M., Porcellati, S., Emiliani, C., & Martino, S. (2019). Insight into mechanobiology: How stem cells feel mechanical forces and orchestrate biological functions. *International Journal of Molecular Sciences*, *20*(21). https://doi.org/10.3390/ijms20215337

26. Chuang, L. S. H., & Ito, Y. (2021). The Multiple Interactions of RUNX with the Hippo–YAP Pathway. *Cells*, *10*(11). https://doi.org/10.3390/CELLS10112925

27. Dupont, S., Morsut, L., Aragona, M., Enzo, E., Giulitti, S., Cordenonsi, M., … Piccolo, S. (2011). Role of YAP/TAZ in mechanotransduction. *Nature*, *474*(7350), 179–184. https://doi.org/10.1038/nature10137

28. Dasgupta, I., & McCollum, D. (2019, November 15). Control of cellular responses to mechanical cues through YAP/TAZ regulation. *Journal of Biological Chemistry*. American Society for Biochemistry and Molecular Biology Inc. https://doi.org/10.1074/jbc.REV119.007963

29. Heng, B. C., Zhang, X., Aubel, D., Bai, Y., Li, X., Wei, Y., … Deng, X. (2020, July 30). Role of YAP/TAZ in Cell Lineage Fate Determination and Related Signaling Pathways. *Frontiers in Cell and Developmental Biology*. Frontiers Media S.A. https://doi.org/10.3389/fcell.2020.00735

30. Cobbaut, M., Karagil, S., Bruno, L., Loza, M. D. C. D. de la, Mackenzie, F. E., Stolinski, M., & Elbediwy, A. (2020). Dysfunctional Mechanotransduction through the YAP/TAZ/Hippo Pathway as a Feature of Chronic Disease. *Cells*, *9*(1). https://doi.org/10.3390/CELLS9010151

31. Hong, J. H., Hwang, E. S., McManus, M. T., Amsterdam, A., Tian, Y., Kalmukova, R., … Yaffe, M. B. (2005). TAZ, a transcriptional modulator of mesenchymal stem cell differentiation. *Science*, *309*(5737), 1074–1078. https://doi.org/10.1126/science.1110955

32. Shi, Y. U., Li, H., Zhang, X., Fu, Y., Huang, Y., Po, P., … Dai, A. K. (2011). Continuous Cyclic Mechanical Tension Inhibited Runx2 Expression in Mesenchymal Stem Cells Through RhoA-ERK1/2 Pathway. *J. Cell. Physiol*, *226*, 2159–2169. https://doi.org/10.1002/jcp.22551

33. Zhang, Y. Y., Li, X., Qian, S. W., Guo, L., Huang, H. Y., He, Q., … Tang, Q. Q. (2012). Down-regulation of type I Runx2 mediated by dexamethasone is required for 3T3-L1 adipogenesis. *Molecular Endocrinology*, *26*(5), 798–808. https://doi.org/10.1210/me.2011-1287

34. Humphries, D. L., Grogan, J. A., & Gaffney, E. A. (2017). Mechanical Cell–Cell Communication in Fibrous Networks: The Importance of Network Geometry. *Bulletin of Mathematical Biology*, *79*(3), 498–524. https://doi.org/10.1007/S11538-016-0242-5/FIGURES/13

35. Lee, W. C., Shi, H., Poon, Z., Nyan, L. M., Kaushik, T., Shivashankar, G. v., … van Vliet, K. J. (2014). Multivariate biophysical markers predictive of mesenchymal stromal cell multipotency. *Proceedings of the National Academy of Sciences of the United States of America*, *111*(42), E4409–E4418. https://doi.org/10.1073/pnas.1402306111

36. Gu, Y., Li, T., Ding, Y., Sun, L., Tu, T., Zhu, W., … Sun, X. (2016). Changes in mesenchymal stem cells following long-term culture in vitro. *Molecular Medicine Reports*, *13*(6), 5207–5215. https://doi.org/10.3892/mmr.2016.5169

37. Yang, Y. H. K., Ogando, C. R., Wang See, C., Chang, T. Y., & Barabino, G. A. (2018). Changes in phenotype and differentiation potential of human mesenchymal stem cells aging in vitro. *Stem Cell Research & Therapy2*, *9*(131), 1–14. Retrieved from https://stemcellres.biomedcentral.com/articles/10.1186/s13287-018-0876-3

38. Irianto, J., Lee, D. A., & Knight, M. M. (2014). Quantification of chromatin condensation level by image processing. *Medical Engineering and Physics*, *36*(3), 412–417. https://doi.org/10.1016/j.medengphy.2013.09.006

39. Jambu, M. (1991). 1-D Statistical Data Analysis. *Exploratory and Multivariate Data Analysis*, 27–62. https://doi.org/10.1016/B978-0-08-092367-3.50007-1

40. Riffenburgh, R. H. (2012). Descriptive Statistics. *Statistics in Medicine*, 95–116. https://doi.org/10.1016/B978-0-12-384864-2.00005-6

41. Team, R. C. (2021). R: A language and environment for statistical computing. Vienna, Austria: R Foundation for Statistical Computing.

42. Constantin, A.-E., & Patil, I. (2021). {ggsignif}: R Package for Displaying Significance Brackets for {'ggplot2'}. PsyArxiv. https://doi.org/10.31234/osf.io/7awm6

43. FC, M., & Davis, T. L. (2022). ggpattern: "ggplot2" Pattern Geoms.

44. Dai, E. N., Heo, S. J., & Mauck, R. L. (2020). "Looping In" Mechanics: Mechanobiologic Regulation of the Nucleus and the Epigenome. *Advanced Healthcare Materials*, *9*(8), 1–14. https://doi.org/10.1002/adhm.202000030

45. Kimura, K., Breitbach, M., Schildberg, F. A., Hesse, M., & Fleischmann, B. K. (2021). Bone marrow CD73+ mesenchymal stem cells display increased stemness in vitro and promote fracture healing in vivo. *Bone Reports*, *15*, 101133. https://doi.org/10.1016/J.BONR.2021.101133

46. Kihara, T., Haghparast, S. M. A., Shimizu, Y., Yuba, S., & Miyake, J. (2011). Physical properties of mesenchymal stem cells are coordinated by the perinuclear actin cap. *Biochemical and Biophysical Research Communications*, *409*(1), 1–6. https://doi.org/10.1016/j.bbrc.2011.04.022

47. Khatau, S. B., Hale, C. M., Stewart-Hutchinson, P. J., Patel, M. S., Stewart, C. L., Searson, P. C., … Wirtz, D. (2009). A perinuclear actin cap regulates nuclear shape. *Proceedings of the National Academy of Sciences of the United States of America*, *106*(45), 19017–19022. https://doi.org/10.1073/pnas.0908686106

48. Miroshnikova, Y. A., Nava, M. M., & Wickstro, S. A. (2017). Emerging roles of mechanical forces in chromatin regulation. *Journal of Cell Science*, *130*, 2243–2250. https://doi.org/10.1242/jcs.202192

49. Yim, E. K. F., & Sheetz, M. P. (2012). Force-dependent cell signaling in stem cell differentiation. *Stem Cell Research and Therapy*, *3*(5), 1–12. https://doi.org/10.1186/SCRT132/TABLES/1

50. Gaspar-Maia, A., Alajem, A., Meshorer, E., & Ramalho-Santos, M. (2011). Open chromatin in pluripotency and reprogramming. *Nature reviews. Molecular cell biology*, *12*(1), 36. https://doi.org/10.1038/NRM3036

51. Tan, K., Zhu, H., Zhang, J., Ouyang, W., Tang, J., Zhang, Y., … Deng, X. (2019). CD73 Expression on Mesenchymal Stem Cells Dictates the Reparative Properties via Its Anti-Inflammatory Activity. https://doi.org/10.1155/2019/8717694

52. Xu, J. H., Li, Z. H., Hou, Y. D., & Fang, W. J. (2015). Potential mechanisms underlying the Runx2 induced osteogenesis of bone marrow mesenchymal stem cells. *American Journal of Translational Research*, *7*(12), 2527. Retrieved from /pmc/articles/PMC4731654/

CHAPTER 3: MECHANICAL STIFFNESS REGULATES CHROMATIN REMODELING IN MESENCHYMAL STROMAL CELLS DURING MONOLAYER CULTURE

Background

Epigenetics

Gene transcription is dynamically regulated across a range of cellular processes including the maintenance of stemness – characterized by self-renewal ability, differentiation to specific cell type, and proliferation through symmetric/ asymmetric cell division. The eukaryotic genome is organized within the cell nucleus where about 6 billion base pairs of DNA are compacted into an intricate and dynamic structure called chromatin. The complex architecture is composed of DNA and many accessory proteins including histones. The fundamental unit of chromatin is a nucleosome where 146 base pairs of DNA are wrapped about 1.65 times around an octamer of core histone proteins consisting of H2A, H2B, H3, and H4, resembling a "beads on a string" structure. Hierarchical folding of chromatin renders the intricate chromatin architecture, affecting the accessibility of genes.

The expression level of most eukaryotic genes is dependent on the state of accessibility of its associated chromatin domain. The overall higher-order chromatin structure can be classified into heterochromatin which represents a transcriptionally inactive state, and euchromatin which represents a transcriptionally active state. The compacted state of heterochromatin poses a hindrance to regulators of cellular processes i.e., cell cycle regulation and differentiation, thus alteration and status of the chromatin structure in order to regulate these processes are critical for the cell phenotype. The two most frequently observed mechanisms of regulation are DNA

methylation and post-translational modification of histone tails by histone modifying enzymes, while the ATP-dependent chromatin remodeling is emerging as a new frontier of chromatin architecture modulation [1].

Covalent modifications of histone tails cause alterations in DNA-histone interactions, promoting changes in nucleosome assembly and conformation. Post-translational modifications of histones such as methylation or acetylation happen in an ATP-dependent manner through enzymes such as histone acetyltransferases (HATs), histone deacetylases (HDACs), or histone methyltransferases (HMTs). Histone 3 lysine 4 di or tri methylation (H3K4me2/3,) and Histone 4 acetylation (H4Ac) at target gene promoters are indicative of active transcription whereas histone 3 lysine 9 methylation (H3K9me) or histone 3 lysine 27 trimethylation (H3K27me3, heterochromatin) are indicative of silent genes [1]. These epigenetic modifications control many cellular mechanisms, including mechanosensing.

Effects of Substrate Stiffness on MSC

Substrate mechanics is known to affect the MSC fate, as elucidated by many researchers starting with the seminal work by the Denis Discher group [2]. MSC-derived lineage specifications such as their commitment to chondrocyte, osteoblast, etc. are profoundly affected by the mechanical environment through multiple mechanosensitive pathways. Recently, it was shown that the mechanics of the cellular environment can define the tissue-specific cellular phenotype through the modulation of intranuclear mechanics and chromatin architecture via epigenetic mechanisms [3, 4]. Subsequently, recent studies are emerging to indicate that irrespective of the differentiation status, the MSC phenotype maintenance in culture is also affected by the mechanical environment thus having implications in culturing MSCs on a substrate for further application in cell therapy.

It was previously shown that [5, 6] that MSC phenotypes are better preserved on softer substrates over multiple passages when compared to growth on stiffer substrates i.e., tissue culture plastic (TCP) or glass. Cells on soft substrates have been shown to have no significant change in proliferation through passaging, have relatively low levels of senescence in late passages, have increased expression of pluripotency genes, and have better differentiation outcomes compared to TCP (Figure 14). Overall, a softer substrate leads to better MSC survival and performance although the exact reason behind why it is more beneficial is still under investigation.

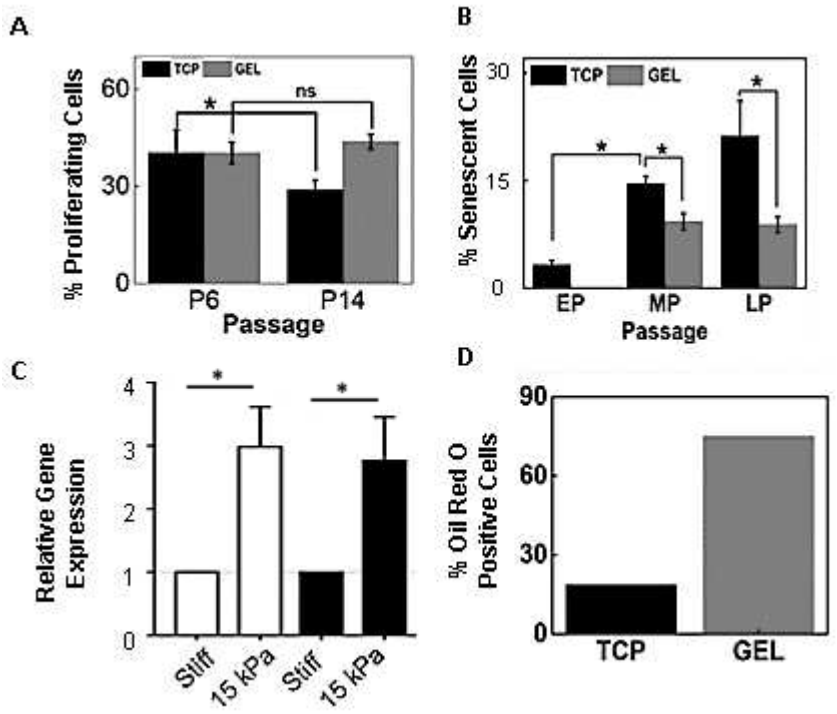

Figure 14. Soft substrates lead to better MSC survival and performance. (A) Percent proliferating cells from passage 6 to passage 14 show no significant change when cultured on a soft gel. (B) Percent senescent cells remain low in late passages. (C) Relative gene expression of two pluripotency markers, Nanog (white) and Oct4 (black) are significantly increased on soft substrates. (D) Improved differentiation on soft gel is indicated by a higher percentage of oil red o positive cells upon induction of adipogenesis. *$p<0.05$. Adapted from Kureel et al. and Gerardo et al.

Some groups have hypothesized that the mechanics of the cellular environment can define these specific phenotypes through epigenetic mechanisms [6, 7], and they indicated that the

underlying reason is the chromatin architecture and epigenetic status in MSCs. Upon culture on a soft substrate, the overall euchromatin content increases (Figure 15). The DNA in the nucleus exists in two forms that reflect the level of activity of the cell: heterochromatin and euchromatin, as mentioned before. Heterochromatin is most abundant in cells that show little to no activity while euchromatin is prevalent in cells that are transcriptionally active. An open chromatin architecture, associated with euchromatin, is a hallmark of all stem cells, including MSCs, and a soft substrate promotes this transcriptionally active cell state through the maintenance of more open chromatin. Our objective in this work is to understand how the mechanics affect the maintenance of MSC phenotype and the deviation from the MSC-like characteristics in culture through epigenetic mechanisms and chromatin remodeling complexes. Subsequently, our long-term goal is to exploit such a mechanism in maintaining the MSC phenotype in dish culture without compromising its proliferation ability.

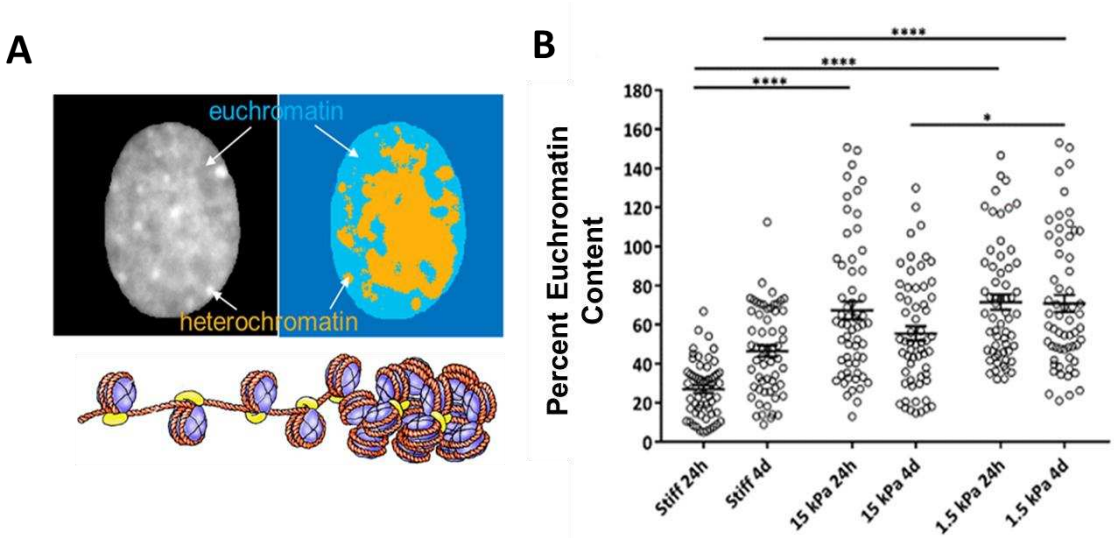

Figure 15. (A) Euchromatin is the transcriptionally active, unwound region of chromatin and is characterized by a less bright DAPI stain. Adapted from Ghosh et al. (B) Gerardo et al. evaluated euchromatin content over varying substrate stiffnesses and it was shown that the softer substrate leads to more euchromatin content.

Chromatin Remodeling

Epigenetic modification to define chromatin architecture is traditionally attributed to histone modifications and DNA methylation. More recently, the chromatin remodeling complex and its accessorial mechanisms are evolving as a new frontier of epigenetic modification. Chromatin-associated multi-subunit protein complexes, referred to as chromatin remodeling complexes (CRC), can affect whether a gene is activated or repressed by nucleosome ejection, compaction, or sliding. There are 4 classes of CRC in mammals. The primary CRC of interest for our group is the SWItch/Sucrose Non-Fermentable (SWI/SNF), which is a family of evolutionarily conserved complexes that require ATP to regulate chromatin structure. SWI/SNF is known to alter transcription through nucleosome reassembly, using ATP to physically remodel nucleosome structure and facilitate the binding of transcriptional factors, either activators or repressors, to nucleosomal DNA.

The mammalian SWI/SNF complex consists of a central catalytic subunit that is either Brahma-related gene 1 (BRG1, also known as SMARCA4) or Brahma (BRM), alternative ATPases that catalyze the CRC along with 8-15 other subunits termed BRG1/BRM-associated factors (BAFs) [8, 9]. These BRG1-containing SWI/SNF complexes can be further distinguished into pBAF or the BAF complexes. pBAF complexes uniquely contain BAF200 and BAF180 while the BAF uniquely contains BAF250A and BAF250B.

Many complexes are unique to specific tissues or biological functions, so it is not solely the BAF complex itself that controls biological processes, but the expression of distinct BAF complexes with unique subunit compositions is a major part of the regulatory process [8]. It has various subunits, but we chose to examine the following subunits as they are the key proteins in the CRC for our study.

SMARCA4 (BRG1) is the central catalytic subunit of numerous chromatin-modifying enzymatic complexes and is capable of promoting some nucleosome remodeling *in vitro* [10]. It plays a role in cellular proliferation and differentiation by interacting with specific promoters, serves as a tumor suppressor, and can either activate or repress transcription through interactions with specific protein partners. Loss of its expression leads to abnormal proliferation, anomalous cell cycle control, and impairs osteoblast differentiation [11], with total inactivation being embryonic lethal in murine homozygotes [1].

The distinguishing subunit of human SWI/SNF is ARID1 (BAF250) which exists in two forms ARID1A (BAF250A) and ARID1B (BAF250B). They are expressed across most human cells and tissues, with mutations associated with a wide array of developmental disorders and cancers. This suggests a role for them in the maintenance of cell type, transcriptional status, and the determination of cell fate [12]. ARID1A is implicated in a variety of cellular processes such as stem cell differentiation [44], [45], [48], [50]. ARID1A knockouts in mouse and human embryonic stem cells exhibit failure to maintain pluripotency, demonstrate spontaneous differentiation and dysregulated expression of pluripotency genes, and finally a failure to differentiate into specific cell types such as cardiomyocytes or adipocytes [12, 13]. ARID1B knockout mouse embryonic stem cells failed to maintain pluripotency and showed dysregulation as well as pluripotency gene expression [14]. Therefore, both subunits are critical in defining the cell transcriptional status and phenotype.

ARID2 (BAF200) is involved in the overall stabilization of pBAF. It has roles in transcriptional progression and initiation [10], while its depletion shows the promoter does not switch from BRM to BRG1, not allowing subsequent gene expression [11]. ARID2 has suggested roles in embryogenesis and organ development as well as maintaining cellular identity. Loss of

ARID2 profoundly impairs osteogenic lineage gene expression and osteogenesis but does not compromise adipogenesis [15].

Actin-like 6A, ACTL6A (BAF53A) is a component of various complexes with chromatin remodeling and histone acetyltransferase activity. ACTL6A and β-actin bind to form the actin-related protein (ARP) subunit in BAF complexes which binds to the BRG1 [16]. Mutation-driven impairments of ACTL6A binding to nuclear β-actin and SMARCA4 affect the integrity of the BAF complex [10]. It also plays a role in stem cell maintenance and when complexed with the primary BAF, plays a direct role in targeting the BAF complex to the TEAD-YAP enhancers, preparing the chromatin landscape and allowing transcriptional activation of their targets [16].
When cells experience a high force through cytoskeletal tension, the nuclear strain increases [17]. The reason is that mechanical force can be transduced from the cytoskeleton to the nucleus through connected nuclear envelope proteins, such as the LINC complexes and nuclear lamina. Disruption of these linking proteins does not allow external forces to be "felt" by the nucleus, causing a lowered intranuclear deformation and strain. It was previously shown that cells grown on stiff substrates show high cytoskeletal tension and increased stress fibers.

Walker et al. [18]investigated the effects of actin on chromatin remodeling in persistently activated fibroblasts (myofibroblasts) which are behind fibrotic disease. They applied treatments of cytochalasin D to inhibit actin polymerization and Y27632 to inhibit actin-myosin contraction. Both treatments resulted in a significantly reduced amount of F-actin, nuclear tension, and chromatin condensation. This was found to be due to chromatin accessibility, with a higher HDAC activity in the persistent myofibroblasts when compared with healthy, transient fibroblasts. Upon applying an HDAC inhibitor, persistent myofibroblasts could not be "rescued" or reverted back to a transient state, suggesting that simply opening chromatin is not enough. All these studies indicate

that mechanical stretching of the MSC via the underlying soft substrate can interact with the epigenetic landscape to define the MSC phenotype.

Mechanistic understanding of how substrate mechanics drive the change in MSC stemness has reached a new frontier because of recent findings that point to a non-transcription factor related changes in chromatin architecture. Such changes in chromatin architecture can directly affect the epigenetic landscape inside the MSC nucleus, directly activating or repressing the genes, by opening or closing the specific chromatin region. Specifically, it was found that histone deacetylase is responsible for chromatin condensation and loss of MSC stemness on a stiff substrate [18]. Recently, it has emerged that mechanical stiffness can initiate the shuttling of transcription factors from the cytoplasm to the nucleus and can also change the localization of epigenetic markers such as H3K27me3. Additionally, mechanical stiffness mediates the nuclear envelope protein Lamin A/C to chromatin interaction, leading to heterochromatin formation inside the nucleus. Together, this data points to the need of understanding through what precise mechanism the chromatin architecture is changed by the mechanical stiffness and what is the implication of that in MSC stemness and phenotype.

In this project, we investigated how the mechanics drive the chromatin architecture through the investigation of several epigenetic modifiers. We looked into their relative level in cells and intranuclear localization using high-resolution microscopy and advanced image analysis. We hypothesized that the localization and expression of the epigenetic modifiers are substrate mechanics dependent and their distribution inside the nucleus can be differentially memorized by the MSC, depending on the priming duration. The functional meaning of the epigenetic modifier localization was correlated with MSC cell and nuclear shape, and also with CD73 expression. Finally, based on the acquired mechanobiological insight, we applied drugs to selectively inhibit

specific component proteins in the cell and the nucleus to achieve higher quality and quantity of MSCs even on a stiff plastic culture substrate. Knowledge of the mechanisms to maintain a high quality and quantity MSC population in two-dimensional culture can provide future intervention strategies to gain more control over MSCs during their longer-term expansion in the clinical setting without requiring a specialized bioreactor system. Further, the knowledge of mechanical memory and its retention will provide us with unique design principles to manufacture MSCs at scale, and also to design cellular engineering protocol post *in vivo* transplant.

Materials and Methods

MSC culture

Passage 2 primary human bone marrow-derived MSCs (PT-2501) were purchased from Lonza for all the experiments. These cells are a mixed population of cells derived from the bone marrow of healthy adult individuals. Cells were maintained in bulletkit (Lonza) growth medium kit consisting of the MSC Basal medium (PT-3238) and the supplemental kit (PT-4105) as stated in the manufacturer's protocol to obtain passage 3 cells. The culture condition was 5% CO2, 37°C temperature and 90% relative humidity. For all the experiments, cells were seeded in a 75 cm^2 T-flask and passaged at 90% confluency at 5000 cells/ cm^2. Trypsin-EDTA (0.05%) was used for subculturing. The medium was replenished every 3 days. For mechanical memory experiments, passage 3 cells were seeded after directly thawing, serially passaged to passage 4 and passage 5 cells.

MSC culture on substrates with varying mechanical stiffness and cell density

Three substrate stiffness groups were prepared for cell culture. Soft: Sylgard 527 PDMS (*E*~5 kPa), medium stiffness: Sylgard 184 PDMS (*E*~1 MPa), and stiff: polymer resembling cell culture plastic (*E*~1 GPa). Those mechanical stiffness conditions represent the physiological bone marrow stiffness, pathological fibrotic condition, and the standard T-flask cell culture condition respectively. Cells were cultured on 8 well chamber slides (ibidi, 80821) with thin bottom for high-resolution imaging using a confocal microscope. For the stiff group, untreated polymer bottom slides or plastics were used followed by bovine Type 1 collagen coating (50 µg/ml, A10644-01, Gibco). For the soft and medium stiffness groups, the bottom polymer coverslip was removed, and custom-made chamber slides were refabricated with a thin PDMS substrate as described in the next section. For maintenance and subculture, cells were cultured in 60 mm diameter petri dishes, and the PDMS was cast directly inside those dishes. Petri dish groups were also treated with type 1 collagen to maintain the same protocol between experiments. Figure 16 details the workflow of the serial passaging experiments performed in this work.

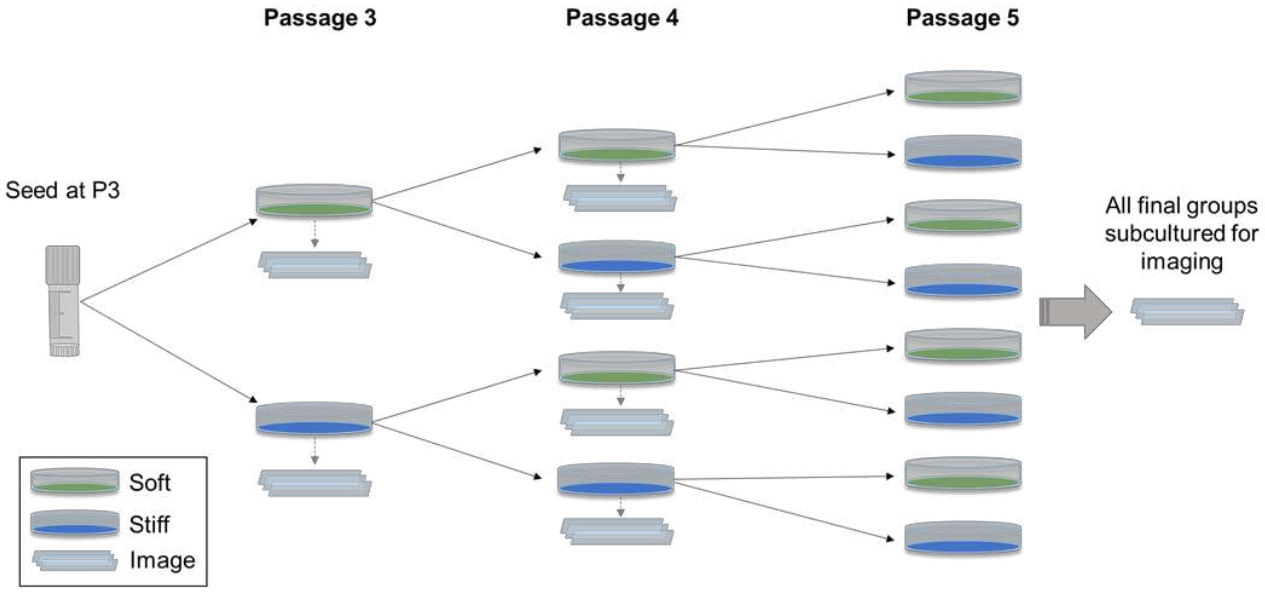

Figure 16. Schematic of the experimental workflow. For the investigation of mechanical stiffness and passaging-driven chromatin architecture change and epigenetic modifications. The passaging on soft to stiff vs soft to stiff substrates was designed to understand the effect of mechanical priming on the cell phenotype.

Preparation of thin PDMS substrate

Polydimethylsiloxane (PDMS) substrates were prepared using Sylgard 527 and Sylgard 184 (Dow Corning). To fabricate the thin soft PDMS substrate (~ 5 kPa), Sylgard 527 was mixed at a 1:1 ratio of each solution provided by the manufacturer. The mixture was then placed in a water bath at 37°C for 20-30 minutes to begin the curing process. Sylgard 184 thin PDMS sample was prepared by mixing ten parts of base with one part of curing agent and vigorous mixing. A small amount of each mixture (~70 µl) was distributed across a glass coverslip (24x60 mm). The glass coverslips were then placed in a vacuum chamber for 20 minutes to remove any bubbles. For attachment of the coverslip to the bottomless chamber slide (ibidi, 80821), the coverslip was partially cured for 2 hours at 75°C and Sylgard 184 (10:1 mixture) was used to mount the coverslip to the chamber slide. To completely cure, it was placed in a 75°C oven overnight. Cured PDMS was then plasma treated (BD-20AC, Electro-Technic) to facilitate the collagen coating. Then they were sterilized in the cell culture cabinet with a 70% ethanol soak under UV light for 20 minutes, followed by incubation in a type I collagen coating (50 µg/ml, A10644-01, Gibco) for 1 hour to improve cell attachment and proliferation. The stiff group with polymer bottom was also treated with the plasma and the same type I collagen solution to maintain the same biochemical treatment between the groups. Cells were seeded on these prepared substrates and cultured with the previously stated culture condition.

Live imaging of cell nucleus during cell attachment

Cells were seeded on thin PDMS or polymer bottom 8 well slides after directly thawing P4 cells. After thawing, cells were stained with Nucblue (ThermoFisher), a live stain for the DNA. Subsequently, time-lapse wide field images were obtained using the DAPI filter for 24 hours. 3D images were captured at each timepoint to ensure that an appropriate imaging plane could be obtained later, for the subsequent chromatin segregation index analysis.

Cell Staining for immunofluorescence, actin, and DNA

For all imaging tasks, cells were fixed with 4% PFA (in 1X PBS: Phosphate Buffer Solution) for 10 minutes at room temperature. Cells were permeabilized with 0.1% Triton X-100 in 1X PBS, washed with 1X PBS, and blocked for the non-specific binding sites with bovine serum albumin and normal goat serum. Primary antibodies were diluted in antibody dilution buffer and incubated overnight at 4°C. Next, secondary antibodies were diluted and added at room temperature for 2 hours. All antibodies were purchased from ThermoFisher Scientific. Then, cells were stained for the DNA using DAPI (ThermoFisher Scientific) and for the F-actin, using phalloidin conjugated with a fluorescent protein (ThermoFisher Scientific). Cells were imaged across their midsection using a confocal microscope (Zeiss LSM 980). Cells were imaged either at low resolution with 20X air objective or at high resolution with 63X oil objective for all subsequent analyses. For all imaging, the imaging setting (laser power, gain, etc.) was maintained constant between the groups. List of dilution of antibodies (all from Invitrogen): CD73-1:100, Runx2 – 1:100, ARID1A – 1:400, H3K9me3 – 1:400, H3K9Ac – 1:400. H3K27me3 and H3K4me3 were conjugated antibodies from Cell Science Technologies, and they were used at 1:50 dilution. All secondary antibodies (Invitrogen) were used at 1:200 dilution.

Quantification of cell and nuclear morphology and stress fiber formation

Cell area quantification: A custom MATLAB code was used to calculate the cell area.

Nuclear area and other geometrical parameters calculation: Nuclear morphology quantification was performed on the tiled images of the entire growth surface for robust image analysis. Images were binarized and watershed separation was applied to separate cells that were touching or very close using ImageJ. These images were then imported into MATLAB. Subsequently, disk structuring elements were created through the strel() function, to create masks over each identified nucleus, which were then smoothed and filled to create a solid element. The size filtering for the nucleus images was critical to avoid any small background particles that may remain or any nuclei that were not separated by the watershed function. The final allowable elements were labeled for later reference and then measured with the regionprops() function to calculate the nucleus area and circularity.

Quantification of chromatin architecture

To calculate chromatin segregation from the DAPI stained nucleus images, a technique was adapted from a previous approach described by Irianto et al. The high-resolution images of nuclei were cropped and apportioned into images of individual nuclei. To calculate the chromatin segregation index based on the DAPI stain, gradient-based Sobel edge detection algorithm produced an edge map, then a thinning algorithm reduced strong border edge lines so they could be excluded. Next, the edge areas were measured, and this value was divided by the cross-sectional area of the nucleus.

Quantification of immunofluorescence images

For quantification of protein fluorescence, 20x images of cells stained for DAPI, actin, and other proteins were imaged together. ImageJ was used for measuring the intensity values for each channel. Briefly, cells were randomly chosen throughout the well, and the cell and nucleus shapes were outlined and added as a region of interest (ROI). The mean intensity was then calculated by ImageJ in the ROI. For localization of the signal, the nuclear area was divided into inner, middle, and outer regions using a custom-made PYTHON code.

Cell treatments with drugs

Drug treatments were applied to understand the effect of targeting several key proteins in the MSC phenotype. For all drug treatments, cells were seeded on a soft substrate at passage 3 directly after thawing. After they reached confluency, cells were trypsinized and seeded on T25 flasks at 5000 cells/ cm^2. Drugs were applied 6 hours after cell seeding when the cells were completely attached. Actomyosin contraction in the cytoplasm was inhibited using Y27632 (Tocris Biosciences) at a concentration of 4 μM. All other drugs were purchased from Sigma Aldrich. Verteporfin (2 μM) was used to inhibit cytoplasmic YAP. CADD522 (2 μM) was used to inhibit Runx2. ARID1A function was blocked by using GSK126 (10 μM). H3K27me3 (10 μM) was downregulated by inhibiting EZH2 using GSK343. H3K9me3 (10 μM) was downregulated using the drug chaetocin which inhibits the methyltransferase SUV39H1/2. All the control groups for these experiments were vehicle-treated (DMSO). Cells were left in the medium for 3 days for subsequent harvesting by trypsinization and counting and gene expression analysis.

Cell counting and gene expression analysis

After trypsinization, cells were counted using a manual hematocytometer to estimate the total number of cells in the petri dish. Subsequently, total RNA was extracted from the cells using Qiagen total RNA Mini Kit, reverse transcribed into cDNA via Qiagen Reverse Transcription. Real-time quantitative PCR was performed with SsoAdvanced Universal SYBR Green Supermix in a CFX96 Touch thermocycler (all kits and devices from Bio-Rad Laboratories) using 10 ng of cDNA/reaction. All data was normalized to the reference genes GAPDH. Pre-designed and validated VEGF primer was purchased from IDT.

Statistical Analysis

Statistical analysis was performed using Student's t-test (RStudio). Results are expressed as mean ± standard deviation, with differences considered statistically significant at $p < 0.05$ or $p < 0.01$, as specified in the figure legends. Sample and replicate numbers are provided in the figure legends.

Results

Serial passaging on a soft substrate increases a stemness marker but decreases the chromatin segregation

Serial passaging on the soft substrate showed a gradually higher intensity of the CD73 marker, while serial passaging on a stiff substrate showed a gradually lower intensity of the CD73 marker (Figure 17A, B, B1.A). If the MSCs were first cultured on the soft substrate, their memory was retained later even though they were cultured on a stiff substrate later. Stiff priming with two rounds could not rescue the CD73 intensity even when they were cultured later on the soft substrate. However, culturing them first on soft, then on stiff, and then again on the soft substrate

shows that they can revert back to their stemness. Therefore, early priming after cell thawing seemed to be a decisive factor for cell fate and mechanical memory retention in later passages. Quantifying the chromatin segregation index (CSI), resulted in a counterintuitive finding (Figure 17C, B1.B). CSI is a marker of chromatin openness as stated in several previous studies including our own work [19–21]. Initially, we found that CSI is higher on soft and lower on the stiff substrate, as expected. With more passaging, the CSI value started becoming the same, and they were indistinguishable in passage 5 irrespective of their serial passaging history on soft vs stiff substrates. Investigation of Lamin A/C showed that stiff substrates lead to high intensity of Lamin A/C along with high-stress fiber formation, with the opposite trend seen on soft substrates by passage 5. Overall, this data suggests that CSI and resulting chromatin openness calculation is not an appropriate marker of MSC stemness after serial passaging. Therefore, we looked into the epigenetic modifiers which are a more specific measure of the overall active/ repressive status of MSCs.

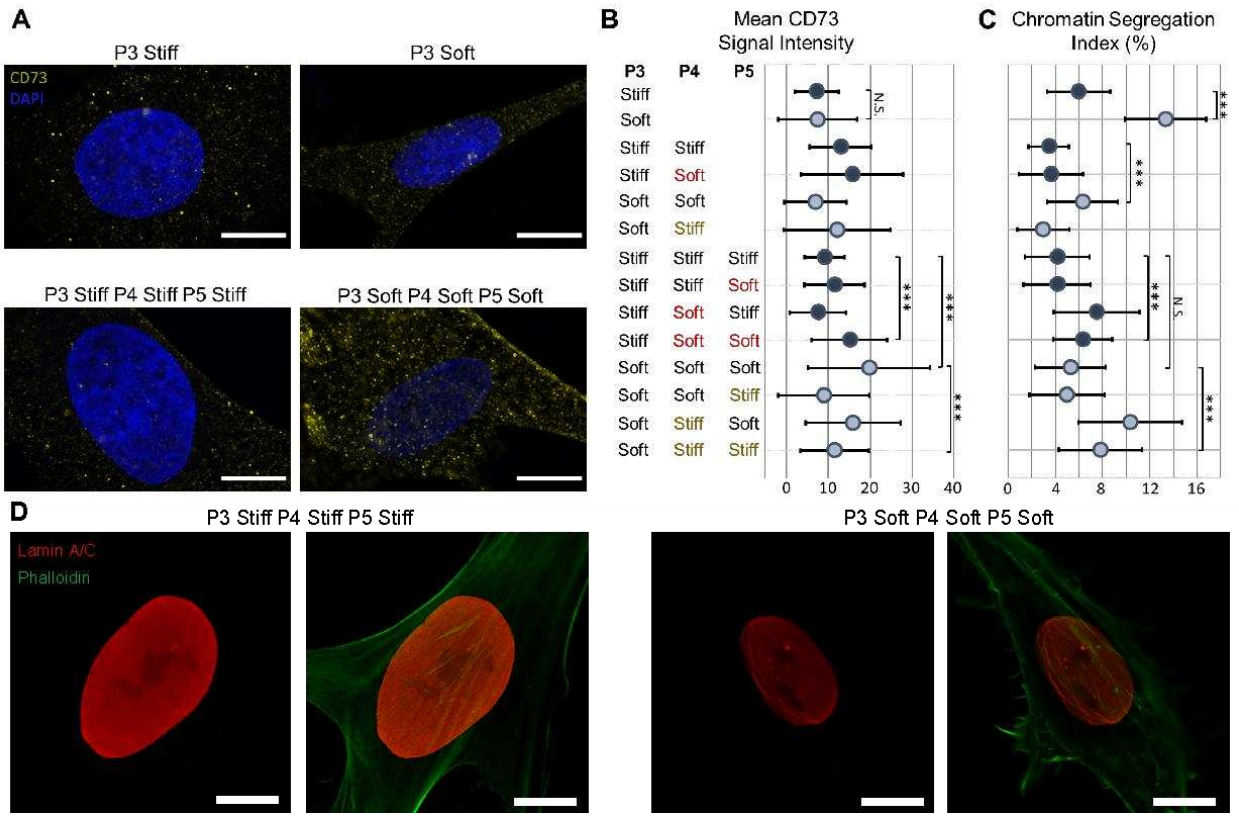

Figure 17. Mechanical stiffness of the substrate affects the intranuclear architecture, cytoskeletal architecture, and MSC phenotype. (A) Super-resolution images of the key groups showing higher CD73 intensity on soft substrates passaging through P5. (B) The stemness of MSCs gradually increases on soft substrate serial passaging, shown by quantification of the CD73 marker intensity. (C) Serial passaging of MSCs on the soft substrate keeps the overall chromatin architecture open compared to a stiff substrate in early passages, but chromatin architecture openness becomes quantitatively similar in later passages (D) Stiff substrate not only promotes a higher amount of stress fiber formation, but also it causes the Lamin A/C intensity in the nucleus. Results are reported based upon n > 20 nuclei for each group. Scale bar: 10 µm. *p<0.05, ** p<0.01, *** p<0.001.

Serial passaging leads to a flatter cell shape and more rounded nucleus on the stiff substrate

Next, we looked into some classic markers of MSC phenotype such as cell and nuclear area and shape (Figure 18, B2). We found that on the stiff substrate the cells were flatter, characterized by larger area, and nuclei were more rounded which changed to some extent with serial passaging. Interestingly, serial passaging on the soft substrate made the cells more elongated in later passages, and this mechanical memory of cell/ nuclear phenotype was retained when they were first cultured

on the soft substrate. Overall, this data from cell and nucleus shape or area shows the same trend as the changes in CD73, described in Figure 17.

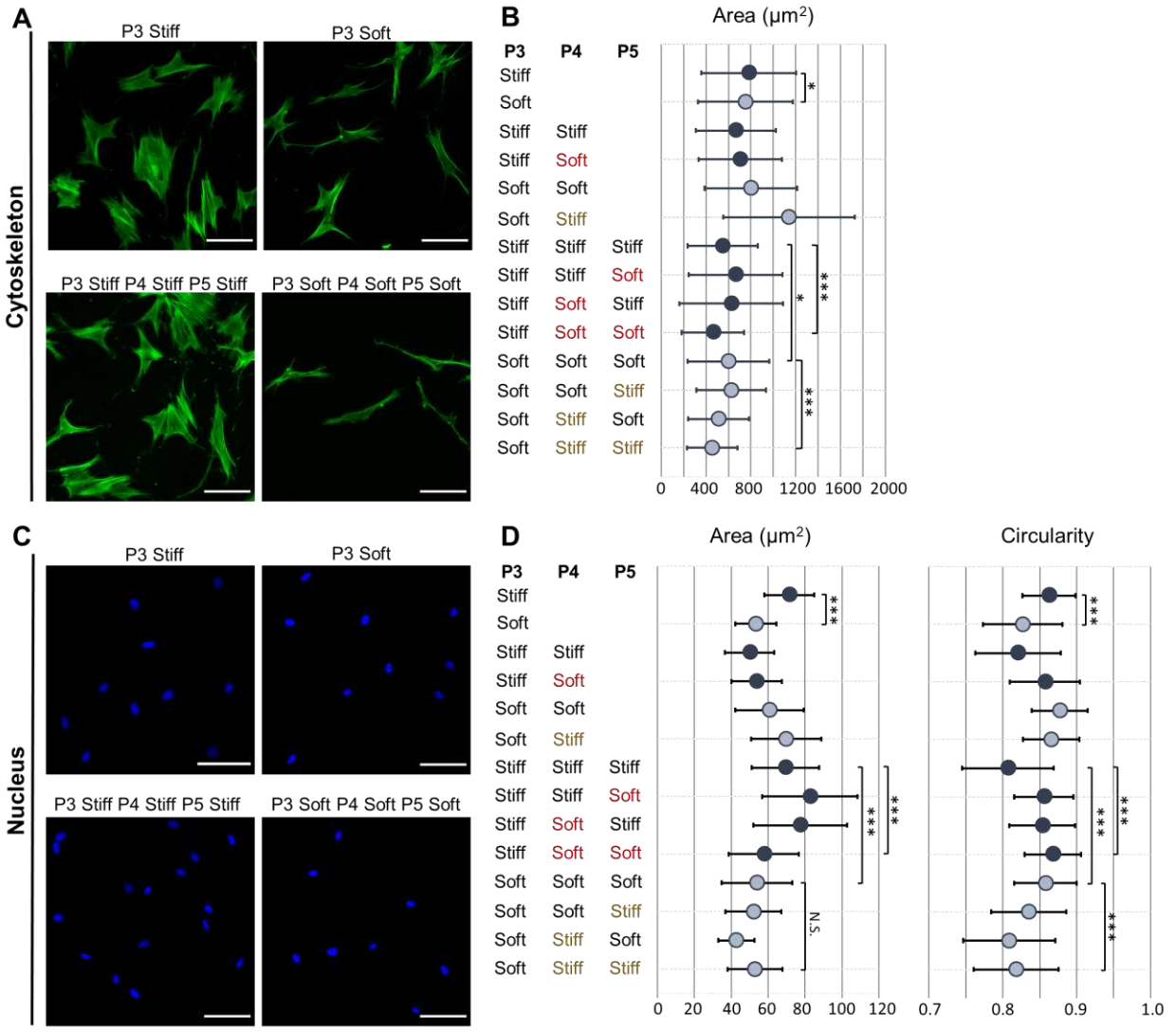

Figure 18. Mechanical stiffness of the substrate affects cell and nuclear geometric phenotype. Serial passaging on the soft substrate makes the cells more elongated and cell area decreases. (A) Representative images of cells along with the quantification of their area (B). (C) Representative images of nuclei along with the quantification of their area and circularity (D). Results are reported based upon n>1000 cells or nuclei for each group. Scale bar: 50 μm. *p<0.05, ** p<0.01, *** p<0.001.

Soft substrate affects the localization and expression of the facultative repressive marker H3K9me3 but not the constitutive repressive marker H3K27me3

Loss of stemness and hence, transcription of genes is associated with global repression. Therefore, we investigated the expression and localization of the repressive epigenetic markers H3K9me3 and H3K27me3 in the nucleus. H3K27me3 is a constitutive heterochromatin marker and H3K9me3 is a facultative marker that represents a more dynamic/ compliant region heterochromatin. When we looked into the nucleus, we found that in all groups, the H3K27me3 was mostly localized at the center of the nucleus, compared to the periphery (Figure 19 A, C). The intensity map showed that all the groups have the same intensity for H3K27me3 (Figure 20 A, B). This data suggests that the constitutive repressive modification characterized by H3K27me3 is probably not the key driver of epigenetic repression in MSCs during serial passaging.

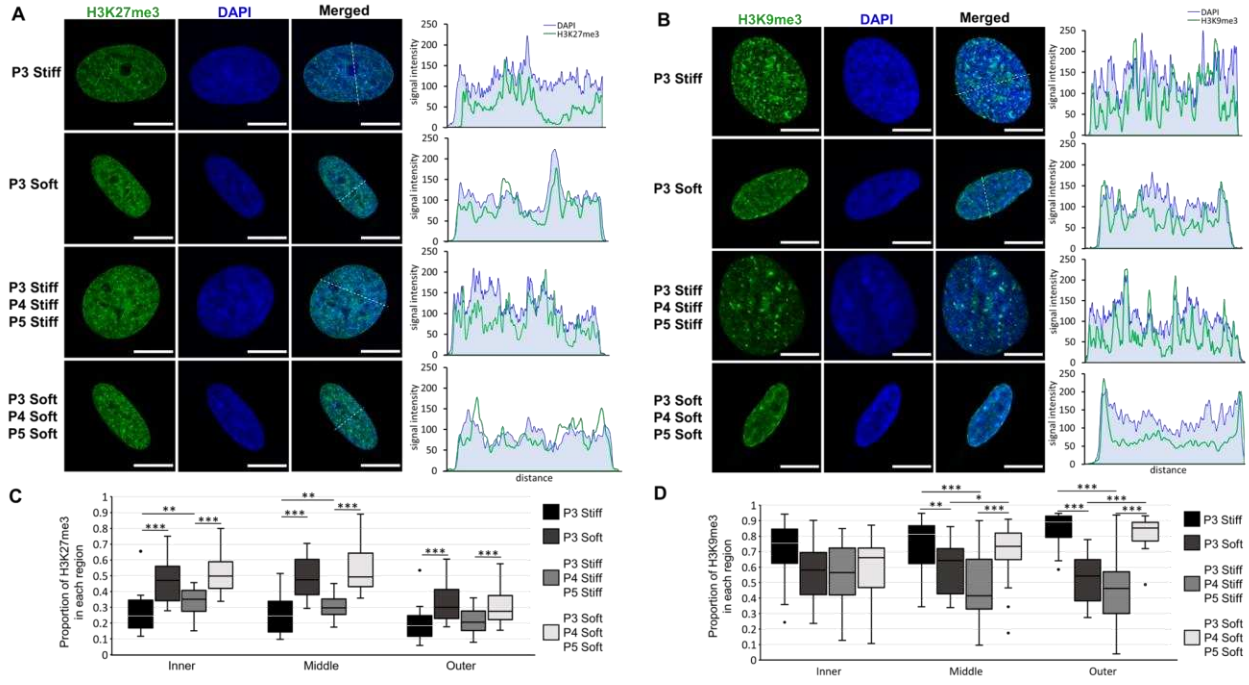

Figure 19. Gene repression-specific epigenetic markers have different localization on soft vs stiff substrates. Representative images of the nucleus stained for DNA and the repressive epigenetic markers H3K27me3 (A) and H3K9me3 (B). (C) Overall enrichment of the constitutive epigenetic marker H3K27me3 in the nucleus center does not change in a mechanics-dependent manner. (C) The facultative epigenetic marker H3K9me3 showed more peripheral enrichment on

the soft substrate in later passages compared to early passages. On the stiff substrate, it is homogeneously distributed throughout the nucleus, with larger puncta size in later passages. Results are reported based upon n>20 nuclei for each group. Scale bar: 10 μm. *p<0.05, ** p<0.01, *** p<0.001.

Interestingly, when we investigated the H3K9me3 marker, we found that it was more localized in the nuclear periphery on the soft substrate at passage 5, compared to passage 3 (Figure 19 B, D). For stiff substrates, H3K9me3 tends to be more localized as puncta in the entire nucleus and those puncta grew bigger over passaging on the stiff substrate. Overall, a key finding was that MSC culture on the soft substrate promotes the localization of H3K9me3 to the periphery, opening more regions inside the nucleus for gene transcription. Moreover, the intensity of H3K9me3 remained the same on the soft substrate while it increased on the stiff substrate by serial passaging (Figure 20 C, D, B3). Overall, this data shows that H3K9me3 is a key driver of mechanics-mediated chromatin architecture and repressive status during serial passaging of MSCs.

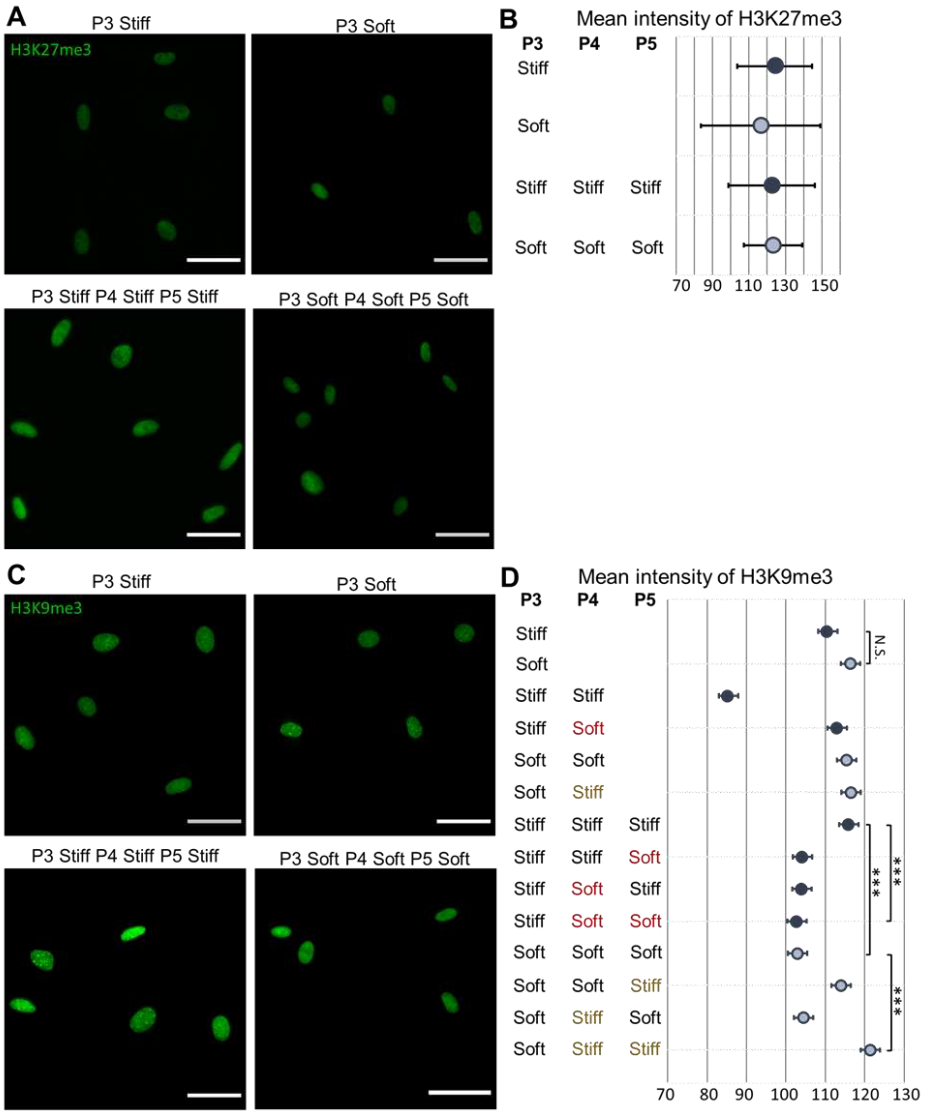

Figure 20. Gene repression-specific epigenetic markers have different expression levels on soft vs stiff substrates. (A) Representative images of H3K27me3 intensity levels for each group. (B) Quantification of H3K27me3 intensity level shows no significant changes based on the substrate stiffness. (C) Representative images of H3K9me3 intensity levels for each group. (D) H3K9me3 intensity increases on the stiff substrate with serial passaging. Results are reported based upon n>20 nuclei for each group. Scale bar: 50 μm. N.S. $p>0.05$, *** $p<0.001$.

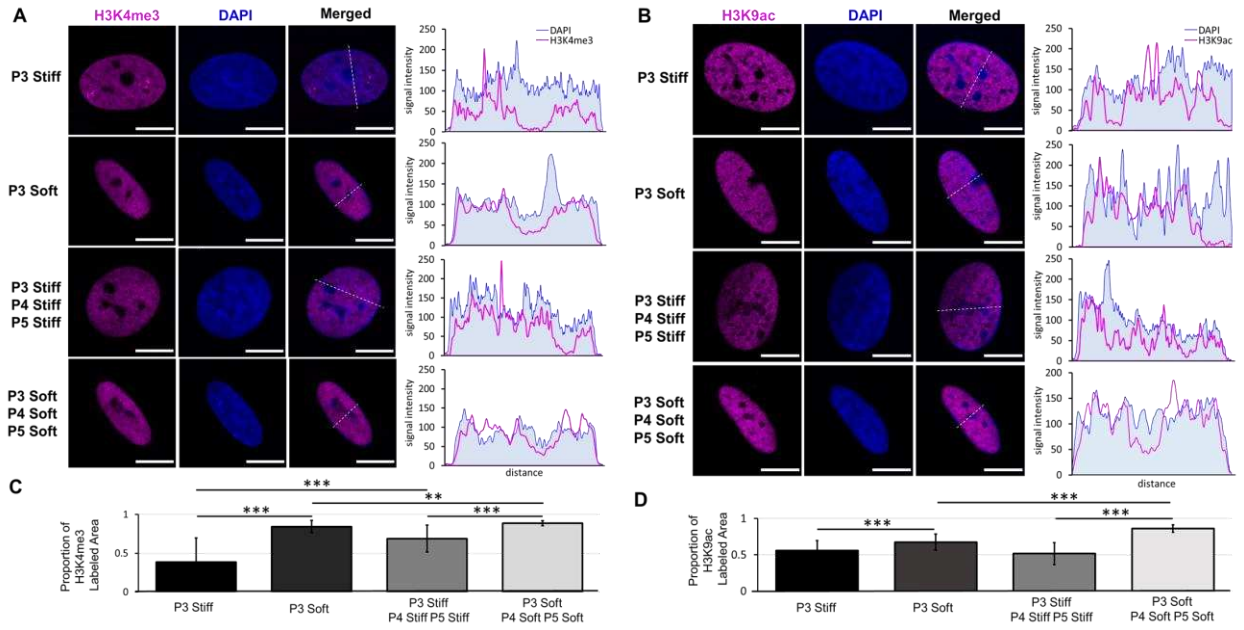

Figure 21. Gene activation-specific epigenetic markers localize differently on soft vs stiff substrates. Representative images of the nucleus stained for DNA and the active epigenetic markers H3K4me3 (A) and H3K9ac (B). (C,D) Both transcriptionally active markers H3K9ac and H3K4me3 show a higher proportion of nuclear localization on soft substrate. They did not show any peripheral enrichment or central enrichment – as compared to the transcriptionally repressive markers. Results are reported based upon n>20 nuclei for each group. Scale bar: 10 µm. ** p<0.01, *** p<0.001.

Soft substrate promotes a higher localization of active epigenetic markers in the nucleus

Because the soft substrate promotes MSC stemness, we wanted to look into key epigenetic drivers of such MSC behavior. When we looked into the H3K9ac and the H3K4me3 markers, we found that on P3 the H3K9ac labeled area was high in the nucleus on the soft substrate which further increased with passaging (Figure 21 B, D, B4.A). The same behavior was visible for the H3K4me3 marker. The stiff substrate had an H3K9ac level lower than soft which stayed low on stiff. However, on the stiff substrate, the H3K4me3 labeled area in the nucleus also increased with passaging. This was a bit surprising because H3K4me3 was also supposed to stay low on the stiff substrate. When we looked into the overall intensity values of these markers (Figure 22, B4.B) it

showed the same trend as their proportional enrichment as shown in Figure 21. Of note, we did not find any specific localization of the markers in the nucleus, such as in the center vs the peripheral regions. Overall, this data suggests that H3K9ac is a more dynamic active epigenetic modifier compared to H3K4me3 in the context of mechanics-driven epigenetic changes in MSCs.

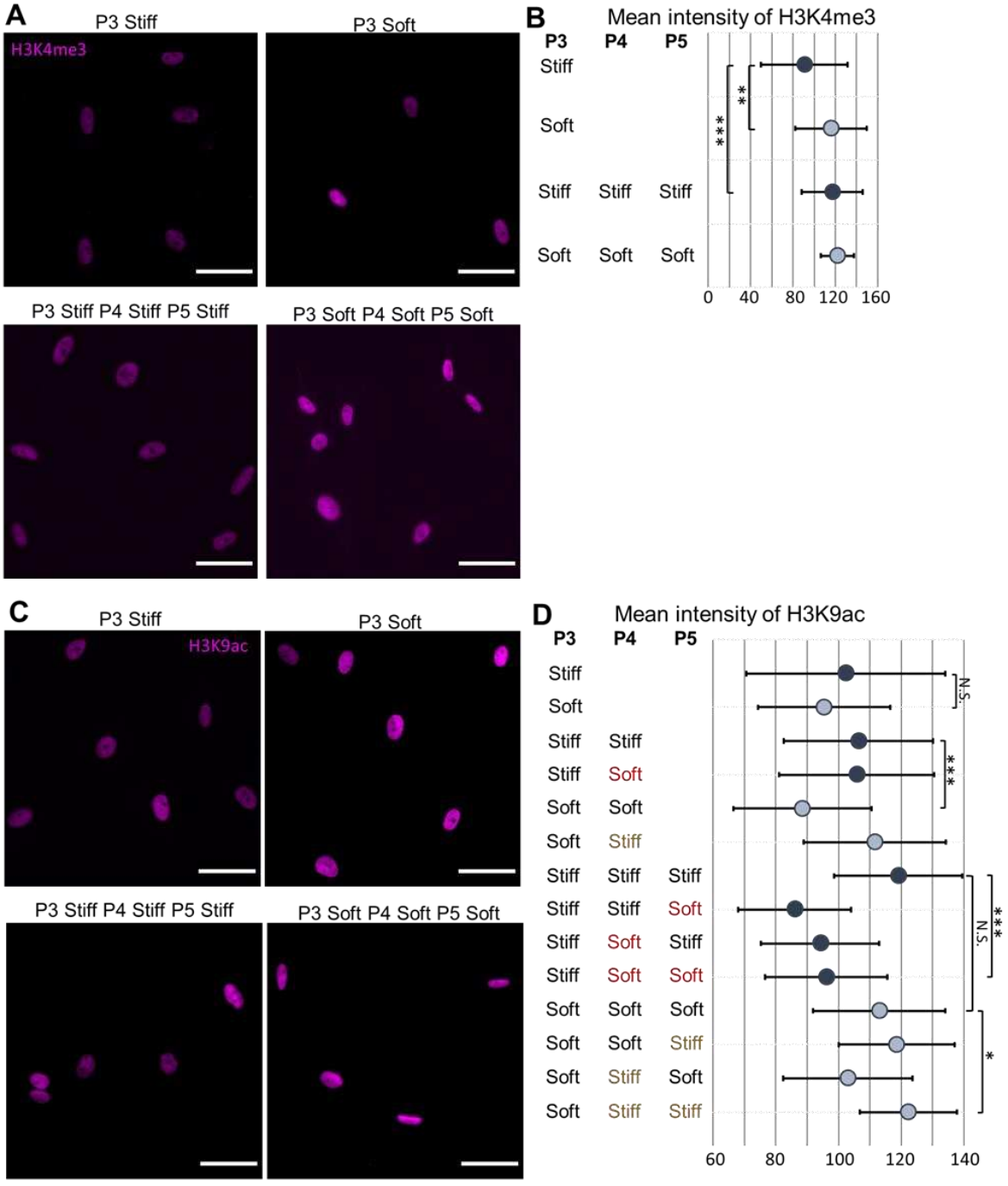

Figure 22. Gene activation-specific epigenetic markers have different expression levels on soft vs stiff substrates. (A) Representative images of H3K4me3 intensity levels for each group. (B) Quantification of H3K4me3 intensity level shows no significant changes based on the substrate stiffness. (C) Representative images of H3K9ac intensity for each group. (D) H3K9ac intensity levels are more dynamic and sensitive to substrate stiffness. Results are reported based upon n>20 nuclei for each group. Scale bar: 50 µm. N.S. p> 0.05, *p<0.05, *** p<0.001.

Soft substrate promotes the increased activity of SWI/SNF chromatin remodeling complex

Histone acetylation and methylations are signatures of chromatin architecture status in MSCs. However, it is not clear what really causes the chromatin architecture change. Of note, H3K9me3 showed more peripheral enrichment on the soft substrate, especially during serial passaging. This suggests that the chromatin is dynamic on the soft substrate. To investigate the possible cause of such dynamic chromatin architecture, we visualized ARID1A, the core subunit of the CRC SWI/SNF. SWI/SNF is highly conserved in mammals in cells and has never been investigated before in the context of mechanobiology of MSCs. We found that on the soft substrate the intensity of ARID1A is high, but also, large clusters form, which further increases in the later passage (Figure 23 A-C, B5). On the stiff substrate, the intensity is not only low but they also make smaller puncta which further decreases in size in later passages. We further found that the gene expression of several SWI/SNF CRC complex subunits also increased on the soft substrate (Figure 23 D, E). When the MSCs on the stiff substrate were treated with cytoskeletal mechanics disrupting drugs, their expression increases again, indicating a clear role of mechanics in gene expression. Overall, this data suggests that SWI/SNF CRC-mediated chromatin remodeling is critical to maintain the stemness and to maintain the dynamic chromatin architecture for MSCs on the soft substrate.

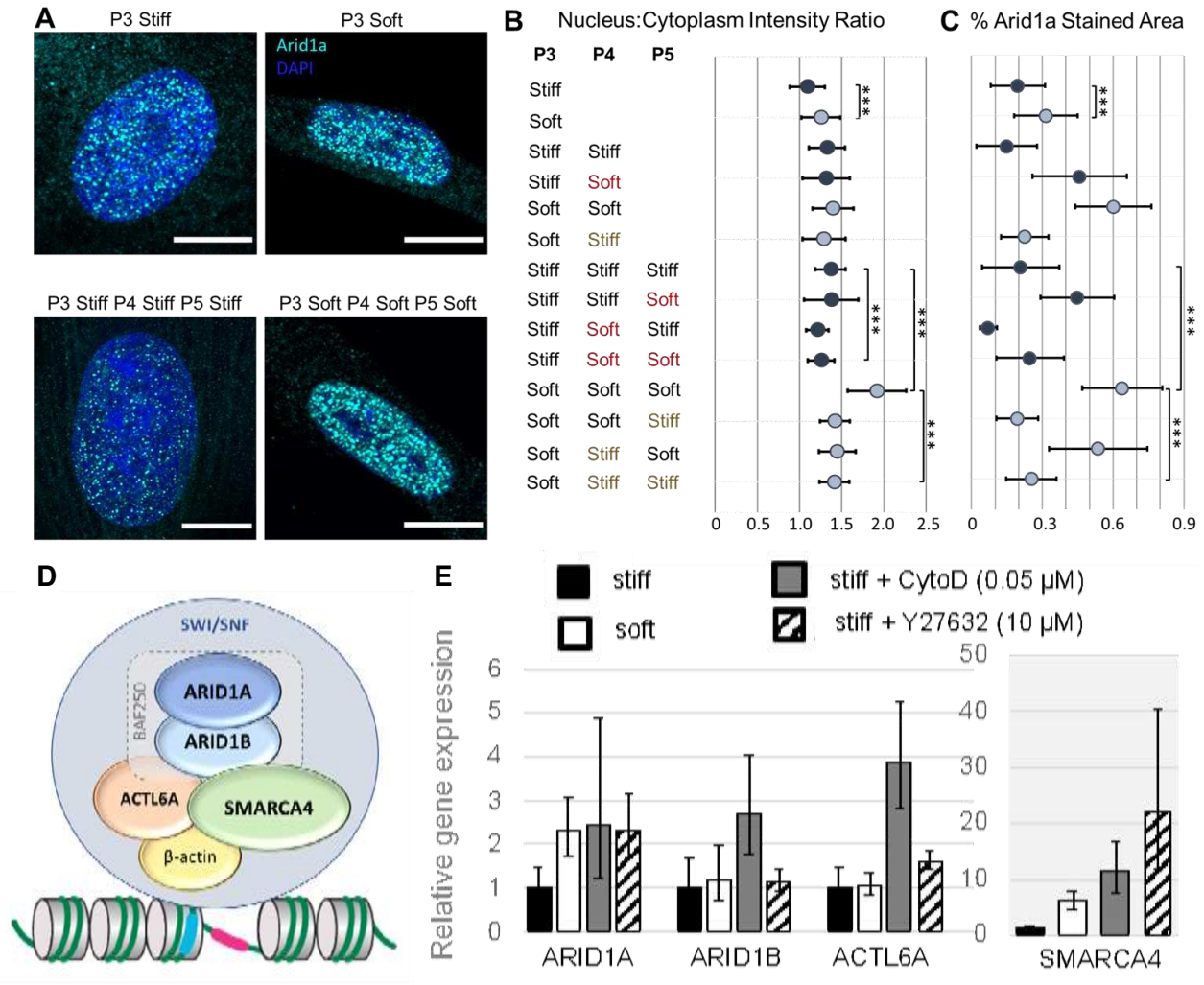

Figure 23. MSC stemness is associated with high SWI/SNF core complex activity in a mechanics-dependent manner. (A) Representative images of nuclei stained for DAPI and ARIDA, demonstrating the nucleus localization within the nucleus. (B) Quantification of the ARID1A localization in the nucleus (n>20 cells per group). (C) To examine the clusters of ARID1A in the nucleus, the percent Arid1a-stained area within the nucleus was quantified (n>20 nuclei per group). (D) Schematic of the SWI/SNF complex key subunits. (E) Gene expression of the SWI/SNF subunits in a mechanics-dependent manner. Mean reported with min/max bars from one sample per group run in triplicate. Scale bar: 10 μm. *** p<0.001.

Chromatin segregation has slowed temporal dynamics

So far, our data suggested that chromatin is dynamic in a mechanics-dependent manner. Next, we were curious to understand how chromatin segregation changes once seeded under two different mechanical conditions. To investigate this, we seeded P4 cells on soft and stiff substrates and

tracked the chromatin segregation index in living cells using a live nuclear stain (Figure 24). We found that for the first two hours of cell seeding, the CSI values are similar but later over 24 hours the CSI value changes. The MSCs on the soft substrate end up with a higher CSI value while MSCs on the stiff substrate end up with a lower CSI value. Overall, this data suggests that early during the cell seeding the mechanobiological pathways can be intervened to potentially maintain high stemness in MSCs even though they are previously cultured on a stiff substrate. This data corresponds with the overall chromatin condensation and increased H3K9me3 expression in MSCs cultured on the stiff substrate.

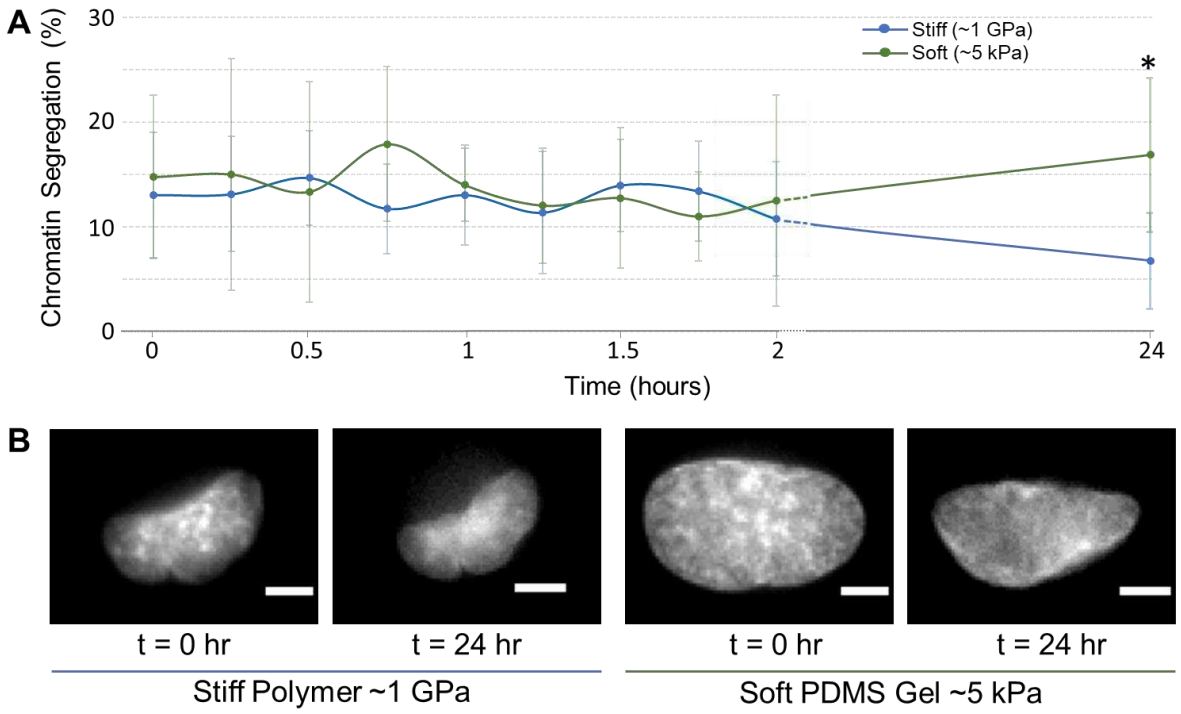

Figure 24. Chromatin architecture change occurs early but stabilizes in the longer term after seeding the cells. (A) Quantification of chromatin segregation over time (n = 2-5 nuclei per group). On the soft substrate, the chromatin segregation index increases over 24 hours while on the stiff substrate it decreases. (B) Representative images of nuclei on each substrate at the beginning and end points. Scale bar: 5 µm. *p<0.05.

Targeting the mechanobiological and epigenetic pathways is a potential strategy to maintain MSC stemness

From a preliminary study, we found that adding intervening drugs during the seeding process causes a completely abnormal cell and nuclear shape. Accordingly, we added the drugs 6 hours after cell seeding when the cells are well attached but have not completely committed to a phenotype. As a functional measure, we quantified the VEGF expression of the drug-treated cells and compared it with the control group. The rationale of the drug treatment is shown in Figure 25A, in a proposed mechanobiological model. We found, with the exception of GSK126 treatment, that cell proliferation is maintained similarly in the control case even on the stiff substrate. The halt of proliferation by GSK126, which blocks the chromatin remodeling drastically, is not surprising as chromatin condensation requires the SWI/SNF CRC, and halting that will stop cell division.

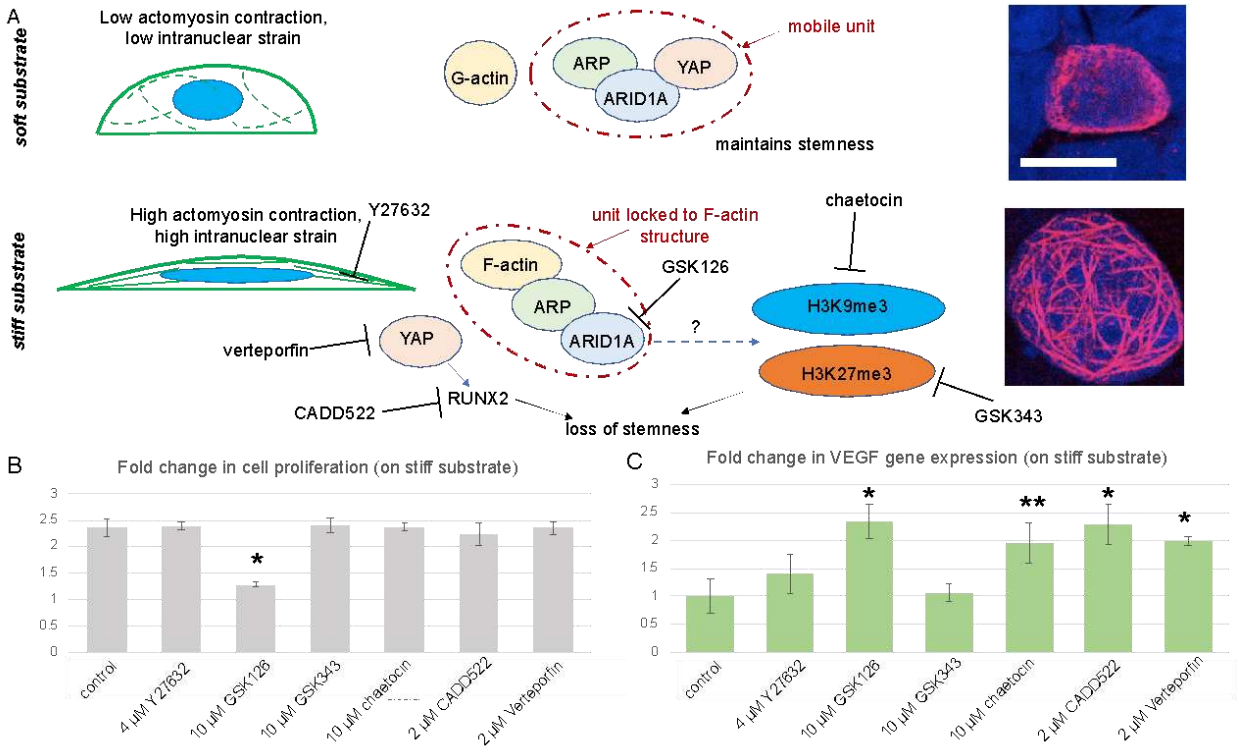

Figure 25. Mechanistic understanding-based targeting has the potential to expand MSCs to larger numbers without compromising the MSC phenotype. (A) Soft substrates exhibit more MSC-like phenotypes and show less actomyosin contraction and low intranuclear strain. Monomeric G-actin is present in the nucleus, leaving ARP, ARID1A, and YAP to form one unit that is mobile within the nucleus. Stiff substrates exhibit high actomyosin contraction and intranuclear strain. This leads to the presence of nuclear F-actin (bottom nucleus image) which binds to ARP and ARID1A to form a unit that is locked in place. The use of select inhibitors used experimentally target the specified locations within the diagram. (B) Cell number after treatment with the listed inhibitors. Only treatment with GSk126 had a significant decrease in cell count from the stiff control group. (C) VEGF gene expression evaluation after treatment with the listed inhibitors. *p< 0.05, **p<0.01, based on three technical replicates.

When we investigated the VEGF expression of the drug-treated group compared to the control group, we found that GSK126 treatment increases the VEGF expression, but it is translationally not beneficial because it leads to a low number of cells. However, blocking the H3K9me3, Runx2 and YAP causes significantly higher VEGF gene expression along with high cell proliferation opening possibilities of using those drugs for scalable MSC expansion.

Discussion

In this study, we demonstrated a mechanics-dependent memory aspect to the epigenetic landscape in MSCs during 2D culture. We found that serial passaging on soft substrates resulted in cells with increased expression of stemness-associated markers accompanied by an MSC-like phenotype. This may be advantageous in therapeutic applications because problems with fibrotic tissue post-transplantation could be mitigated with soft substrate priming. For a better mechanistic understanding, repressive and active epigenetic markers were evaluated.

Distinct localization patterns of epigenetically marked chromatin were seen in a substrate-dependent manner. Soft substrates localized the repressive H3K9me3 mark to the nuclear periphery, opening up the nuclear interior, accompanied by a corresponding increase in the active

H3K9ac and H3K4me3 marked chromatin. This study identified H3K9me3 and H3K9ac as the key drivers of mechanics-mediated chromatin architecture changes and genetic status during serial passaging. H3K9me3 being functionally relevant is not unique to MSCs but is seen in other cell types as well [22, 23], such as distinct reorganization of H3K9me3 under nuclear deformation in contractile cardiomyocytes [24]. This is reasonable because though H3K9me3 is generally considered a constitutive heterochromatin modification, genome-wide studies have shown a clear role in stem cells as a facultative heterochromatin, explaining the dynamics we see in this study [25].

The SWI/SNF complex is well studied in other cell systems and is a known inhibitor of YAP in cancer cells [26], but has not been investigated regarding MSC mechanotransduction. This inhibitory interaction that occurs between SWI/SNF and YAP occurs in cells experiencing low stress. Under stress and the subsequent formation of nuclear F-actin, however, the SWI/SNF complex binds to the F-actin and YAP can no longer bind. In this study, soft substrates exhibit more MSC-like phenotypes and show less actomyosin contraction and low intranuclear strain. Monomeric G-actin is thus present in the nucleus, leaving ARP, ARID1A, and YAP to form one unit that is mobile within the nucleus. This bound YAP is thus unavailable as a transcription factor, and stemness is maintained. On the other hand, stiff substrates exhibit high actomyosin contraction and intranuclear strain. This leads to the presence of nuclear F-actin which binds to ARP and ARID1A to form a unit that is essentially locked in place. YAP is now free to act as a transcription factor, initiating the Runx2 pathway, leading the cells down the osteoprogenitor pathway. By using select inhibitors to target various proteins within this pathway, we can obtain a large amount of MSCs without compromising their function. The drug targets used in this study showed promising

results in terms of maintaining proliferation without decreasing functionality when culturing cells on standard tissue culture plastic.

This study provides new mechanistic insight into the mechanical memory of MSCs and proposes specific targets within the pathway to intervene in order to maintain high proliferation as well as the MSC's beneficial properties. The major limitation of this study is that despite considerable characterization, the connecting dots are still missing. VEGF is a good preliminary indicator but performing RNA-seq with a soft and stiff control in combination with the drug treatments would give a more complete picture. Further studies are needed to understand the actin-driven process and how the histone modifications happen downstream of SWI/SNF, if at all.

REFERENCES

1. Aras, S. (2015). *Role of SWI/SNF Chromatin Remodeling Enzymes in Melanocyte Differentiation and DNA Damage Response to Ultraviolet Radiation*. University of Toledo.

2. Engler, A. J., Sen, S., Sweeney, H. L., & Discher, D. E. (2006). Matrix Elasticity Directs Stem Cell Lineage Specification. *Cell*, *126*(4), 677–689. https://doi.org/10.1016/J.CELL.2006.06.044

3. Ghosh, S., Seelbinder, B., Henderson, J. T., Watts, R. D., Scott, A. K., Veress, A. I., & Neu, C. P. (2019). Deformation Microscopy for Dynamic Intracellular and Intranuclear Mapping of Mechanics with High Spatiotemporal Resolution. *Cell Reports*, *27*(5), 1607-1620.e4. https://doi.org/10.1016/j.celrep.2019.04.009

4. Le, H. Q., Ghatak, S., Yeung, C. Y. C., Tellkamp, F., Günschmann, C., Dieterich, C., … Wickström, S. A. (2016). Mechanical regulation of transcription controls Polycomb-mediated gene silencing during lineage commitment. *Nature Cell Biology*, *18*(8), 864–875. https://doi.org/10.1038/ncb3387

5. Kureel, S. K., Mogha, P., Khadpekar, A., Kumar, V., Joshi, R., Das, S., … Majumder, A. (2019). Soft substrate maintains proliferative and adipogenic differentiation potential of human mesenchymal stem cells on long-term expansion by delaying senescence. *Biology Open*, *8*(4). https://doi.org/10.1242/bio.039453

6. Gerardo, H., Lima, A., Carvalho, J., Ramos, J. R. D., Couceiro, S., Travasso, R. D. M., … Grãos, M. (2019). Soft culture substrates favor stem-like cellular phenotype and facilitate reprogramming of human mesenchymal stem/stromal cells (hMSCs) through mechanotransduction. *Scientific Reports*, *9*(1), 1–18. https://doi.org/10.1038/s41598-019-45352-3

7. Killaars, A. R., Grim, J. C., Walker, C. J., Hushka, E. A., Brown, T. E., & Anseth, K. S. (2019). Extended Exposure to Stiff Microenvironments Leads to Persistent Chromatin Remodeling in Human Mesenchymal Stem Cells. *Advanced Science*, *6*(3). https://doi.org/10.1002/advs.201801483

8. Alfert, A., Moreno, N., & Kerl, K. (2019). The BAF complex in development and disease. *Epigenetics and Chromatin*, *12*(19). https://doi.org/10.1186/s13072-019-0264-y

9. Chen, D.-M., & Zhong, X.-Q. (2015). SWI/SNF Chromatin Remodeling Complex in Regulating Mesenchymal Stem Cell Lineage Specification. *Journal of Tissue Science & Engineering*, *06*(03), 1–5. https://doi.org/10.4172/2157-7552.1000154

10. Hadidy, N. El, & Uversky, V. N. (2019). Intrinsic disorder of the baf complex: Roles in chromatin remodeling and disease development. *International Journal of Molecular Sciences*, *20*(21). https://doi.org/10.3390/ijms20215260

11. Xu, F., Flowers, S., & Moran, E. (2012). Essential role of ARID2 protein-containing SWI/SNF complex in tissue-specific gene expression. *Journal of Biological Chemistry*, *287*(7), 5033–5041. https://doi.org/10.1074/jbc.M111.279968

12. Pagliaroli, L., & Trizzino, M. (2021, March 4). The Evolutionary Conserved SWI/SNF Subunits ARID1A and ARID1B Are Key Modulators of Pluripotency and Cell-Fate Determination. *Frontiers in Cell and Developmental Biology*. Frontiers Media S.A. https://doi.org/10.3389/fcell.2021.643361

13. Lei, I., West, J., Yan, Z., Gao, X., Fang, P., Dennis, J. H., … Wang, Z. (2015). BAF250a protein regulates nucleosome occupancy and histone modifications in priming embryonic stem cell differentiation. *Journal of Biological Chemistry*, *290*(31), 19343–19352. https://doi.org/10.1074/jbc.M115.637389

14. Yan, Z., Wang, Z., Sharova, L., Sharov, A. A., Ling, C., Piao, Y., … Ko, M. S. H. (2008). BAF250B-Associated SWI/SNF Chromatin-Remodeling Complex Is Required to Maintain Undifferentiated Mouse Embryonic Stem Cells. *Stem Cells*, *26*(5), 1155–1165. https://doi.org/10.1634/stemcells.2007-0846

15. Sinha, S., Biswas, M., Subhra Chatterjee, S., Kumar, S., & Sengupta, A. (2020). Pbrm1 Steers Mesenchymal Stromal Cell Osteolineage Differentiation by Integrating PBAF-Dependent Chromatin Remodeling and BMP/TGF-β Signaling. *Cell Reports*, *31*. https://doi.org/10.1016/j.celrep.2020.107570

16. Chang, C.-Y., Shipony, Z., Kuo, A., Loh, K. M., Greenleaf, W. J., & Crabtree, G. R. (2021). Increased ACTL6A Occupancy Within mSWI/SNF Chromatin Remodelers Drives Human Squamous Cell Carcinoma. *bioRxiv*, 2021.03.22.435873. https://doi.org/10.1101/2021.03.22.435873

17. Lammerding, J., & Kirby, T. J. (2018). Emerging views of the nucleus as a cellular mechanosensor. *Nature Cell Biology*, *20*(4), 373–381. https://doi.org/10.1038/s41556-018-0038-y.Emerging

18. Walker, C. J., Crocini, C., Ramirez, D., Killaars, A. R., Grim, J. C., Aguado, B. A., … Anseth, K. S. (2021). Nuclear mechanosensing drives chromatin remodelling in persistently activated fibroblasts. *Nature Biomedical Engineering*. https://doi.org/10.1038/s41551-021-00709-w

19. Killaars, A. R., Grim, J. C., Walker, C. J., Hushka, E. A., Brown, T. E., & Anseth, K. S. (2019). Extended exposure to stiff microenvironments leads to persistent chromatin remodeling in human mesenchymal stem cells. *Transactions of the Annual Meeting of the Society for*

Biomaterials and the Annual International Biomaterials Symposium, *40*, 670. https://doi.org/10.1002/advs.201801483

20. Kaonis, S., Aboellail, Z., & Ghosh, S. (2022). Characterization of Mechanics Driven Heterogeneity in Mesenchymal Stromal Cells. *bioRxiv*, 2022.07.25.501486. https://doi.org/10.1101/2022.07.25.501486

21. Gaspar-Maia, A., Alajem, A., Meshorer, E., & Ramalho-Santos, M. (2011). Open chromatin in pluripotency and reprogramming. *Nature reviews. Molecular cell biology*, *12*(1), 36. https://doi.org/10.1038/NRM3036

22. Nava, M. M., Miroshnikova, Y. A., Biggs, L. C., Niessen, C. M., Dahl, K. N., & Wickströ M Correspondence, S. A. (2020). Heterochromatin-Driven Nuclear Softening Protects the Genome against Mechanical Stress-Induced Damage. *Cell*, *181*, 800-817.e22. https://doi.org/10.1016/j.cell.2020.03.052

23. Sun, J., Chen, J., Mohagheghian, E., & Wang, N. (2020). Force-induced gene up-regulation does not follow the weak power law but depends on H3K9 demethylation. Retrieved from https://www.science.org

24. Seelbinder, B., Ghosh, S., Schneider, S. E., Scott, A. K., Berman, A. G., Goergen, C. J., … Neu, C. P. (2021). Nuclear deformation guides chromatin reorganization in cardiac development and disease. *Nature Biomedical Engineering*, *5*, 1500–1516. https://doi.org/10.1038/s41551-021-00823-9

25. Becker, J. S., Nicetto, D., & Zaret, K. S. (2016). H3K9me3-Dependent Heterochromatin: Barrier to Cell Fate Changes. *Trends in genetics : TIG*, *32*(1), 29. https://doi.org/10.1016/J.TIG.2015.11.001

26. Chang, L., Azzolin, L., di Biagio, D., Zanconato, F., Battilana, G., Lucon Xiccato, R., … Piccolo, S. (2018). SWI/SNF as mechanoregulated inhibitor of YAP/TAZ. *Nature*, *563*(7730), 265. https://doi.org/10.1038/S41586-018-0658-1

CHAPTER 4: INVESTIGATION OF THE PHYSIOXIA RELATED PATHWAYS IN MSC PROLIFERATION

Background

Bone marrow derived MSCs are traditionally cultured under 20% oxygen (hyperoxia) in the cell culture incubator, yet human bone marrow oxygen tension (physioxia) can range from less than 1% to 6% [1], which is a considerably low oxygen tension compared to the incubator. This discrepancy between *in vitro* and *in vivo* growth conditions can cause a major change in MSC performance (Figure 26) [2]. Physioxic culture of stem cells has been studied in a variety of cell types and has been shown to increase the proliferation and differentiation capacity of MSCs [3] and other stem cells, while also providing better immunomodulatory effects.

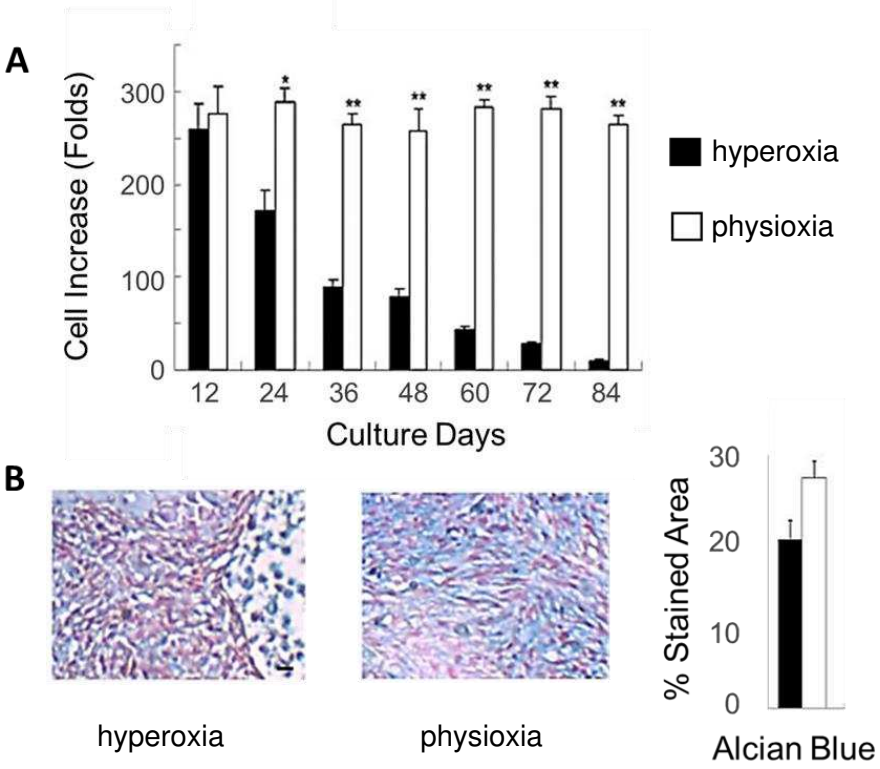

Figure 26. MSCs maintain expansion rate and differentiation capacity better under physioxia. (A) Cell number is maintained throughout long-term culture under normoxia, whereas it is significantly lowered over time under normoxia. (B) Hyperoxic and physioxic cells at passage 6

were induced to chondrogenic differentiation for 21 days followed by Alcian Blue staining. Adapted from Tsai et al. (2011).

MSC Performance Under Physioxia: Multiple Pathways Intersect

Ohnishi et al. [4] examined the gene expression profiles for bone marrow-derived mononuclear cells and their MSC subpopulation under hyperoxic and physioxic conditions in depth. Focusing on genes that encode secretory proteins in cells under physioxia, they found that the genes upregulated in the mononuclear, mixed population cells were proinflammatory cytokines. Meanwhile, the secretory protein genes upregulated in physioxic MSCs were related to cell proliferation and survival, such as vascular endothelial growth factor (VEGF) [4]. VEGF provides crucial signaling for angiogenesis, promoting vascularization in normal wound healing as well, being involved in various cellular processes. Evidence suggests that diabetes attenuates VEGF production and diminished levels have been observed in the myocardial tissue of diabetic patients as well as in animal models of diabetic wound repair [5, 6]. In diabetes, multiple tissues are low in oxygen, with physioxia representing an early event in the development and progression of diabetic neuropathy [7]. The normal adaptive responses to physioxia are impaired in diabetes patients due to hyperglycemia and elevated fatty acid levels that inhibit HIF-1α stability and function [8]. VEGF expression is associated with plenty of beneficial cellular processes while also being a downstream target of the physioxic pathway, so it is a logical marker to investigate.

HIF-1α is one factor that is overexpressed under physioxia. Sun et al. over-expressed HIF-1α in MSC-conditioned medium to rescue hypoxia-injured human umbilical cord vein endothelial cells, mitigating their impaired angiogenic ability, migratory function, and proliferation [9]. Such increased VEGF expression through physioxic treatment could positively impact the MSC clinical

outcomes for cell therapies (Figures 27 and 28). There are other factors that come into effect proliferation, such as the cyclin-dependent kinase inhibitor p21.

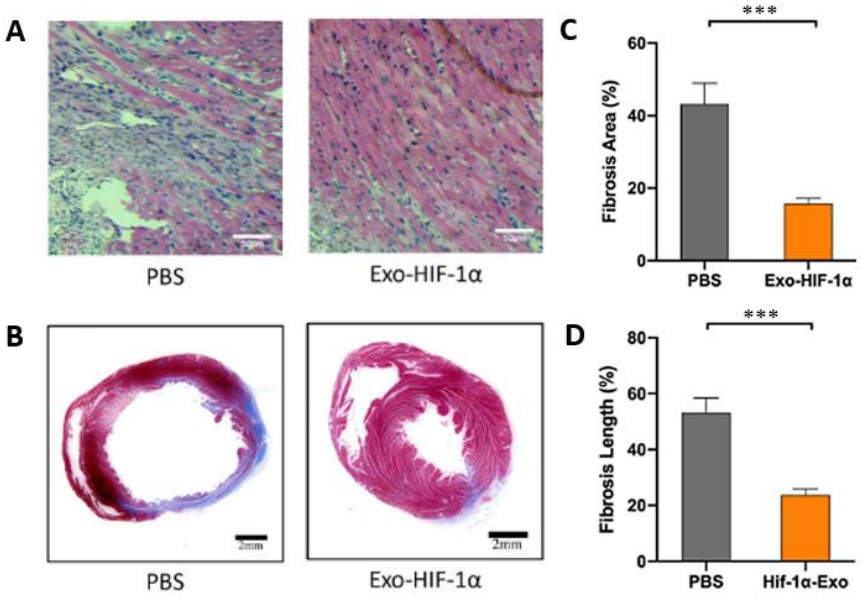

Figure 27. Histological assessment of the effect of physioxia primed MSC exosomes on an infarcted heart. (A) H&E staining showed different levels of fibrocyte infiltration in the ischemic area. (B) Masson trichrome staining of heart slides at 28 days after myocardial infarction: red, myocardium; blue, scarred fibrosis. (C), (D) percentage of fibrotic area and length calculated and averaged. ***p<0.001, n = 5. Adapted from J.Sun et al (2020).

Lv et al. [10] overexpressed HIF-1α through transfection in murine BM-MSCs resulting in significantly increased cell viability and a decrease in apoptotic cells as well as significantly suppressing the level of p21. HIF-1α knockdown produced the opposite effect in every case, except for p21 levels which did not change significantly from the control levels [10]. This indicates that p21 is involved in a separate HIF-1α-independent pathway that needs to be considered while investigating the combined effect of HIF-1α and p21 under physioxia.

Tsai et al. (2011) [2] evaluated MSC performance under physioxia and found that physioxic culture increases expansion efficiency (Figure 28), decreases senescence, and maintains

MSC properties by suppressing p21 expression. siRNA against p21 in hyperoxic cells enhanced proliferation and increased differentiation potential, whereas overexpression of p21 in physioxic cells induced a decrease in proliferation and a loss of differentiation capacity [2]. In a similar study, knockout of p21 did not affect growth rates of cells, but it did increase the proliferative potential and made mice more susceptible to cancer due to the unregulated growth by cell division [11].

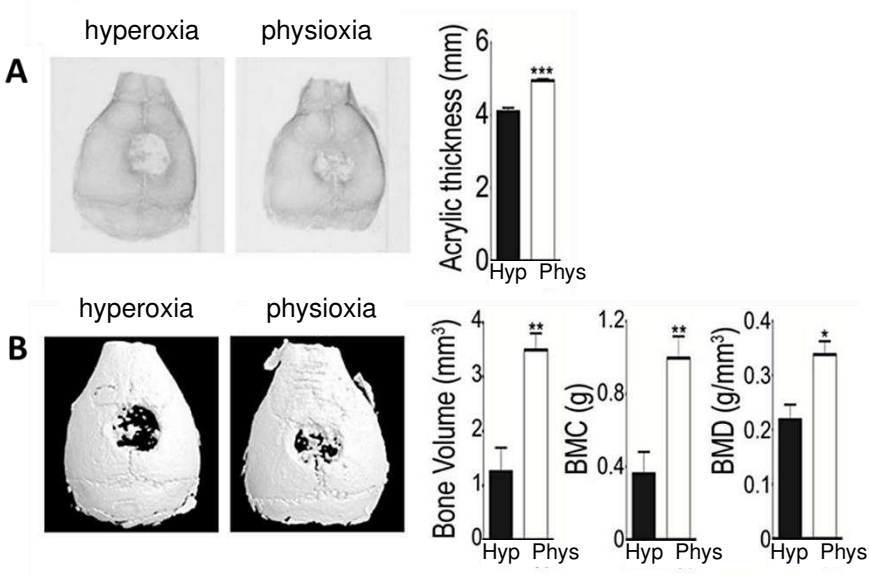

Figure 28. Physioxic cells increase *in vivo* bone repairing ability. Calvarial defects were implanted with hyperoxic (Hyp) or physioxic cells (Phys). (A) Radiographic images and densitometric analyses were performed after 6 weeks. (B) Micro-CT 3D reconstruction imaging and quantification for bone volume, bone mineral content (BMC), and bone mineral density (BMD) of newly formed tissues were performed after 6 weeks. *p<0.05, **p<0.01, ***p<0.005. Adapted from Tsai et al. (2011).

Arthur et al. [12] reviewed results from murine regeneration studies and what specific role p21 plays in the regulation of this *in vivo* regeneration. In this murine ear injury study, the rapid growth rate of fibroblast-like cells in the injured area showed an unusual accumulation of cells in the G_2/M phase of the cell cycle. Deletion of the p21 gene converted a non-regenerating strain of mouse to one capable of multi-tissue regeneration. Studies of p21 in mammalian liver regeneration revealed that p21 gene expression plays a role in both p53-dependent and p53-independent control mechanisms [12]. Overexpression of p21 produced large polyploid nuclei in a portion of the

hepatocytes and the regenerative capacity of the livers was halted. The aggregated knowledge from these studies led us to identify key players and different branches of this physioxia-induced p21 pathway as potential engineered targets.

Role of HIF-1α During Physioxia

A key mediator of the cellular response to physioxia is the hypoxia-inducible factor -1 (HIF-1) [13]. HIF-1 is a heterodimer composed of α and β subunits. Where HIF-1β is constitutively expressed, while HIF-1α has oxygen-dependent expression. Figure 29 gives a general overview of the HIF-1α pathway under hyperoxia and physioxia. Under hyperoxic conditions, HIF-1α is hydroxylated on proline residues by prolyl-4-hydroxylases (PHDs) and polyubiquinated by the von Hippel-Lindau protein (pVHL). That leads to degradation of HIF-1α by a proteasome, keeping HIF-1α levels low. Under physioxic conditions, PHDs are inhibited which stabilizes HIF-1 causing two things to happen. First, in the cytoplasm, the p21 pathway is triggered causing cell cycle arrest, decreasing the MSC proliferation, thereby limiting the beneficial effect of physioxia. Second, stabilized HIF-1α translocates into the nucleus where it binds to HIF-1β, triggering the transcription of target genes conducive to MSC activity and proliferation, such as VEGF, which is implicated in cellular adaptation to physioxia [14].

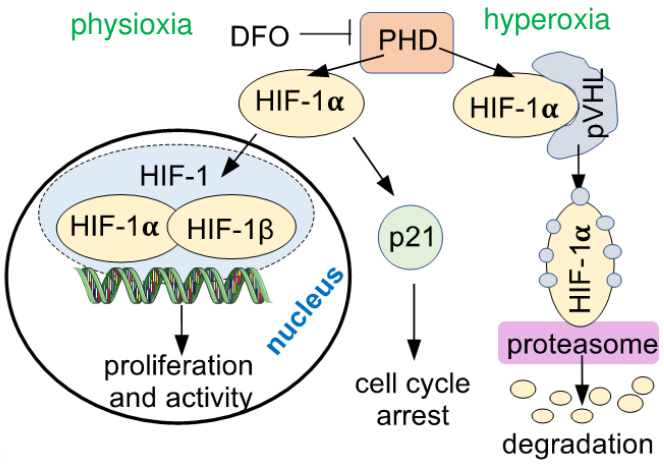

Figure 29. HIF-1α pathway under physioxia (left side) and hyperoxia (right side). HIF-1α levels remain low under hyperoxia due to proteasomal degradation. Under physioxia, PHDs are inhibited by activating the HIF-1α pathway.

Role of p21 in Cell Survival

The eukaryotic cell division cycle is divided into four different phases and begins with Gap 1 (G_1) phase (Figure 30). G1 phase together with synthesis (S) and Gap 2 (G_2) phase, also known as interphase, involves cell growth, biosynthesis of mRNA, and protein and organelles that are all needed for DNA replication [15].

A balance of positive and negative regulators control various restriction points throughout this cycle. Cell-cycle progression and proliferation are regulated by a restriction point when the cells progress from G_1 (cell growth phase) to the S phase (DNA synthesis). Cyclins E, A, B, and cyclin-dependent kinases (CDK) are positive regulators, while an example of a negative regulator is p21 Cip (cyclin-dependent kinase interacting protein) [16]. p21 binds directly to the CDKs, inhibiting the interaction of its activating cyclin. This results in growth arrest, lending a role in cellular senescence.

Recently, p21 is being recognized as a broader regulator of cell function, with key roles in apoptosis, differentiation, cell migration, etc. [17, 18]. The expression of p21 is tightly controlled

at the transcriptional level through p53 and Myc-dependent repression [15], though this cell cycle-specific component of p21 is independent of regulation by p53 [19]. This p53-independent pathway is the target of this project because of its involvement in the cell cycle and implications with senescence.

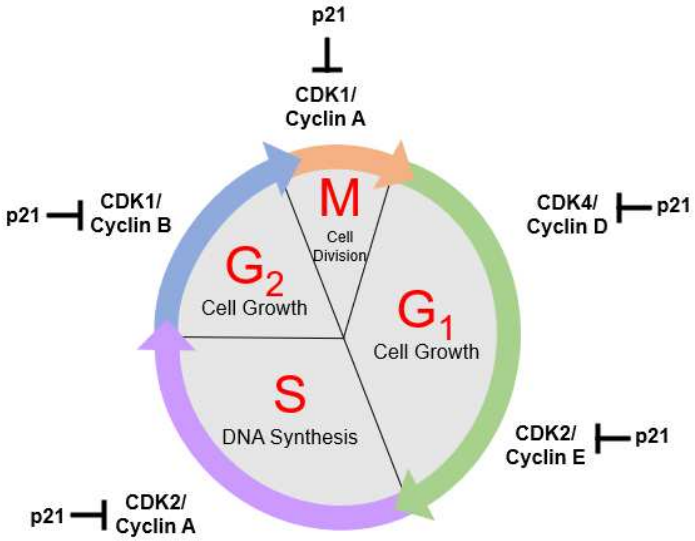

Figure 30. Cell cycle with key regulators. Cyclins that positively regulate the cycle progression are all inhibited by p21 presence through direct binding.

Physioxia Induction in Vitro

Induction of the physioxic pathway can be achieved through culture in a tri-gas incubator that can maintain low oxygen levels or with the use of small molecule drugs, such as deferoxamine mesylate (DFO) which affects specific pathways as explained later. Tri-gas incubators have the advantage of not using drugs that have the potential to alter cell behavior independently of the oxygen tension, however, many types of experimentation cannot be done as oxygen re-enters the incubator at each opening and thus lessens physioxia condition [20] and can lower HIF-1 levels quickly as demonstrated before. Physioxic exposure is usually defined as the time when the doors of the tri-gas incubator close, but it can take minutes to several hours for the oxygen concentration in the culture medium to equilibrate [21]. Opening the incubator door causes instantaneous gas

exchange with the outside air and can take up to 1 hour until physioxic conditions are re-established. To add to the complications, biological reactions such as oxygen sensing by HIF-1α and PHDs will continue even in cell lysates [21]. Due to these issues, large equipment like physiological cell culture workstations is required so that every step can be performed within a physioxic environment. Without that equipment, experiment results using tri-gas incubators can be varied and not provide an accurate picture of the physioxic response. Installation of such infrastructure, especially in large cell manufacturing facilities, is expensive and can be a hurdle.

The use of drugs, such as DFO, allows for an experiment to be performed in an open environment without affecting the "physioxic" condition. DFO is an iron chelator frequently used in the study of cell proliferation and apoptosis. DFO is a physioxia-mimetic agent that stabilizes HIF-1 through the inhibition of PHDs through the chelation of Fe^{2+} that binds to the active site of the PHD required for enzymatic activity. It has been shown to promote BMSC growth, rejuvenate senescent BMSCs [22], and improve neo-vascularization in a murine wound healing model [5]. DFO will be the chosen method of physioxia induction for the experiments in this study due to its ease of use experimentally and to implement on a large scale. To understand the improved MSC proliferation due to physioxia and p21 and to investigate its temporal dynamics, a mathematical model was developed.

Stem Cell-Specific Growth Models

Tabatabai et al. (2005) developed a set of mathematical models to predict self-limited growth behavior in tumors and stem cells. These models are referred to as hyperbolastic models because the outcome is a function of the inverse hyperbolic sine function (arcsinh). The three hyperbolastic growth models described are H1 which generalizes the logistic growth model, H2, a stand-alone,

and H3 which generalizes the Weibull growth model [37]. Tabatabai et al. (2011) then determined the best parameters to fit the H3 model to MSC growth specifically based on experimental data, with the rate of proliferation measured using the MTT (3-(4,5-dimethylthiazol-2-yl)-2,5-diphenyl tetrazolium bromide) reduction assay method. The Deasy model is generally used for modeling cell growth and when compared to experimental data of MSC growth, it had a larger absolute relative error when compared to the ESC-specific H3 growth model (Table 2) [24], demonstrating that this is the most realistic and accurate model of stem cell growth.

Table 2. Observed and estimated number of embryonic stem cells (in units of thousands). The H3 model (red box) had the lowest absolute relative error. Taken from Tabatabai et al. (2011).

Day	Observed number of stem cells	Estimated number of stem cells		Absolute relative error	
		Hyperbolastic H3	Deasy	Hyperbolastic H3	Deasy
1.0	110.000	110.000	74.334	0.000	0.324
2.0	139.375	142.862	137.751	0.023	0.012
3.0	186.875	184.876	227.114	0.013	0.216
4.0	303.750	304.918	353.037	0.002	0.162
5.0	603.125	603.246	530.480	0.000	0.120
6.0	760.000	760.062	780.520	0.000	0.027

This model applies not only to cell count but also to the proliferative index (PI) as a measure of proliferation of stem cells (Equation 1), rather than cell count because this is often more practical for experimental purposes.

$$\text{Proliferative Index} = [(S + G_2/M) / (G_0/G_1 + S + G_2/M)] \quad (1)$$

The PI is a percentage of cells that are in stages S and G_2/M of the cell cycle, giving the best representation of cells in or at the point near proliferation. The G_1 and G_0 phases are excluded from this model because they represent the quiescent and length-determining stages of the cycle [24].

Project Goals

We propose that drug-mediated HIF-1α stabilization and apoptosis suppression through p21 inhibition will lead to similar improved effects as physioxic culture but with the added benefit of ease of use and improved scalability for clinical cell culture. To examine this, we created a predictive mathematical model of MSC proliferation under varying levels of physioxia followed by *in vitro* experiments to examine key differences between physioxic culture conditions and drug-mediated physioxia. Knowledge of the mechanisms to improve MSC proliferation in two-dimensional culture can provide future intervention strategies to gain more control over MSC during clinical long-term expansion without requiring specialized culture conditions.

Materials and Methods

Predictive mathematical model

To understand the improved MSC proliferation due to physioxia and p21 and to investigate its temporal dynamics, a mathematical model was developed in MATLAB.

To model HIF-1α protein dynamics, a compartmentalized model was used to understand its role in both the nuclear and cytoplasmic interactions [13]. The nuclear HIF-1α is synthesized with rate s, spontaneously degraded with rate a, and is engaged into a chemical equilibrium with the pVHL/HIF-1α complex. k_f and k_b are the assembly/disassembly rates of the complex. The degradation of pVHL in the nuclear complex liberates HIF-1α with rate *g*.

$$\frac{dh_n}{dt} = \sigma + (k_b + \gamma)c_n - k_f v_n h_n - \alpha h_n \quad (1)$$

Cytoplasmic HIF-1α equation:

$$\frac{dh_c}{dt} = (k_b + \gamma)c_c - k_f v_c h_c - \alpha h_c \quad (2)$$

Equations (1) and (2) are then added together to get a curve of total HIF-1α levels over time (Equation 4). The intermediate equations can be found in Appendix A.

$$h_{total} = h_n + h_c \tag{3}$$

Next, I present the equation for HIF-1α -dependent p21 levels. Equation (2) was inserted into the [HIF1α] variable in equation (4). k_{sp210} is the basal induction rate of p21, k_{sp21} is the HIF-1α inducible production rate of p21, j_{sp21} is the Michaelis constant of HIF-1α inducible p21 production, and k_{dp21} is the degradation rate of p21.

$$\frac{d[p21]}{dt} = k_{sp210} + k_{sp21}\frac{[HIF1\alpha]^4}{[HIF1\alpha]+^4 {j_{sp21}}^4} - k_{dp21}[p21] \tag{4}$$

The proliferation equation is a hyperbolastic model [24] which has been demonstrated to be highly accurate for modeling biological growth, specifically stem cells. The PI is a percentage of cells that are in stages S and G2/M of the cell cycle, giving the best representation of cells in at the point near proliferation. The G1 and G0 phases are excluded from this model because they represent the quiescent and length-determining stages of the cycle [24]. The solved total HIF-1α and p21 equations were incorporated into the carrying capacity variable, the limiting value of the size of the population, to investigate their effects on the proliferative index over 3 passages. After several baseline testing, it was determined that this was the most relevant variable to incorporate total HIF-1α and p21 equations. Inhibition of p21 was modeled by removing the *p21(t)* term, thus not accounting for the biologically negative effects of p21.

$$\frac{dP}{dt} = (h_{total}(t) - p21(t) - P(t))\left(\delta\gamma t^{\gamma-1} + \frac{\theta}{\sqrt{1+\theta^2 t^2}}\right) \tag{5}$$

MSC Culture

Passage 2 primary human bone marrow-derived MSCs (PT-2501) were purchased from Lonza for all the experiments. These cells are a mixed population of cells derived from the bone marrow of

healthy adult individuals. Cells were maintained in bulletkit (Lonza) growth medium kit consisting of the MSC Basal medium (PT-3238) and the supplemental kit (PT-4105) as stated in the manufacturer's protocol. The culture condition was 5% CO_2, 37°C temperature and 90% relative humidity. For all the experiments, cells were seeded in a 75 cm^2 T-flask and passaged at 90% confluency at 5,000 cells/ cm2. Trypsin-EDTA (0.05%) was used for subculturing.

For low oxygen cell culture, growth medium was equilibrated overnight in a tri-gas incubator set to 2% O_2. Standard culture methods were used, with the cells staying in the 2% O_2 incubator for the specified periods of time between 2 and 24 hours. Cells were harvested for RNA extraction immediately at each endpoint Passage4 cells were seeded on petri dishes and kept in a standard incubator for 6 hours so cells could attach and stabilize. Concurrently, a tri-gas incubator was brought to 5% O_2 to bring the level down, then it was set to 2% O_2, in which the MSC growth medium was maintained for 2 hours to equilibrate. Once equilibrated, the growth medium was changed to the 2% O_2 -primed medium for cells to undergo physioxic culture. Cells were then harvested immediately at the given time points and pellets were left in RNAlater (Invitrogen) until the last sample was collected. Within 1 hour of the last sample collection, all cell pellets were processed for RNA extraction.

Cell treatments with physioxia-mimetic drugs

For cell treatments, DFO (Sigma-Aldrich) was added to the growth medium at a concentration of 120 μM for 8 or 24 hours followed by replacement with fresh medium. The p21 inhibitor was added to the growth medium at a concentration of 2 uM for the same time period as the corresponding DFO treatment. Cells were then harvested immediately at the given time points and

pellets were left in RNAlater until the last sample was collected. Within 1 hour of the last sample collection, all cell pellets were processed for RNA extraction.

RNA Extraction and Reverse Transcription

Cell pellets were homogenized using the QiaShredder (Qiagen) and then total RNA was extracted from cells using the RNeasy MiniKit (Qiagen) according to the manufacturer's protocol, but with an additional 15-second spin at 8,000 x g between steps 6 and 7 (between buffer RW1 and the buffer RPE washes) to minimize any phenol contamination that is picked up during quantification. RNA concentration and quality were quantified using the NanoDrop One Spectrophotometer (ThermoFisher). RNA was then reverse transcribed into cDNA using the iScript gDNA Clear cDNA Synthesis Kit (BioRad) following the manufacturer's protocol in 20 µl reactions. Samples are then stored at -80°C.

Quantitative Real-Time PCR

For reverse transcription quantitative PCR (RT-qPCR), cDNA was diluted to 15 ng/µl and used with the SYBR Green Master Mix and transcript-specific primers that were pre-designed from IDT (Integrated DNA Technologies). Amplification and analysis were performed using the QuantStudio 3 (Applied Biosystems) using amplification settings according to the SYBR green specifications. 30 ng of cDNA was used in each well, 100 µM of each primer sequence, with each sample run in quadruplicate. $\Delta\Delta C_t$ analysis was performed using the QuantStudio Design and Analysis Software with gene expression data normalized to GAPDH and reported as relative fold change.

Statistics

Statistical analysis was performed using Student's t-test in RStudio. Results are expressed as mean ± standard deviation, with differences considered statistically significant at $p < 0.05$ or $p<0.01$, as specified in the figure legends.

Results

Mathematical model determines optimal parameters in physioxia-dependent cell proliferation

Analysis of MSC proliferation under physioxia requires an understanding of p21 and HIF-1α dynamics. The intermediate equations that get input to the proliferation equation were modified slightly for our purposes and the individual curves are plotted in Figure 6. Hyperoxia resulted in low p21 protein levels and HIF-1α levels compared to physioxic conditions (Figure 31) returning to basal levels in a short period of time due to PHD facilitated degradation. Physioxia priming time of 1 hour also resulted in a p21 level under 1, leading to a wider HIF-1α curve upon reoxygenation suggesting that p21 levels less than HIF-1α levels can extend the activation of HIF-1α. The p21 peak level and duration were affected by physioxia priming time, while the oxygen level mainly changed the initial slope of the p21 curve. HIF-1α peaks were influenced by oxygen level, while physioxic priming time directed the time HIF-1α remains at an elevated level. Together, low physioxia increases activation of HIF-1α accompanied by sustained p21 levels during the physioxic period.

Understanding how these dynamics affect MSC proliferation under varied physioxic conditions was modeled next. Proliferation curves were modeled over 20 days to simulate about 3 passages of MSC expansion. Proliferation was modeled under different levels of physioxia: low, moderate, and hyperoxic, representing an estimated 3%, 5%, and 20% oxygen respectively. The

original proliferation model from Tabatabai et al. [24] before any modifications had a peak proliferative index peak and plateau of about 0.85, which represents standard hyperoxic culture conditions of MSC. When the equations for HIF-1α and p21 were incorporated into the base proliferation equation, the effects of various oxygen levels could be examined (Figure 32). Interestingly, it was specifically the addition of p21 to the model, that led to slope changes after 10 days, rather than a flat plateau. This highlights the delayed detrimental effects of the p21 protein, resulting in the plateau beginning to take on a negative slope (-0.01) after day 10. Conversely, when p21 inhibition was modeled, these slopes became slightly positive (0.002). Moderate physioxia (orange lines) resulted in a slight peak increase, just above 1, but low physioxia (blue lines) showed a peak PI around 1.3. Optimization of these conditions were tested next to determine minimal time periods that would theoretically be needed for *in vitro* physioxic culture.

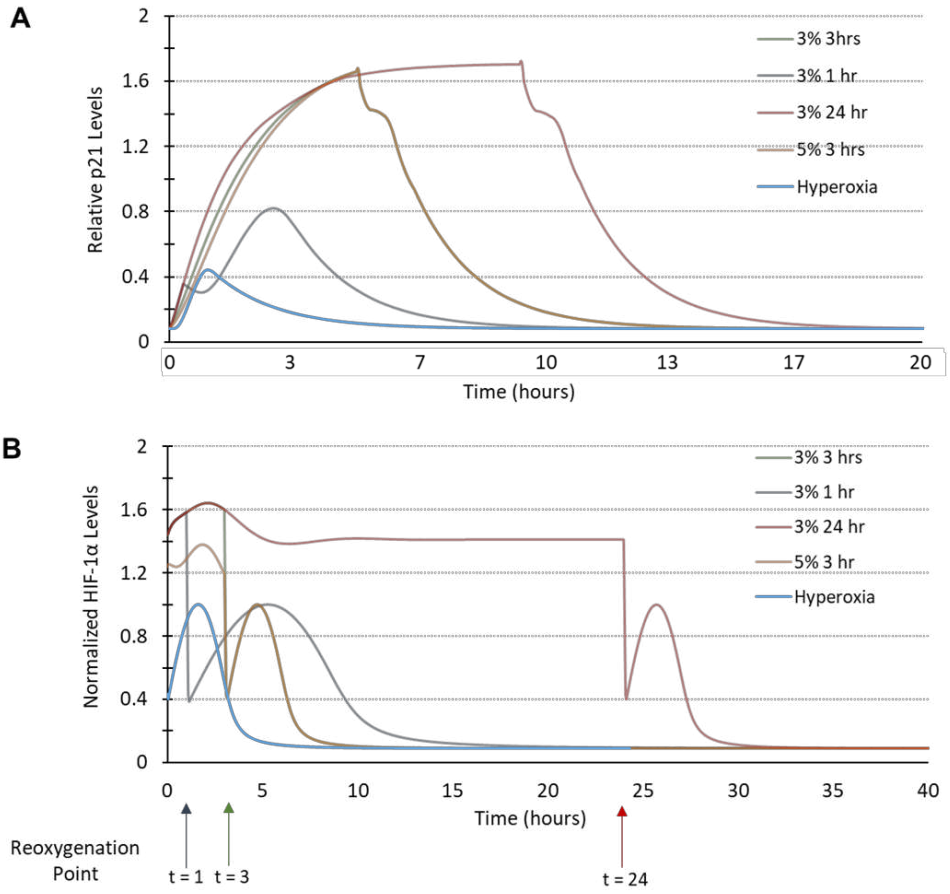

Figure 31. Intermediate results for the physioxia-dependent proliferation model. Physioxia applied at t = 0 and reoxygenated at the listed time points. (A) p21 protein levels are less than 1 in hyperoxia and short low physioxic priming times. Longer priming times sustain a high level of p21 in the cells, returning to a basal rate by 17 hours. (B) HIF-1α levels normalized to the hyperoxic condition. Physioxia level determines peak, with the priming time determining the time of sustained HIF-1α levels before return to basal levels.

Priming time was incorporated into the model using a piecewise method. The model was solved using physioxic conditions for the specified priming times and was then concatenated to the model solved under hyperoxic conditions for the rest of the time period. The results showed that 3 hours of low physioxic priming (3% O_2) led to the highest peak proliferative index and a flattened slope (-.009) after day 10 (Figure 32). 1 hour of low physioxia priming showed similar PI peaks at each oxygen level, but the PI decreases faster after day 10 (slope = -.01). Priming times of longer than 3 hours did not show significant changes in the PI peak or PI values over time, with

24 hours at 3% O_2 matching 3 hours at 3% O_2. When p21 inhibition was incorporated into the model, the PI continued to increase after day 10 (slope = 0.002), accompanied by an increase in PI peak. 3 hours under low physioxia with the p21 inhibitor produced a PI peak of 1.49, whereas the longer priming time of 24 hours resulted in a peak of 1.57. A key limitation of this model, however, is the lack of diffusion equations that directly relate to *in vitro* experiments. This makes translating the determined physioxia priming times unclear, so *in vitro* experiments were performed to better understand the model results.

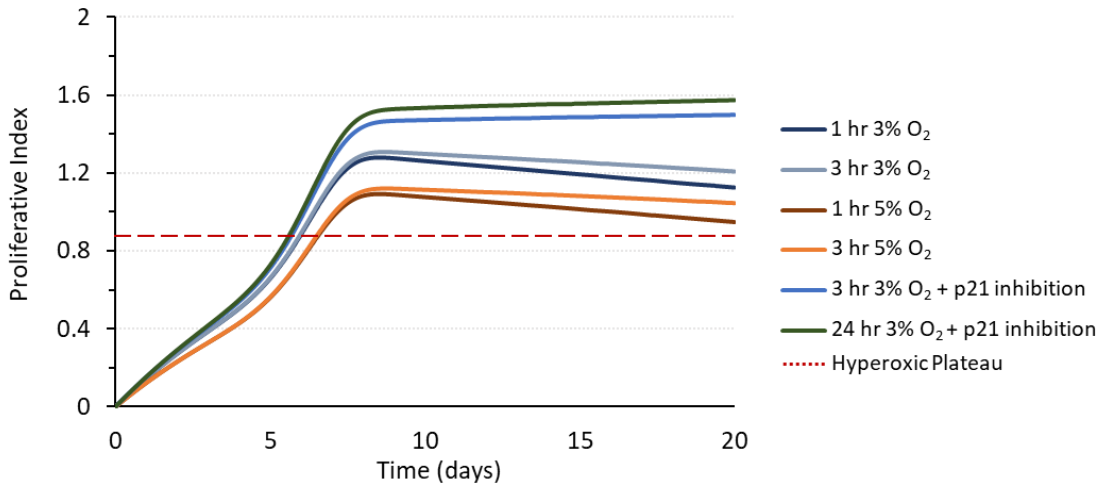

Figure 32. MSC proliferative index predictive model over 20 days (~3 passages) under low (3% O_2) or moderate (5% O_2) physioxia for varying priming times. Inhibition of p21 under low physioxia for 24 hours resulted in an extended interval of increased PI. Moderate physioxia showed the lowest PI, yet is still an improvement over hyperoxic culture.

DFO treatment can similarly induce a physioxic response at the gene expression level

To evaluate physioxia exposure *in vitro*, VEGF expression, a downstream gene in the HIF-1α pathway, was examined (Figure 33). Culture in a tri-gas incubator at 2% O_2 showed increasing VEGF expression with additional time under physioxia from 2-fold at 4 hours up to 10-fold at 24 hours. Similarly, DFO treatments in cells cultured under hyperoxia showed a large fold increase of VEGF as well, increasing with treatment time from 12- to 18-fold. The addition of p21 inhibitors

to DFO treatments did not show any considerable changes in VEGF expression when compared to DFO alone, instead decreasing in the 24-hour DFO treated group.

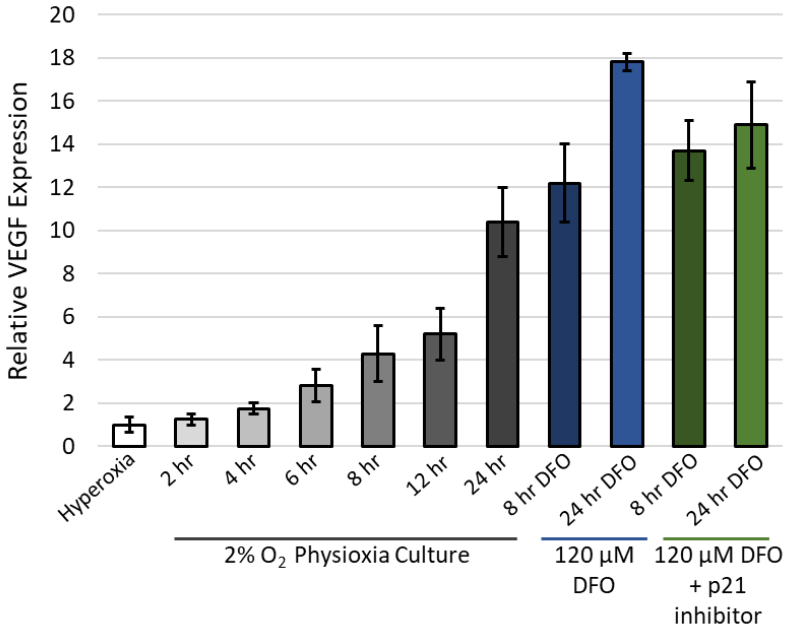

Figure 33. Relative VEGF expression in MSC cultured under hyperoxia (21% O_2), various times under physioxia (2% O_2), or with drug treatments under hyperoxia. VEGF levels under 24 hours of physioxia are close to that of 8 hr DFO treatment under hyperoxia. DFO treatments with p21 inhibitors did not show advantages in VEGF expression.

Discussion

Limited periods of physioxia exposure have been shown to have beneficial effects on MSC [10, 15–17], but the pathways are still under investigation. In this preliminary study, we developed a mathematical model to predict MSC proliferation under varying physioxic conditions. A model period of 20 days represents about 3 passages, which is a standard amount of passaging for MSC during *in vitro* studies. The proliferative index (PI) represents the proportion of cells that are actively proliferating [24], and this value was highest under modeled 3% O_2 primed for 3 hours followed by hyperoxic culture. Low physioxic culture conditions mimic the native bone marrow oxygen tension [1] and have been shown to increase MSC proliferation [4, 25], which is reinforced by this model. Modeling extreme cases (Figure S1) of anoxia and over-oxygenation had a large

reduction in PI, which is expected *in vitro*. The inclusion of p21 in this model was key to investigating the opposing factors of this physioxic pathway. Priming times longer than 3 hours may not have an effect on peak PI or long-term dynamics due to the concomitant upregulation of p21 as seen in the 24-hour 3% O_2 case. These antagonist effects most likely diminish any improvements expected from elevated HIF-1α levels for a long period. Modeling of p21 inhibition 24 hours of low physioxia with modeled p21 inhibition resulted in the highest peak PI value most likely because the HIF-1α factors were unhindered by the negative regulation by p21. The positive PI slope over time suggests the potential for unregulated proliferation, which could lead to problems *in vitro*, so checking limited time periods with p21 inhibitor in the culture medium will be important to examine. In the varying conditions tested, this model supports literature results and can be used to predict MSC proliferation under specific physioxic culture conditions.

Comparing VEGF expression under the different physioxia culture methods *in vitro* indicated that 2% O_2 for longer than 4 hours activated the HIF-1α pathway. The DFO addition to the culture medium under hyperoxic culture conditions similarly activated the HIF-1α pathway. This is determined through VEGF expression levels since it is downstream of the HIF-1α pathway and is more stable than the HIF-1α protein itself. The addition of a p21 inhibitor with DFO treatments did not make considerable changes in VEGF expression most likely due to VEGF expression occurring in the nucleus with HIF-1α acting as a transcription factor [26], while cytoplasmic p21 has less impact. When determining which treatments are comparable, the 24-hour physioxic culture most closely matched the 8-hour DFO treatment. These groups will be used for future comparison studies between physioxic culture and simple drug additions to the culture medium in MSC.

The preliminary results from this study are promising towards a simple solution to achieve MSC with increased proliferation through drug-mediated HIF-1α stabilization and apoptosis suppression. The ability to culture a large amount of MSC under standard hyperoxic conditions with a small molecule addition to the culture medium could improve the scalability of physioxia-primed MSC and their beneficial properties. Future studies will examine the functional differences between DFO treatment and physioxic culture in more detail to understand the possibilities and limitations of drug-mediated physioxia pathway activation.

REFERENCES

1. Johnson, R. W., Sowder, M. E., & Giaccia, A. J. (2017, August 1). Hypoxia and Bone Metastatic Disease. *Current Osteoporosis Reports*. Current Medicine Group LLC 1. https://doi.org/10.1007/s11914-017-0378-8

2. Tsai, C.-C., Chen, Y.-J., Yew, T.-L., Chen, L.-L., Wang, J.-Y., Chiu, C.-H., & Hung, S.-C. (2011). Hypoxia inhibits senescence and maintains mesenchymal stem cell properties through down-regulation of E2A-p21 by HIF-TWIST. *Blood*, *117*(2). https://doi.org/10.1182/blood-2010-05-287508

3. Iommarini, L., Porcelli, A. M., Gasparre, G., & Kurelac, I. (2017, November 27). Non-canonical mechanisms regulating hypoxia-inducible factor 1 alpha in cancer. *Frontiers in Oncology*. Frontiers Media S.A. https://doi.org/10.3389/fonc.2017.00286

4. Ohnishi, S., Yasuda, T., Kitamura, S., & Nagaya, N. (2007). Effect of Hypoxia on Gene Expression of Bone Marrow-Derived Mesenchymal Stem Cells and Mononuclear Cells. *Stem Cells*, *25*(5), 1166–1177. https://doi.org/10.1634/stemcells.2006-0347

5. Wahl, E. A., Schenck, T. L., Machens, H. G., & Balmayor, E. R. (2016). VEGF released by deferoxamine preconditioned mesenchymal stem cells seeded on collagen-GAG substrates enhances neovascularization. *Scientific Reports*, *6*(1), 1–12. https://doi.org/10.1038/srep36879

6. Thangarajah, H., Yao, D., Chang, E. I., Shi, Y., Jazayeri, L., Vial, I. N., … Gurtner, G. C. (2009). The molecular basis for impaired hypoxia-induced VEGF expression in diabetic tissues. *Proceedings of the National Academy of Sciences of the United States of America*, *106*(32), 13505–13510. https://doi.org/10.1073/pnas.0906670106

7. Foyt, D. A., Taheem, D. K., Ferreira, S. A., Norman, M. D. A., Petzold, J., Jell, G., … Gentleman, E. (2019). Hypoxia impacts human MSC response to substrate stiffness during chondrogenic differentiation. *Acta Biomaterialia*, *89*, 73. https://doi.org/10.1016/J.ACTBIO.2019.03.002

8. Takiyama, Y., & Haneda, M. (2014). Hypoxia in diabetic kidneys. *BioMed Research International*, *2014*. https://doi.org/10.1155/2014/837421

9. Sun, J., Shen, H., Shao, L., Teng, X., Chen, Y., Liu, X., … Shen, Z. (2020). HIF-1α overexpression in mesenchymal stem cell-derived exosomes mediates cardioprotection in myocardial infarction by enhanced angiogenesis. *Stem Cell Research and Therapy*, *11*(1), 1–13. https://doi.org/10.1186/s13287-020-01881-7

10. Lv, B., Li, F., Fang, J., Xu, L., Sun, C., Han, J., … Jiang, X. (2017). *Hypoxia inducible factor 1α promotes survival of mesenchymal stem cells under hypoxia*. *American Journal of Translational Research* (Vol. 9). Retrieved from www.ajtr.org

11. Cho, Y. S., Bae, J. M., Chun, Y. S., Chung, J. H., Jeon, Y. K., Kim, I. S., … Park, J. W. (2008). HIF-1α controls keratinocyte proliferation by up-regulating p21(WAF1/Cip1). *Biochimica et Biophysica Acta (BBA) - Molecular Cell Research*, *1783*(2), 323–333. https://doi.org/10.1016/j.bbamcr.2007.11.017

12. Arthur, L., & Heber-Katz, E. (2011, June 29). The role of p21 in regulating mammalian regeneration. *Stem Cell Research and Therapy*. BioMed Central. https://doi.org/10.1186/scrt71

13. Bedessem, B., & Stéphanou, A. (2014). Role of compartmentalization on HiF-1α degradation dynamics during changing oxygen conditions: A computational approach. *PLoS ONE*, *9*(10), e110495. https://doi.org/10.1371/journal.pone.0110495

14. Zhou, C. H., Zhang, X. P., Liu, F., & Wang, W. (2015). Modeling the interplay between the HIF-1 and p53 pathways in hypoxia. *Scientific Reports*, *5*(1), 1–10. https://doi.org/10.1038/srep13834

15. Ortmann, B., Druker, J., & Rocha, S. (2014, May 25). Cell cycle progression in response to oxygen levels. *Cellular and Molecular Life Sciences*. Birkhauser Verlag AG. https://doi.org/10.1007/s00018-014-1645-9

16. Lees, S. J., Childs, T. E., & Booth, F. W. (2008). p21Cip1 expression is increased in ambient oxygen, compared to estimated physiological (5%) levels in rat muscle precursor cell culture. *Cell Proliferation*, *41*(2), 193–207. https://doi.org/10.1111/j.1365-2184.2008.00512.x

17. Abbas, T., & Dutta, A. (2009). P21 in cancer: Intricate networks and multiple activities. *Nature Reviews Cancer*. Nature Publishing Group. https://doi.org/10.1038/nrc2657

18. Kreis, N. N., Louwen, F., & Yuan, J. (2014, May 26). Less understood issues: P21Cip1 in mitosis and its therapeutic potential. *Oncogene*. Nature Publishing Group. https://doi.org/10.1038/onc.2014.133

19. Ritt, M. G., Mayor, J., Wojcieszyn, J., Smith, R., Barton, C. L., & Modiano, J. F. (2000). Sustained nuclear localization of p21/Waf-1 upon growth arrest induced by contact inhibition. *Cancer Letters*, *158*, 73–84. https://doi.org/10.1016/S0304-3835(00)00507-3

20. Wu, D., & Yotnda, P. (2011). Induction and testing of hypoxia in cell culture. *Journal of Visualized Experiments*, (54), 2899. https://doi.org/10.3791/2899

21. Wenger, R., Kurtcuoglu, V., Scholz, C., Marti, H., & Hoogewijs, D. (2015). Frequently asked questions in hypoxia research. *Hypoxia*, *3*, 35. https://doi.org/10.2147/hp.s92198

22. Yi, L., Ju, Y., He, Y., Yin, X., Xu, Y., & Weng, T. (2021). Intraperitoneal injection of Desferal® alleviated the age-related bone loss and senescence of bone marrow stromal cells in rats. *Stem Cell Research & Therapy*, *12*(45), 1–13. https://doi.org/10.1186/s13287-020-02112-9

23. Ahmadi, H., & Mottaghitalab, M. (2007). Hyperbolastic models as a new powerful tool to describe broiler growth kinetics. *Poultry Science*, *86*(11), 2461–2465. https://doi.org/10.3382/ps.2007-00086

24. Tabatabai, M. A., Bursac, Z., Eby, W. M., & Singh, K. P. (2011). Mathematical modeling of stem cell proliferation. *Medical and Biological Engineering and Computing*, *49*(3), 253–262. https://doi.org/10.1007/s11517-010-0686-y

25. Antebi, B., Rodriguez, L. A., Walker, K. P., Asher, A. M., Kamucheka, R. M., Alvarado, L., … Cancio, L. C. (2018). Short-term physiological hypoxia potentiates the therapeutic function of mesenchymal stem cells. *Stem Cell Research & Therapy*, *9*(1). https://doi.org/10.1186/S13287-018-1007-X

26. Ren, H., Cao, Y., Zhao, Q., Li, J., Zhou, C., Liao, L., … Zhao, R. C. (2006). Proliferation and differentiation of bone marrow stromal cells under hypoxic conditions. *Biochemical and Biophysical Research Communications*, *347*(1), 12–21. https://doi.org/10.1016/j.bbrc.2006.05.169

CHAPTER 5: FUTURE DIRECTIONS AND POTENTIAL IMPACT

Overall, this research is aimed to advance our understanding of the fundamental science of mesenchymal stromal cells and to design mechanism-based novel bioengineering strategies for scalable MSC manufacturing for clinical applications. Each aspect discussed in this thesis investigates a separate pathway to find engineering targets with the end goal to culture MSCs in standard conditions while exhibiting high proliferation, but not sacrificing their stemness and homogeneity.

Mechanical stiffness-driven heterogeneity through the Runx2 pathway

In summary, in Chapter 2 we found that substrate stiffness plays a key role in defining the heterogeneity of the MSC population. Soft substrates (~5 kPa) promoted a more homogeneous population of cells with the characteristic MSC cellular and nuclear phenotype, accompanied by increased expression of CD73. Conversely, MSCs grown on the stiff substrate (~1 GPa) not only resulted in phenotypical abnormalities, the presence of perinuclear actin caps, and Runx2 nuclear localization, but also caused significant phenotypical heterogeneity at the population level. Drug treatment can lower the heterogeneity at the population level, as the data showed, but this work opens new avenues for future research.

Future directions of this study might focus on several aspects as described below.

(1) Single cell RNA-sequencing, single cell ATAC-sequencing, CUT & RUN to further characterize the heterogeneity in the MSC population in their transcriptome and epigenome. Such work will provide us with more specific targets for each population of cells for maintaining population-level heterogeneity.

(2) The inhibitors we already identified for the mechanobiological targets can be optimized for minimizing heterogeneity. After we achieve a more homogeneous MSC population, they can be tested through bulk RNA sequencing and proteomics to verify the quality of the MSC population. Subsequently, they can be differentiated to a tissue-specific pathway such as chondrogenesis to find if a homogenous population of MSC ultimately leads to higher quality and larger cartilage tissue.

Mechanics-induced epigenetic pathways as a potential strategy to maintain MSC stemness

In Chapter 3, we found several mechanistic understanding and epigenetic characteristics that can be further investigated for future studies. We not only discovered several mechanics-dependent epigenetic features, but also we showed how the pathways can be intervened to obtain MSC in higher quantity along with maintaining their quality (characterized through VEGF expression) The investigation of SWI/SNF CRC can bring a potentially transformative knowledge in the fundamental understanding MSC, and it can provide us with novel bioengineering targets for obtaining MSC of high quality and quantity.

Future directions emerging from Chapter 3 are described below.

(1) Finding the mechanism of if and how the SWI/SNF affects the epigenetic localization such as H3K9me3. Further, it can be investigated how the mechanical memory is coded inside the chromatin.

(2) Finding the mechanism of how the substrate stiffness mediated intracellular and intranuclear strain impact the chromatin remodeling through the accumulation of nuclear actin.

(3) Drug treatments followed by RNA sequencing can provide more details of how the MSC quality is maintained through inhibition. An optimal protocol might be created for serial passage of the MSC on the soft substrate followed by drug treatment on the plastic substrate to obtain a large number of high-quality MSC. Subsequent differentiation property and trophic properties of the final MSC product can be verified for functional applications.

Drug-mediated HIF-1α stabilization to increase MSC proliferation

The results from Chapter 4 are promising towards a relatively simple solution to achieve high-quality MSC with increased proliferation through drug-mediated HIF-1α stabilization and apoptosis suppression. The ability to culture a large amount of MSC under standard hyperoxic conditions with a small molecule addition to the culture medium could improve the scalability of physioxia-primed MSC and their beneficial properties. This can be especially useful in large cell manufacturing facilities.

Future studies will take an in-depth look at the functional differences between DFO treatment and physioxic culture through:

(1) RNA-sequencing

(2) Western Blot

(3) tri-lineage differentiation.

The optimal combination and duration of the small molecules can be investigated with the goal of scalable MSC manufacturing.

APPENDIX A

Supplementary Figures

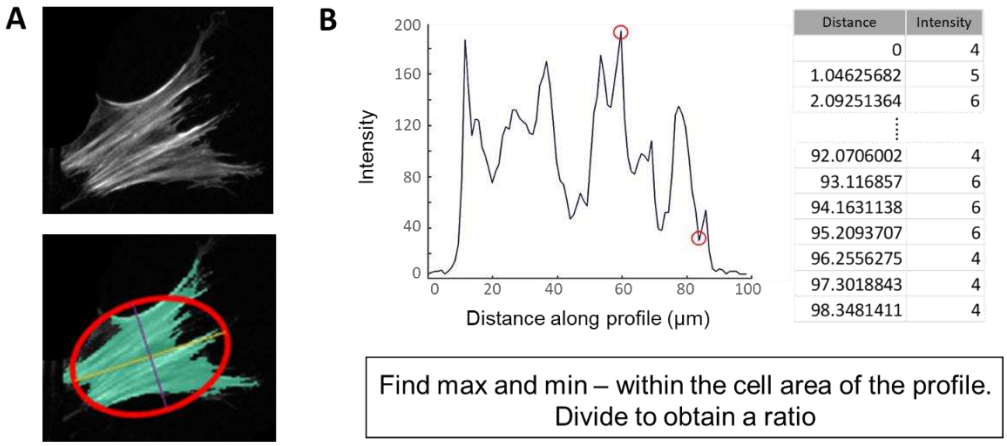

Figure A1. F-actin intensity quantification method. A custom MATLAB code was used to identify individual cells in an image (colored for confirmation). An ellipse fit based on the major and minor axes. Intensity maps and corresponding tables are then printed for each major and minor axis to the screen and saved. The cell number is noted on the graph and in the tables for reference. In general, the minor axis is used because it is usually aligned perpendicular to the actin fibers, but this is confirmed for each cell. Then the maximum value was divided by the minimum value within the bounds of the cell area to obtain an intensity ratio.

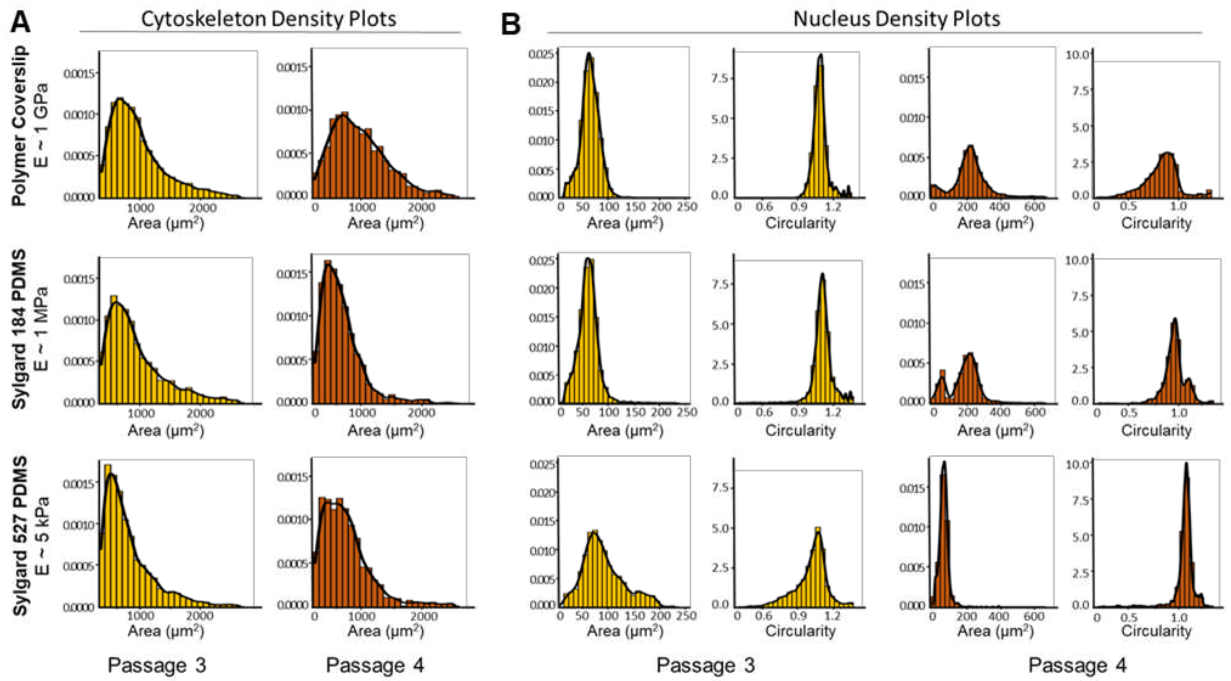

Figure A2. Density plots using a kernel density estimate to show the probability density function of each variable in Passage 3 or Passage 4. (A) Cytoskeleton area quantification density plots for the violin and box plot reported in Figure 1B. (B) Nucleus area and circularity quantification density plots for the violin and box plots reported in Figure 2B.

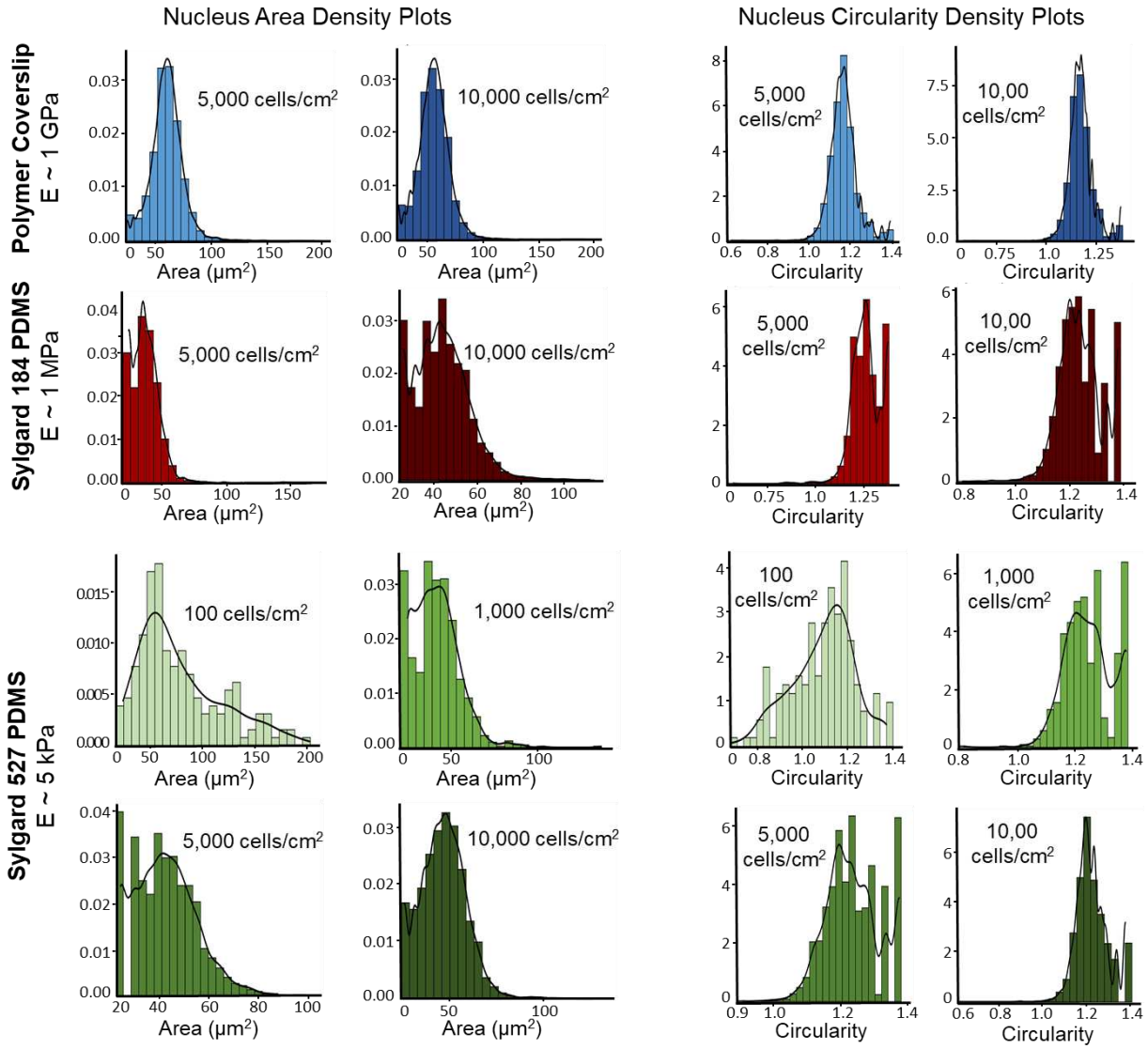

Figure A3. Density plots using a kernel density estimate to show the probability density function of each variable under various seeding densities. Nucleus area and circularity were quantified on each substrate stiffness and under increasing seeding densities, listed in each graph. These density plots correspond to the violin and box plots reported in Figure 2C.

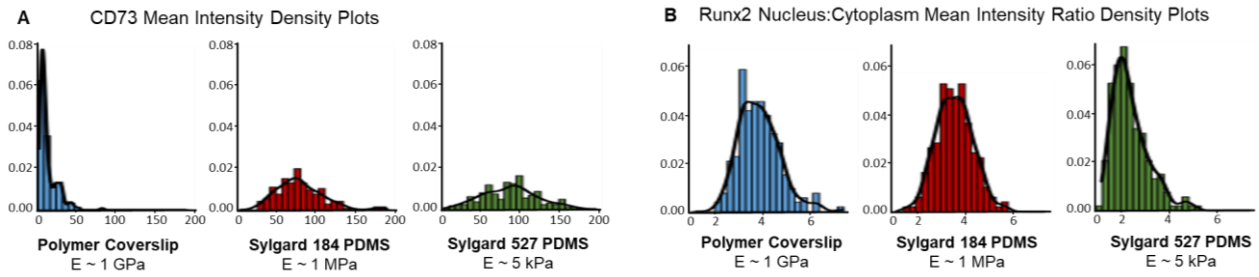

Figure A4. Density plots using a kernel density estimate to show the probability density function of (A) CD73 mean fluorescent intensities or (B) Runx2 nucleus to cytoplasmic mean intensity ratios on each substrate stiffness. These density plots correspond to the violin and box plots reported in Figure 4.

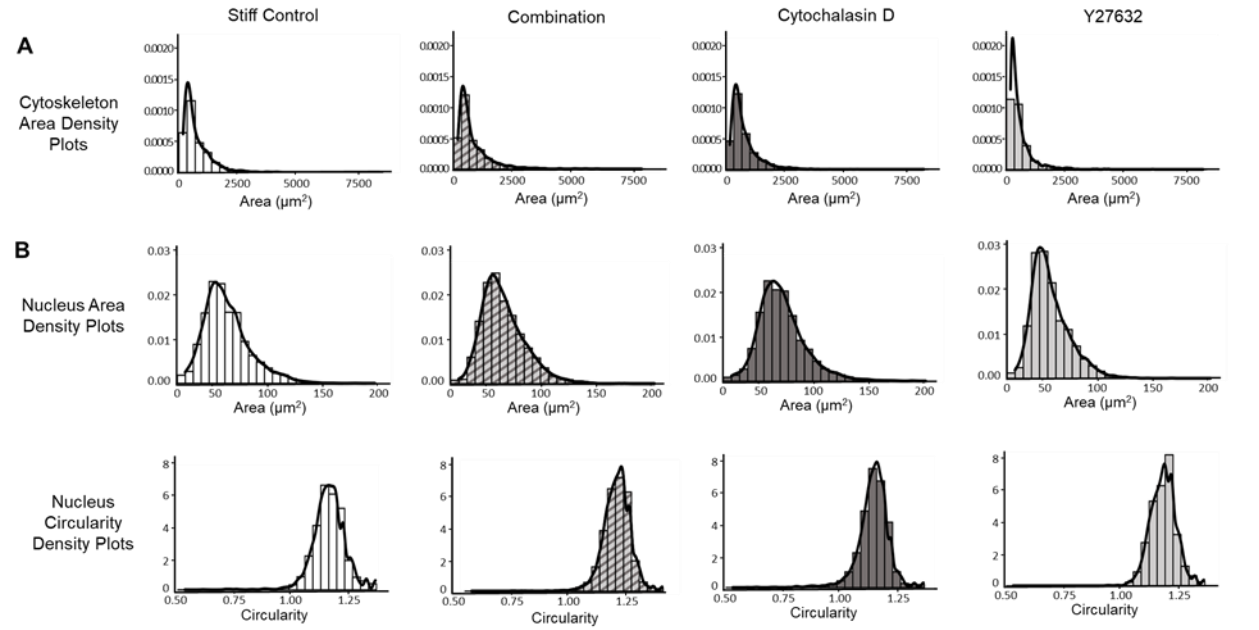

Figure A5. Density plots using a kernel density estimate to show the probability density function of each variable after undergoing treatment with various drug treatments. Passage 5 cells were cultured on a stiff substrate and were treated with cytochalasin D (cyto-D), the ROCK inhibitor Y27632, or a combination treatment of cyto-D and Y27632. (A) Cytoskeleton area quantification density plots for the violin and box plot reported in Figure 5C. (B) Nucleus area and circularity quantification density plots for the violin and box plots reported in Figure 5A.

Quantification of stress fiber formation

Stress fiber intensity quantification was performed using a custom MATLAB code. Cropped confocal images were converted to grayscale and a pixel value threshold was set to create a binary mask around that threshold. Then arbitrary structuring elements were created through the 'strel' function, which created masks over each identified cell in the image. The edges of the identified elements were smoothed and small holes in the element were filled so a solid mask could be visualized over the original image. To avoid any background noise that may have been included, a size filter was run to exclude any elements that would be too small to be considered a cell. The final allowable elements were labeled for later reference and then measured with 'regionprops', which included an estimated ellipse from the major and minor axes of each identified cell. Then the intensity maps and corresponding tables were separately printed and saved for the major and minor axis of each numbered cell. Generally, the minor axis aligned perpendicular to the actin fibers, though each cell was manually checked to confirm. The code relied heavily on aligned F-actin fibers so in some experiment groups with harder to discern F-actin fiber alignment, such as the Y27632 treated cells, the axis of intensity calculation was done manually in ImageJ. After the perpendicular axis was determined and located in the output table for each identified cell, the maximum and local minimum was then divided to obtain a ratio of intensities (Figure S1). Cell morphology quantification underwent the same process of initial image processing and masking of identified and filtered elements; however, images of the entire cell growth surface could be measured at once for a robust analysis. A table of the calculated parameters from regionprops() was exported for further evaluation in R Studio.

APPENDIX B

Significance Tables

Table B1. Significance tables with more comparisons corresponding to the data presented in Figure 4 B, C.

A CD73 Mean Intensity

Comparisons	p value
Soft : Stiff	0.447372
Soft Soft : Stiff Stiff	0.001337
Soft Soft Soft : Stiff Stiff Stiff	1.03E-05
Soft : Soft Soft	0.409676
Soft Soft : Soft Soft Soft	5.1E-06
Stiff : Stiff Stiff	5.63E-06
Stiff Stiff : Stiff Stiff Stiff	0.001351
Soft Soft : Soft Stiff	0.031339
Soft Soft Soft : Soft Soft Stiff	9.38E-05
Soft Soft Soft : Soft Stiff Soft	0.086284
Soft Soft Soft : Soft Stiff Stiff	0.000544
Stiff Stiff : Stiff Soft	0.103301
Stiff Stiff Stiff : Stiff Stiff Soft	0.036866
Stiff Stiff Stiff : Stiff Soft Stiff	0.094408
Stiff Stiff Stiff : Stiff Soft Soft	5.75E-05
Stiff Stiff Soft : Soft Soft Stiff	0.108578

B CD73 Mean Intensity

Comparisons	p value
Soft : Stiff	8.79472E-21
Soft Soft : Stiff Stiff	2.98849E-07
Soft Soft Soft : Stiff Stiff Stiff	0.064869471
Soft : Soft Soft	7.59255E-18
Soft Soft : Soft Soft Soft	0.092598044
Stiff : Stiff Stiff	1.46539E-07
Stiff Stiff : Stiff Stiff Stiff	0.061620423
Soft Soft : Soft Stiff	2.30776E-08
Soft Soft Soft : Soft Soft Stiff	0.34366127
Soft Soft Soft : Soft Stiff Soft	1.16596E-07
Soft Soft Soft : Soft Stiff Stiff	0.001214444
Stiff Stiff : Stiff Soft	0.359957933
Stiff Stiff Stiff : Stiff Stiff Soft	0.486770512
Stiff Stiff Stiff : Stiff Soft Stiff	2.08603E-06
Stiff Stiff Stiff : Stiff Soft Soft	6.63359E-05
Stiff Stiff Soft : Soft Soft Stiff	0.090029011

Table B2. Significance tables with more comparisons corresponding to the data presented in Figure 5 B, D.

A Cytoskeleton Area

Comparisons	p value
Soft : Stiff	0.05687875
Soft Soft : Stiff Stiff	1.19867E-12
Soft Soft Soft : Stiff Stiff Stiff	0.031182981
Soft : Soft Soft	0.003583303
Soft Soft : Soft Soft Soft	2.60027E-19
Stiff : Stiff Stiff	1.57085E-09
Stiff Stiff : Stiff Stiff Stiff	3.17842E-11
Soft Soft : Soft Stiff	5.61874E-25
Soft Soft Soft : Soft Soft Stiff	0.171036743
Soft Soft Soft : Soft Stiff Soft	7.25732E-05
Soft Soft Soft : Soft Stiff Stiff	1.83163E-12
Stiff Stiff : Stiff Soft	0.034121955
Stiff Stiff Stiff : Stiff Stiff Soft	1.46936E-10
Stiff Stiff Stiff : Stiff Soft Stiff	3.33596E-06
Stiff Stiff Stiff : Stiff Soft Soft	9.03614E-12
Stiff Soft Soft : Soft Soft Stiff	6.48124E-17

B Nucleus Area

Comparisons	p value
Soft : Stiff	8.7041E-188
Soft Soft : Stiff Stiff	2.79231E-35
Soft Soft Soft : Stiff Stiff Stiff	1.14558E-17
Soft : Soft Soft	7.84687E-93
Soft Soft : Soft Soft Soft	6.42489E-14
Stiff : Stiff Stiff	1.3792E-109
Stiff Stiff : Stiff Stiff Stiff	6.67677E-78
Soft Soft : Soft Stiff	9.57918E-13
Soft Soft Soft : Soft Soft Stiff	5.75569E-27
Soft Soft Soft : Soft Stiff Soft	3.00515E-19
Soft Soft Soft : Soft Stiff Stiff	0.185855093
Stiff Stiff : Stiff Soft	1.78352E-05
Stiff Stiff Stiff : Stiff Stiff Soft	6.93573E-31
Stiff Stiff Stiff : Stiff Soft Stiff	2.11656E-17
Stiff Stiff Stiff : Stiff Soft Soft	1.63295E-44
Stiff Soft Soft : Soft Soft Stiff	7.29178E-07

C Nucleus Circularity

Comparisons	p value
Soft : Stiff	2.50666E-63
Soft Soft : Stiff Stiff	3.35321E-56
Soft Soft Soft : Stiff Stiff Stiff	8.40095E-07
Soft : Soft Soft	2.53874E-30
Soft Soft : Soft Soft Soft	2.63642E-05
Stiff : Stiff Stiff	5.11256E-36
Stiff Stiff : Stiff Stiff Stiff	0.000176777
Soft Soft : Soft Stiff	1.14761E-16
Soft Soft Soft : Soft Soft Stiff	7.73999E-06
Soft Soft Soft : Soft Stiff Soft	1.68541E-30
Soft Soft Soft : Soft Stiff Stiff	4.85124E-30
Stiff Stiff : Stiff Soft	2.40129E-23
Stiff Stiff Stiff : Stiff Stiff Soft	5.45817E-67
Stiff Stiff Stiff : Stiff Soft Stiff	1.37194E-66
Stiff Stiff Stiff : Stiff Soft Soft	1.3982E-107
Stiff Soft Soft : Soft Soft Stiff	2.77406E-21

Table B3. Significance tables with more comparisons corresponding to the data presented in Figure 7.

H3K9me3 Intensity

Comparisons	p value
Soft : Stiff	0.425844
Soft Soft : Stiff Stiff	0.14141
Soft Soft Soft : Stiff Stiff Stiff	0.000536
Soft : Soft Soft	0.003732
Soft Soft : Soft Soft Soft	0.461658
Stiff : Stiff Stiff	0.02924
Stiff Stiff : Stiff Stiff Stiff	0.012344
Soft Soft : Soft Stiff	0.021677
Soft Soft Soft : Soft Soft Stiff	0.007014
Soft Soft Soft : Soft Stiff Soft	0.387286
Soft Soft Soft : Soft Stiff Stiff	9.27E-06
Stiff Stiff : Stiff Soft	0.104255
Stiff Stiff Stiff : Stiff Stiff Soft	0.006084
Stiff Stiff Stiff : Stiff Soft Stiff	0.000729
Stiff Stiff Stiff : Stiff Soft Soft	1.55E-05
Stiff Stiff Soft : Soft Soft Stiff	0.027499

Table B4. Significance tables with more comparisons corresponding to the data presented in Figure 8 D (A) and Figure 9 (D).

A H3K9ac Labeled Area

Comparisons	p value
Soft : Stiff	0.001678424
Soft Soft : Stiff Stiff	8.47777E-06
Soft Soft Soft : Stiff Stiff Stiff	6.25459E-11
Soft : Soft Soft	0.000797822
Soft Soft : Soft Soft Soft	3.40648E-07
Stiff : Stiff Stiff	0.490142083
Stiff Stiff : Stiff Stiff Stiff	0.193258958
Soft Soft : Soft Stiff	0.002860581
Soft Soft Soft : Soft Soft Stiff	0.003862046
Soft Soft Soft : Soft Stiff Soft	0.382661077
Soft Soft Soft : Soft Stiff Stiff	0.002126751
Stiff Stiff : Stiff Soft	2.01366E-05
Stiff Stiff Stiff : Stiff Stiff Soft	1.86589E-05
Stiff Stiff Stiff : Stiff Soft Stiff	1.63005E-05
Stiff Stiff Stiff : Stiff Soft Soft	1.82579E-07
Stiff Stiff Soft : Soft Soft Stiff	0.002358264

B H3K9ac Intensity

Comparisons	p value
Soft : Stiff	0.008088286
Soft Soft : Stiff Stiff	0.04391987
Soft Soft Soft : Stiff Stiff Stiff	0.23923216
Soft : Soft Soft	0.045211621
Soft Soft : Soft Soft Soft	0.187537071
Stiff : Stiff Stiff	0.124229018
Stiff Stiff : Stiff Stiff Stiff	5.62944E-05
Soft Soft : Soft Stiff	0.001327478
Soft Soft Soft : Soft Soft Stiff	0.000139938
Soft Soft Soft : Soft Stiff Soft	0.181230411
Soft Soft Soft : Soft Stiff Stiff	2.76169E-06
Stiff Stiff : Stiff Soft	0.00172506
Stiff Stiff Stiff : Stiff Stiff Soft	0.25470349
Stiff Stiff Stiff : Stiff Soft Stiff	0.285159448
Stiff Stiff Stiff : Stiff Soft Soft	0.225741106
Stiff Stiff Soft : Soft Soft Stiff	1.10722E-05

Table B5. Significance tables with more comparisons corresponding to the data presented in Figure 10 (B).

Arid1a Intensity

Comparisons	p value
Soft : Stiff	0.000135
Soft Soft : Stiff Stiff	0.090648
Soft Soft Soft : Stiff Stiff Stiff	1.13E-17
Soft : Soft Soft	0.002984
Soft Soft : Soft Soft Soft	3E-14
Stiff : Stiff Stiff	4.35E-06
Stiff Stiff : Stiff Stiff Stiff	0.176338
Soft Soft : Soft Stiff	0.025876
Soft Soft Soft : Soft Soft Stiff	3.05E-15
Soft Soft Soft : Soft Stiff Soft	6.94E-12
Soft Soft Soft : Soft Stiff Stiff	2.48E-15
Stiff Stiff : Stiff Soft	0.430034
Stiff Stiff Stiff : Stiff Stiff Soft	0.439882
Stiff Stiff Stiff : Stiff Soft Stiff	9.91E-07
Stiff Stiff Stiff : Stiff Soft Soft	0.000204
Stiff Stiff Soft : Soft Soft Stiff	0.233005

APPENDIX C

Hypoxia Model Intermediate Equations

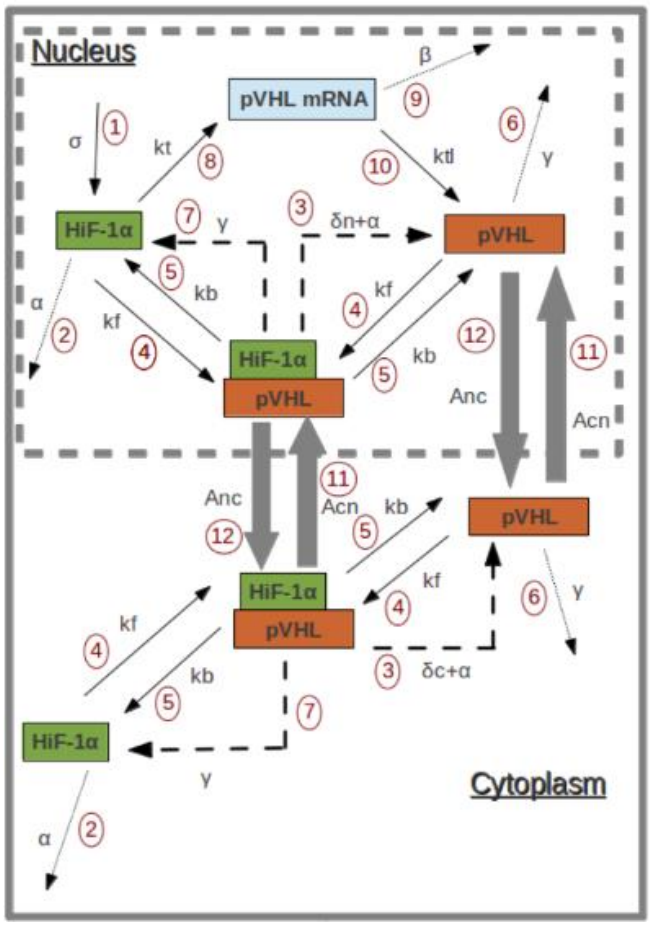

Model Variables

h = total HIF-1

h_n = nuclear HIF-1

h_c = cytoplasmic HIF-1

v_n = nuclear pVHL

v_c = cytoplasmic pVHL

v_m = pVHL mRNA

c_n = nuclear pVHL/HIF-1α complex

c_c = cytoplasmic pVHL/HIF-1α complex

Equation for pVHL mRNA. Its synthesis is promoted by HIF-1 with rate k_t, and it is degraded with rate β

$$\frac{dv_m}{dt} = k_t h_n^2 - \beta v_m \quad (1)$$

Equation for the nuclear pVHL. It is synthesized from mRNA with rate k_{tl}, and naturally degraded with rate ©. It is engaged in chemical equilibrium with the pVHL/HIF complex. k_f and k_b are the assembly/disassembly rates of the complex. This complex leads to the nuclear proteasomal

degradation of HIF-1 with rate ™$_n$ which liberates pVHL. The spontaneous degradation of HIF-1α also liberates pVHL with rate α.

$$\frac{dv_n}{dt} = k_{tl}v_m + k_b c_n + (\delta_n + \alpha)c_n + A_{c,n}v_c - k_f v_n h_n - \gamma v_n - A_{n,c}v_n \quad (2)$$

Equation for cytoplasmic pVHL. Similar to above, but without synthesis term for same reasons as equation 3.

$$\frac{dv_c}{dt} = k_b c_c + (\delta_n + \alpha)c_c + A_{n,c}v_n - k_f v_c h_c - \gamma v_c - A_{c,n}v_c \quad (3)$$

Equation for the nuclear pVHL/HIF-1 complex. It is assembled with rate. k_f, and disassembled with rate k_b. The spontaneous degradations of pVHL and HIF-1α, and the pVHL-induced HIF-1 degradation decreases its concentration with rates α, ©, ™$_n$ and respectively. The nuclear complex is exported to the cytoplasm with rate A_{nc}, and the cytoplasmic complex is imported with rate A_{cn}.

$$\frac{dc_n}{dt} = k_f h_n v_n + A_{c,n}c_c - k_b c_n - \delta_n c_n - (\gamma + \alpha)c_n - A_{n,c}c_n \quad (4)$$

Equation for cytoplasmic pVHL/HIF-1 complex.

$$\frac{dc_c}{dt} = k_f h_c v_c + A_{n,c}c_n - k_b c_c - \delta_c c_c - (\gamma + \alpha)c_c - A_{c,n}c_c \quad (5)$$

The values for these variables can be found in Supplementary Table 1.

Table C1. Table of variable values and ranges that can be used in the model. The variables with ranges are determined based on the oxygen level being modeled.

Parameter	Default Value	Range of Variations
$\int$	1000 nM/h	[200 8000]
$($	0.27/h	
k_f	1000 nM/h	[0 1000]
k_b	7200/h	
$©$	0.8/h	
k_t	.001 nM/h	
β	0.6/h	
k_{tl}	1.4/h	
$™_n$	1/h	
$™_c$	7/h	
A_{cn}	10/h	
A_{nc}	1000/h	[10 1000]